Stony Brook University

The Specificity of Vesicle Trafficking during Prospore Membrane

Formation in Yeast

A Dissertation Presented

by

Hui-Ju Yang

to

The Graduate School

in Partial Fulfillment of the

Requirements

for the Degree of

Doctor of Philosophy

in

Molecular and Cellular Biology

Stony Brook University

December 2010

Stony Brook University

The Graduate School

Hui-Ju Yang

We, the dissertation committee for the above candidate for the

<u>Doctor of Philosophy</u> degree,

hereby recommend acceptance of this dissertation.

Dr. Aaron M. Neiman, Associate Professor
Department of Biochemistry and Cell Biology, Stony Brook University
Dissertation Advisor

Dr. Nancy M. Hollingsworth, Professor
Department of Biochemistry and Cell Biology, Stony Brook University
Chairperson of Defense

Dr. Deborah A. Brown, Professor
Department of Biochemistry and Cell Biology, Stony Brook University

Dr. Neta Dean, Associate Professor
Department of Biochemistry and Cell Biology, Stony Brook University

Dr. Michael A. Frohman, Professor
Department of Pharmacological Sciences, Stony Brook University

Dr. Wei Guo, Associate Professor
Department of Biology, University of Pennsylvania
Outside member

This dissertation is accepted by the Graduate School

Lawrence Marin

Dean of the Graduate School

Abstract of the Dissertation

The Specificity of Vesicle Trafficking during Prospore Membrane Formation in

Yeast

by

Hui-Ju Yang

Doctor of Philosophy

in

Molecular and Cellular Biology

Stony Brook University

2010

This research focuses on the production of new plasma membranes during gametogenesis in yeast. The initiation of these membranes is started by vesicle fusion at spindle pole bodies (SPBs) during Meiosis II. I have asked how these vesicles specifically fuse at SPBs but not at other locations, and demonstrated that binding interactions between soluble NSF attachment protein receptors (SNAREs) confer one layer of specificity to vesicle fusion at SPBs. Furthermore, I showed that SPBs can actively regulate a Rab GTPase, suggesting a role for SPBs in vesicle docking. My work highlights the ancestral dual roles of centrioles in microtubule organization and membrane nucleation, the latter of which is required for cilium formation in mammalian cells.

Table of Contents

List of Tables

List of Figures

Acknowledgements

Frist and foremost, it is my pleasure to acknowledge my advisor, Professor Aaron Neiman, whose guidance and encouragement led me to develop understandings to this research. I have particularly enjoyed many thought-provoking discussions with Aaron.

I am thankful to my committees, Professor Nancy Hollingsworth, Professor Deborah Brown, Professor Neta Dean, Professor Michael Frohman, and Professor Wei Guo whose critics and suggestions enhanced the quality of this work.

Thanks to the yeast community at Stony Brook University for sharing the equipments and reagents, especially people in the Hollingsworth's lab and the Leatherwood's lab. Thanks are also due to Professor Erwin London for helping me to set up the fluorometer, and Dr. Susan Van Horn for teaching me how to use the electron microscope.

I also cherish the friendship with people at the Neiman's lab, including Hideki Nakanishi, Yasuyuki Suda, Jae-Sook Park, Pei-Chen Coney Lin, Erin Mathieson, Aviva Diamond, Alison Coluccio, Rachael Rodriguez, and Carey Kim. I would like to thank them for fruitful discussions and creating a pleasant working environment. Special thanks to Hideki Nakankshi who started the work of Rab GTPases in prospore membrane formation.

Thank many dear friends I met at Stony Brook, especially Huei-Mei Chen, Hui-Ting Cheng, Hsiao-Chi Lo, Wanhe Li and Cai Ying, whose hearty cares had kept my spirit up. I also particularly appreciate the company of my boyfriend, Chia-Hung Dylan Tsai, whose patience and understanding made my life of pursuing Ph.D. much easier.

Last but not least, I would like to express my gratitude to my parents and my sister, whose unconditional loves have supported me to continually challenge myself and pushed me to accomplish this dissertation.

Chapter 1

Introduction

The Life cycle of Saccharomyces cerevisiae

The budding yeast, *Saccharomyces cerevisiae*, can reproduce as diploid or haploid cells by mitotic cell divisions in medium containing sufficient nitrogen and a carbon source, but the mitotic cell cycle is stopped in response to environmental changes. For example, when two haploid cells with different mating types, MAT**a** and MATα, encounter each other, the two cells arrest in G1 phase and mate to form a diploid cell (MAT**a**/α) (Bucking-Throm et al., 1973; Herskowitz, 1988). Moreover, upon nitrogen starvation and in the presence of a nonfermentable carbon source such as acetate, a diploid cell is capable of generating haploid daughter cells (gametes, i.e. spores in yeast) by leaving the mitotic cycle from G1 phase and entering meiosis (Herskowitz, 1988; Neiman, 2005) (Figure 1.1).

During meiosis, a single round of DNA replication is followed by two rounds of division, Meiosis I and Meiosis II. In yeast, meiosis, like mitosis, is closed. That is, the nuclear envelope stays intact throughout the process. Spindle pole bodies (SPBs), the functional homologues of mammalian centrosomes, nucleate the spindle microtubules and span the nuclear envelope (Snyder, 1994). In the G1 phase, there is one SPB present in the cell. The SPB duplicates prior to Meiosis I and forms the Meiosis I spindle. As the cell exits from Meiosis I, the SPBs duplicate again. The separation of sister chromatids during Meiosis II results in four haploid nuclei. These four daughter nuclei are packaged into mature spores by a spore formation process that begins as the chromosomes are segregating in Meiosis II (Neiman, 2005). Spores are quiescent cells, but when nutrients are reintroduced, spores can germinate and re-enter the mitotic cell cycle.
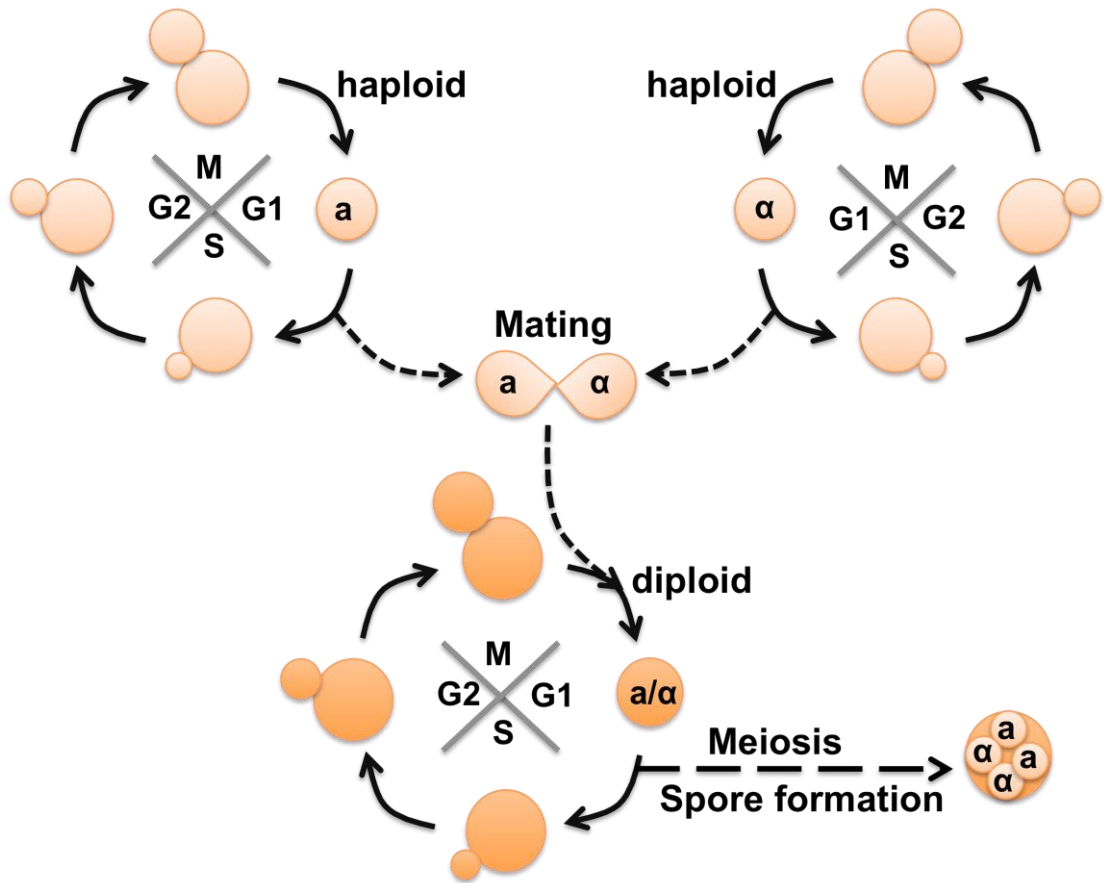
Figure 1.1. Life Cycle of *S. cerevisiae*. Budding yeast can live as haploid (a or α) and diploid (a/α) cells by mitotic cell cycle. Opposite mating types of haploid cells can mate with each other to form diploid cells. Upon nitrogen deprivation and in the presence of a nonfermentable carbon source, diploid cells undergo Meiosis to form spores.

Spore formation involves prospore membrane formation and spore wall assembly

Sporulation, i.e. gametogenesis in yeast, involves an unusual cell biological event in which the four spores are generated inside the cytoplasm of a diploid mother cell (Byers, 1981). After maturation of the spores within the cytoplasm, the mother cell collapses and becomes an ascus surrounding the four ascospores (Neiman, 2005). How is sporulation regulated? In *S. cerevisiae*, starvation signals, as well as *MATα* heteroalleles induce the transcription of *IME1* (Herskowitz, 1988), a master regulator of the sporulation process. Ime1 activates a transcriptional cascade by targeting other transcriptional regulators, (e.g. *NDT80*), and results in sequential waves of gene expression, pushing the sporulation process forward (Chu et al., 1998; Kassir et al., 1988). Many of the genes transcribed in the first wave are required for events of meiotic prophase, such as homologous chromosome pairing and recombination (Chu et al., 1998). Activation of *NDT80* drives the second wave of gene expression. These genes are involved in the simultaneous events of meiotic division and spore formation. Subsequent waves of gene expression are necessary for spore maturation (Chu et al., 1998; Neiman, 2005). Although they are both induced by Ndt80 and occur simultaneously, the meiotic divisions and spore formation can be uncoupled. Genes involved in spore formation do not necessarily affect meiotic division, and *vice versa* (Lo et al., 2008; Nakanishi et al., 2006).

Observations of spore morphogenesis under the electron microscope have linked two phenomena, double membrane formation around the daughter nuclei and spore wall assembly, to spore formation (Coluccio et al., 2004a; Guth et al., 1972; Neiman, 1998). Spore morphogenesis begins with the formation of double membranes, known as prospore membranes, at the beginning of Meiosis II after the second duplication and separation of SPBs (Moens, 1971; Neiman, 2005). Each prospore membrane is found associated with a Meiosis II SPB (Neiman, 1998). Through time-lapse microscopic observations, prospore membrane formation can be dissected into three steps: membrane initiation at the Meiosis II SPB, membrane expansion along the nucleus, and finally membrane closure (cytokinesis) to give rise to an immature prospore (Figure 1.2) (Guth et al., 1972; Neiman, 2005). Mutants defective in assembly of prospore membranes also fail to deposit spore wall material, and lead to

no spore formation, suggesting that prospore membrane formation is prerequisite to spore wall assembly (Diamond et al., 2009; Nakanishi et al., 2006; Nakanishi et al., 2007; Neiman, 1998).

The closure of each prospore membrane creates two distinct membranes. Spore wall materials are deposited in the lumen between the membranes, followed by lysis of the outer membrane (Lynn and Magee, 1970). It is not clear what drives the lysis of the outer membrane. The inner membrane of the prospore membrane serves as the future plasma membrane for the gametes. Spores are in a dormant state and display better resistance to environmental stress than vegetative cells (Coluccio et al., 2008; Smits et al., 2001). The spore wall, which is composed four specific layers, mannan, *beta*-glucan, chitosan, and dityrosine, is responsible for the spores' resistance to environmental damages (Coluccio et al., 2008; Smits et al., 2001). Disruption of spore wall assembly makes spores sensitive to hazards, such as ether (Coluccio et al., 2004a).
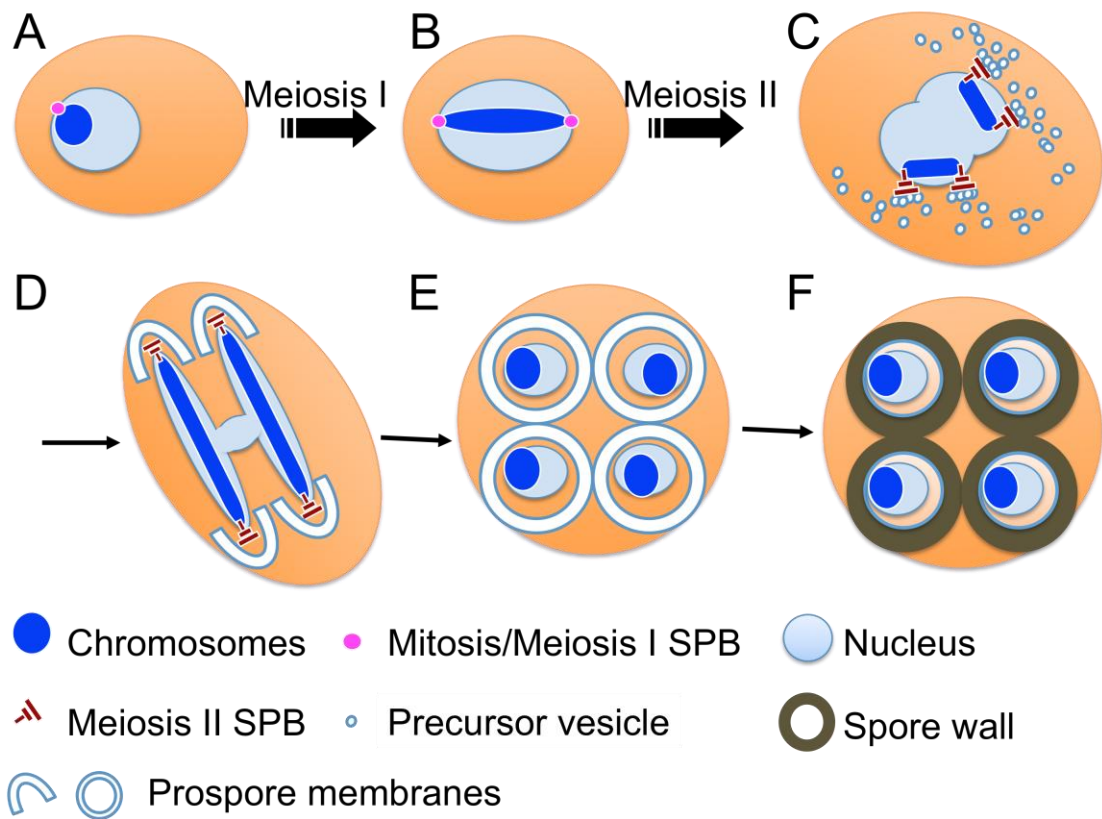
Figure 1.2. Prospore membrane formation. (A)Upon starvation, diploid cells enter Meiosis. (B) First Meiotic nuclear division. (C) Initiation of prospore membrane formation. At the beginning of Meiosis II, the SPBs become docking sites for precusor vesicles. (D) Prospore membrane expansion. (E) Prospore membrane closure. (F) Spore wall assembly.

Initiation of prospore membrane formation requires targeting and fusion of the precursor vesicles at Meiosis II SPBs

An intriguing phenomenon of sporulation is prospore formation inside the cytoplasm of a mother cell. What is the origin of these membranes? Most likely, the prospore membranes are derived from post-Golgi vesicles, analogous to secretory vesicles in vegetative cells (Neiman, 1998). It was shown that the late-*SEC* genes, *SEC1*, *SEC4*, and *SEC8* that mediate fusion of post-Golgi secretory vesicles at the plasma membrane are necessary for spore formation and display defects in prospore membrane formation (Neiman, 1998). In addition, the secreted protein, Gas1, localizes to the prospore membrane compartment during sporulation, suggesting that the secretory vesicles are redirected to the prospore membrane during sporulation (Neiman, 1998).

A specific soluble NSF attachment protein receptor (SNARE) complex drives vesicle fusion at prospore membranes. The membrane fusion machinery at the prospore membrane is similar to but slightly different from the plasma membrane. The SNARE machinery at the plasma membrane consists of Sso1/2, Snc1/2, and Sec9, but at the prospore membrane an alternative complex consisting of Sso1, Snc1/2, and Spo20 is used (Figure 1.3) (Brennwald et al., 1994; Neiman, 1998; Neiman et al., 2000). Sec9 and Spo20 are both the members of the SNAP-25 family; however *SPO20* is a sporulation-specific gene and cannot complement the function of *SEC9* (Neiman, 1998; Neiman et al., 2000). Moreover, although *SSO1* and *SSO2* are functionally redundant at the plasma membrane, *SSO1* is essential for spore formation (Jantti et al., 2002). An *sso1Δ* mutant shows no growth defect but exhibits a complete block of prospore membrane formation. A striking phenotype of the *sso1Δ* mutant seen in the electron microscope is that the precursor vesicles accumulate at the Meiosis II SPB (Nakanishi et al., 2006). This suggests that prospore membranes are initially generated from fusion of vesicles. Noticeably, the accumulated vesicles were found to have direct physical contact with Meiosis II SPBs (Nakanishi et al., 2006).
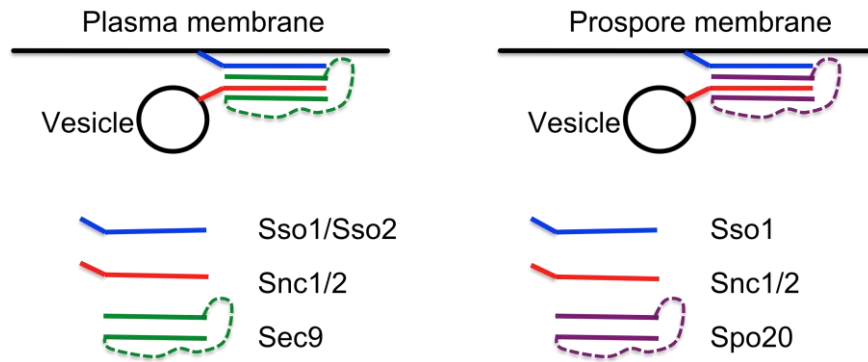
Figure 1.3. Specific pairing of SNARE proteins mediates fusion at the plasma and prospore membranes.

As mentioned above, many of the Ndt80-driven genes are involved in spore morphogenesis and, notably, three of the genes, *MPC54*, *SPO21*, and *SPO74* encode components of Meiosis II SPBs (Bajgier et al., 2001; Knop and Strasser, 2000; Nickas et al., 2003). SPBs are the microtubule-organizing center in yeast. In *S. cerevisiae*, the SPBs span the nuclear envelope and have distinct nuclear and cytoplasmic faces, called the inner and outer plaques, respectively (Jaspersen and Winey, 2004). In mitotic and Meiosis I cells, the outer plaque of the SPB serves as the cytoplasmic microtubule-organizing center due to a localized *gamma*-tubulin binding protein, Spc72 (Knop and Schiebel, 1998); However, Spc72 is replaced by Mpc54, Spo21, and Spo74 at the beginning of Meiosis II (Knop and Strasser, 2000; Nickas et al., 2003). This protein exchange on the outer plaque, which is now called the Meiosis II outer plaque (MOP), accompanies prospore membrane formation (Guth et al., 1972; Moens and Rapport, 1971). Whereas accumulated vesicles were found to be associated with the MOP in the *sso1Δ* mutant, disruption of the MOP by deletion of *MPC54*, *SPO21*, or *SPO74* results in disappearance of the precursor vesicles and prospore membranes (Knop et al., 2005; Nickas et al., 2003) (Figure 1.4). Interestingly, certain missense alleles of *mpc54* exhibit an intermediate phenotype between the *sso1* mutant and the *mpc54* null mutant: accumulation of undocked vesicles at the MOPs (Mathieson et al., 2010). All together, the MOP might serve as a vesicle-tethering complex that facilitates membrane fusion. Yet how the vesicles are directed and tethered to the MOP is not fully understood.

sso1Δ   spo74 Δ

(Nickas et al., 2003)
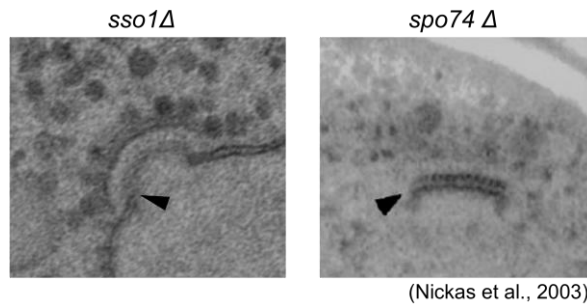
Figure 1.4. The MOP is required for vesicle tethering/docking. Vesicles are accumulated at the MOP in the *sso1Δ* mutant, but dispersed when the MOP is disrupted in the *spo74 Δ* mutant. Arrowheads indicate central plaques.

Forespore membrane formation in Schizosaccharomyces pombe *is a similar process to prospore membrane formation*

The fission yeast, *Schizosaccharomyces pombe*, is another model organism commonly used to study yeast sporulation. *S. pombe* preferentially live as haploid cells (Hayles and Nurse, 1989). Upon nitrogen starvation, two opposite mating types of haploid cells mate with each other to form a zygote, which immediately undergoes meiosis and sporulation. Sporulation in *S. pombe* also involves encapsulation of daughter nuclei by double membranes, called forespore membranes, inside a mother cell (Figure 1.5) (Shimoda, 2004).

As with prospore membrane formation in *S. cerevisiae*, full development of forespore membranes depends on SNARE machinery and modification of the *S. pombe* SPB during Meiosis II (Maeda et al., 2009; Nakamura et al., 2005; Nakase et al., 2008). *psy1+* is an *S. pombe* orthologue of *SSO1* from *S. cerevisiae*. Like Sso1, GFP-Psy1 localizes to the plasma membrane in vegetative cells, but shifts to the forespore membrane during sporulation (Maeda et al., 2009; Nakamura et al., 2008). A *psy1* temperature sensitive mutant leads to defects in forespore membrane assembly (Maeda et al., 2009). In addition, mutants with defects in the early secretory pathway also fail to develop full forespore membranes (Nakamura-Kubo et al., 2003; Nakase et al., 2001), suggesting that the membrane supply for the forespore membrane comes from secretory vesicles. Fusion of the secretory vesicles also starts at the MOP in *S. pombe* (Nakase et al., 2008). Although the proteins that compose the MOP in *S. pombe* do not share sequence similarities with those in *S. cerevisiae*, most of them are predicted as coiled-coil proteins (Knop and Strasser, 2000; Mathieson et al., 2010; Nakase et al., 2008). Many long coiled-coil proteins have been proposed to have a

8

role in vesicle tethering (Whyte and Munro, 2002). It is possible that the MOP in both yeasts utilize similar molecular mechanisms to promote vesicle docking.
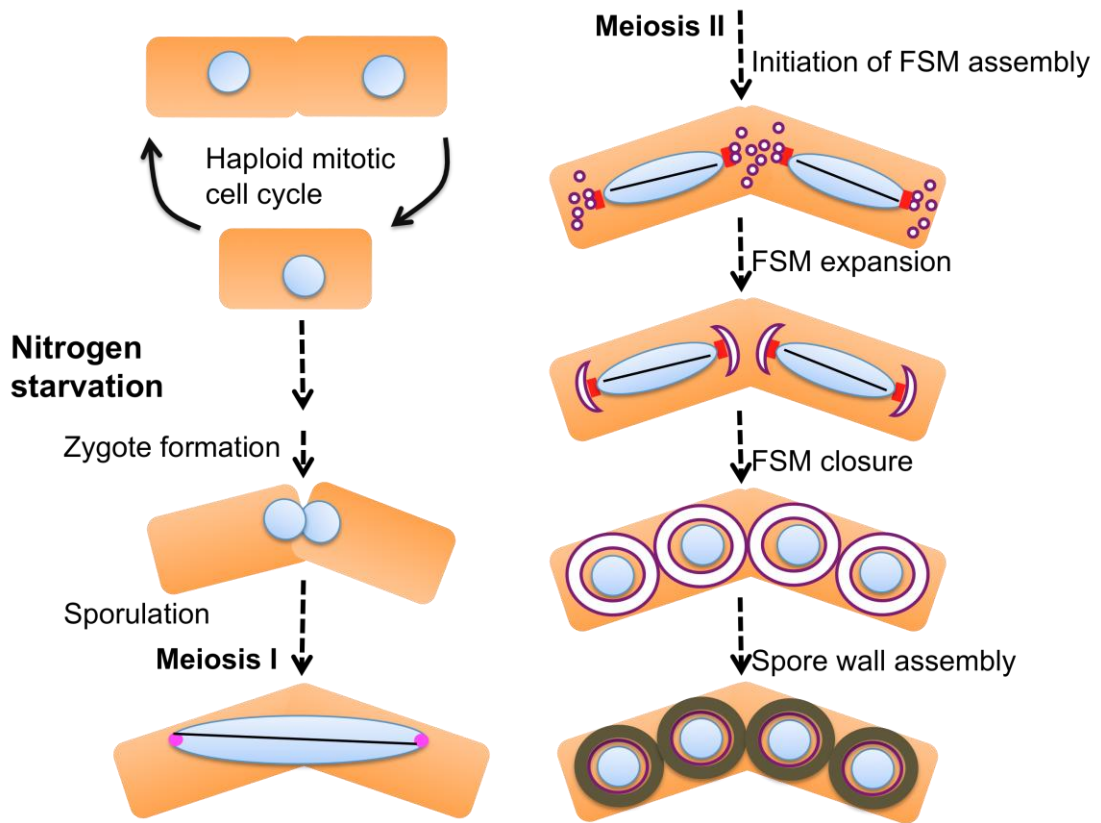
Figure 1.5. Overview of sporulation in *S. pombe*. Fission yeast cells preferentially live as haploids. Upon nitrogen starvation, different mating types mate to form zygotes and immediately enter meiosis and sporulate. The pink dots indicate the Meiosis I SPB. At the onset of Meiosis II, the SPBs, indicated by the red squares, are modified and become vesicle-docking sites (initiation of FSM assembly). The vesicles continuously fuse so that FSMs are elongated (FSM expansion). After nuclear division, the FSMs capture each nucleus and close (FSM closure). Finally, spore wall materials are deposited in the lumen of the double membranes to form the mature spores.

FSM: forespore membrane.

Sporulation in yeass provides a model to study vesicle trafficking specificity

Vesicular transport can be divided into three steps: vesicle budding from the donor membrane, vesicle movement, and vesicle fusion to the acceptor membrane. Specific vesicle fusion to the correct acceptor membrane ensures vesicle trafficking specificity, which is important to maintain cellular organization. The specificity of vesicle fusion can be broadly divided into two aspects (Mellman and Warren, 2000): the first is tethering of transport vesicles to target compartments, and the second is the specific membrane fusion at the right place. The former is thought to be mainly regulated by a Rab GTPase and its downstream effectors (Pfeffer, 1999), and the latter is mediated by SNARE protein complexes (Jahn and Scheller, 2006) (Figure 1.6).

Prospore membrane or forespore membrane formation in yeasts defines a vesicular trafficking step that is developmentally regulated (Nakamura-Kubo et al., 2003; Nakase et al., 2001; Neiman, 1998). With the similarities and differences from vesicle transport to plasma membrane, vesicle trafficking to the prospore membrane provides a good model system to monitor how vesicle trafficking specificity is controlled. For instance, the different requirements for SNARE proteins at the plasma membrane and prospore membrane probably confer the specificity of fusion at the two compartments, and regulation of vesicle tethering could consolidate membrane fusion at the right place.
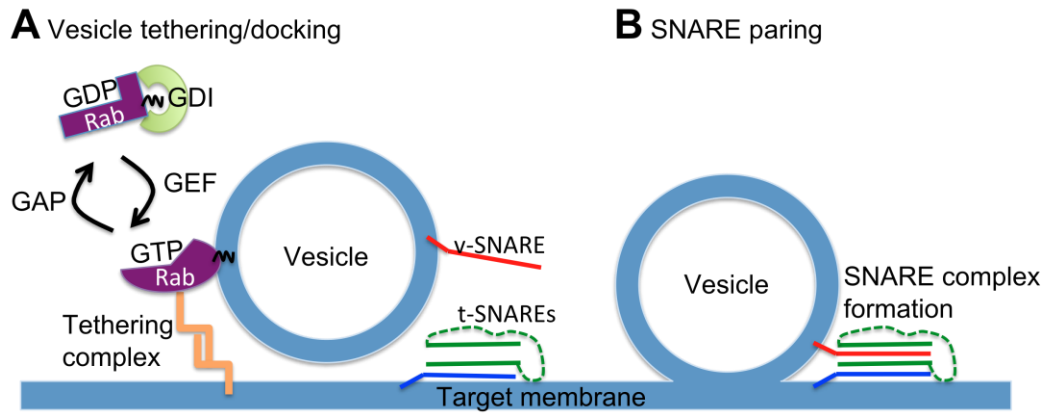
Figure 1.6. Vesicle tethering/docking and SNARE pairing mediate specificity of vesicle fusion. (A) A specific Rab-GDP is recognized by a GEF in the transport vesicle and becomes Rab-GTP. Rab-GTP recruits varying effectors (here it is a tethering factor) and facilitates vesicle docking to the target membrane. After vesicle docking, a specific GAP hydrolyzes the Rab GTP to form Rab-GDP, which is released to the cytosol by binding to a GDP dissociation inhibitor (GDI). (B) SNARE complex formation can bring the opposing membranes close to each other and generates the energy to initiate membrane fusion.

Rab GTPase and its downstream effectors regulate vesicle docking

Ypt (Yeast protein transport) / Rab (<u>Ra</u>s-related proteins in <u>b</u>rain) proteins are members of Ras GTPase superfamily. There are more than 70 Rab family GTPases found in human, 11 such GTPases in *S. cerevisiae*, and 8 reported Rab proteins in *S. pombe*. Rab proteins are key regulators of membrane traffic, and almost every trafficking step involves a specific Rab GTPase (Figure 1.7).

Like other GTPases, Rab GTPases cycle between an inactive GDP-bound and active GTP-bound form. Because of their slow intrinsic enzymatic kinetics, GTPase activating proteins (GAPs) are needed to inactivate Rab GTPases by stimulating GTP hydrolysis, while guanine-nucleotide exchange factors (GEFs) are needed to activate Rab GTPases by facilitating the release of GDP and the uptake of GTP (Pfeffer, 1999; Segev, 2001). Rab proteins associate with membranes through prenylation of their C-terminal cysteines (Zhang, 2003). When in the GDP-bound conformation, Rab GTPases are extracted from membranes and released to the cytosol by binding to GDP dissociation inhibitors (Grosshans et al., 2006b). The specificity of Rab GTPases to distinct vesicle trafficking steps is linked to protein localization, and mediated by co-localized GEFs, and GAPs (Morozova et al., 2006; Rivera-Molina and Novick, 2009; Sclafani et al., 2010). A Rab GTPase is activated by the GEF at the site of action, while the GAP acts at the site to down-regulate the Rab GTPase and confines the action of the Rab GTPase to particular steps of secretory pathway. To ensure the flow and specificity of membrane trafficking, it is suggested that an early-acting Rab protein recruits the GEF for the late-acting Rab while the late acting Rab protein subsequently recruits the GAP for the early-acting Rab (Nottingham and Pfeffer, 2009) (Figure 1.8).
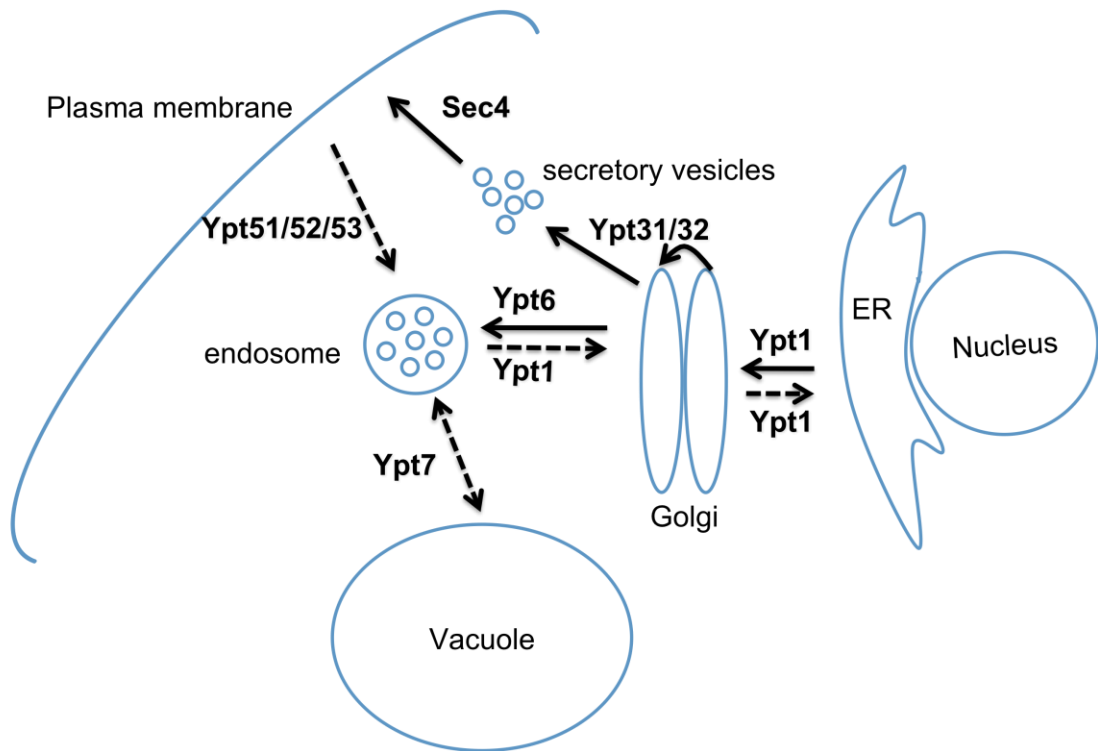
Figure 1.7. Distinct vesicular transport can be assigned to specific Rabs. Intracellular vesicle trafficking broadly involves the secretory pathway and the endocytic pathway. The secretory pathway starts at the endoplasmic reticulum (ER), travels across the Golgi to the plasma membrane. The endocytic pathway runs in a retrograde direction from the plasma membrane, through the endosome, and can lead to the vacuole or back to the Golgi. From the Golgi, the vesicles can go to the plasma membrane, the endosome or back to ER according to their cargo. A specific Rab GTPase regulates each step of vesicle transport pathway.
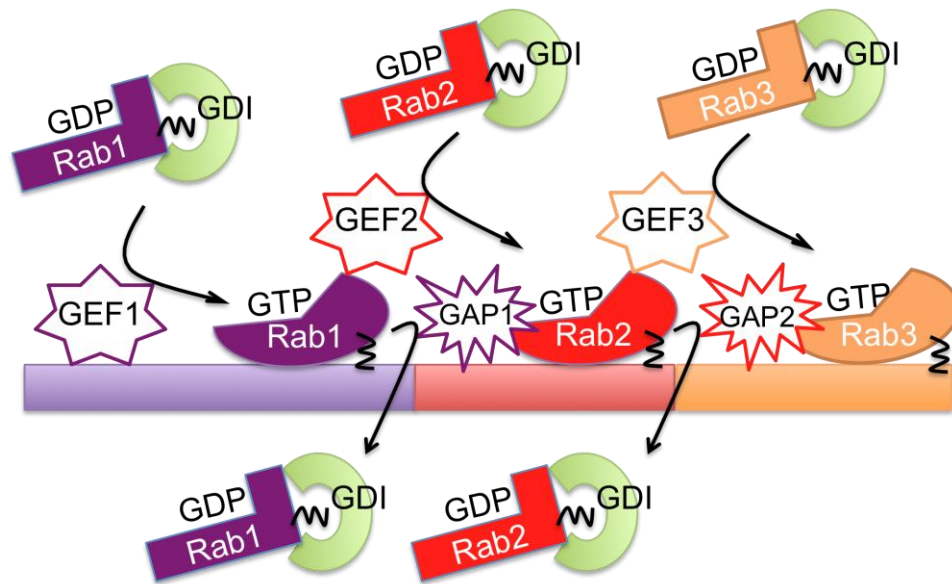
Figure 1.8. Rab specificity is achieved by GEF and GAP cascade. Rab1 is activated by its specific GEF, GEF1, at the first membrane compartment. Rab1-GTP subsequently recruits GEF2 that activates Rab2 at the second membrane compartment. An effector of Rab2-GTP is GAP1 that specifically inactivates Rab1 so that Rab1 can only act on the first membrane compartment. Another effector of Rab2-GTP is the GEF for Rab3. Rab3-GTP binds to GAP2 to inactivate Rab2 and set up the boundary between membrane compartments. Inactive Rab GTPases, Rab-GDP, are retrieved from membranes by binding to the GDP dissociation inhibitor (GDI).

The dynamic GDP/GTP cycle allows Rab GTPases to act as molecular switches to regulate the interactions of transport vesicles and acceptor membranes. It is believed that when a Rab GTPase is in its GTP-bound conformation, it is switched on to interact with downstream effectors. Many interacting proteins of Rab GTPases are tethering factors that are required to support the binding of vesicles to an acceptor compartment; for example, the exocyst complex is a downstream effector of Sec4 (Guo et al., 1999), and the transport protein particle (TRAPP) complex is a tethering complex that binds to Ypt1-GTP (Wang and Ferro-Novick, 2002). It is therefore suggested that one function of Rab GTPases is to facilitate vesicle docking by interacting with tethering effectors (Pfeffer, 1999).

The Rab GTPase, *SEC4*, regulates transport of post-Golgi vesicles to the plasma membrane in vegetative cells of *S. cerevisiae*. It is believed that Sec4 is recruited to the secretory vesicles by binding to the GEF protein, Sec2 (Ortiz et al., 2002; Walch-Solimena et al., 1997). Sec2 activates Sec4 to the GTP-bound conformation, which in turn binds to the downstream effector, Sec15. The association of Sec4 and Sec15 links the exocyst complex to the vesicles and facilitates vesicle docking to the plasma membrane (Guo et al., 1999). *SEC4* is also required for prospore membrane formation and Sec4 is recruited to the precursor vesicles at the SPBs during sporulation (Mathieson et al., 2010; Neiman, 1998); however, no physical connection between Sec4 and the MOP, which defines the site of vesicle tethering, has been identified.

SNARE proteins

A striking feature of SNARE proteins is the highly conserved coiled coil domain (SNARE domain) of 60-70 amino acids (Weimbs et al., 1998). Most SNARE proteins, except for members of the SNAP-25 family, have a single C-terminal transmembrane domain, which is connected to a single SNARE domain by a short linker. The members of the SNAP-25 family lack a transmembrane domain and contain two coiled coil domains. Another feature of SNARE proteins is a cluster of basic amino acids between the transmembrane domain and the SNARE domain. For members of SNAP-25 family, the basic patch is between the two SNARE domains (Weimbs et al.,

1998).

SNARE proteins can be classified as target membrane associated (t)-SNAREs or vesicle associated (v)-SNAREs, and they are further classified as Q- and R-SNAREs depending on the residue found at the center of the SNARE domain (Fasshauer et al., 1998). The structure of SNARE complexes is a parallel four stranded helix bundle (Sutton et al., 1998). It is generally accepted that the formation of the four-helix bundle can bring the opposing membranes close to each other and generate the energy necessary to initiate membrane fusion (Jahn and Scheller, 2006). The helix bundle of SNARE complexes contains 16 layers of interacting side chains, which are mostly hydrophobic, except for the central "0" layer (Figure 1.9). The central "0" layer contains three glutamines (Q) and one arginine (R) (Fasshauer et al., 1998). Accordingly, Q-SNAREs provide glutamine in the ionic "0" layer, while R-SNAREs provide arginine. Most t-SNAREs are included in the classification of Q-SNAREs, and v-SNAREs are included in the R-SNAREs. For example, Sso1, Snc1, and Sec9 are the SNARE proteins that assemble into the SNARE complexes during plasma membrane fusion in *S. cerevisiae*. Sso1 and Sec9 are t-SNAREs which contain Q residues in the ionic "0" layer of their SNARE domain, while Snc1 is a v-SNARE protein which contains an R residue in the "0" layer of its SNARE domain.
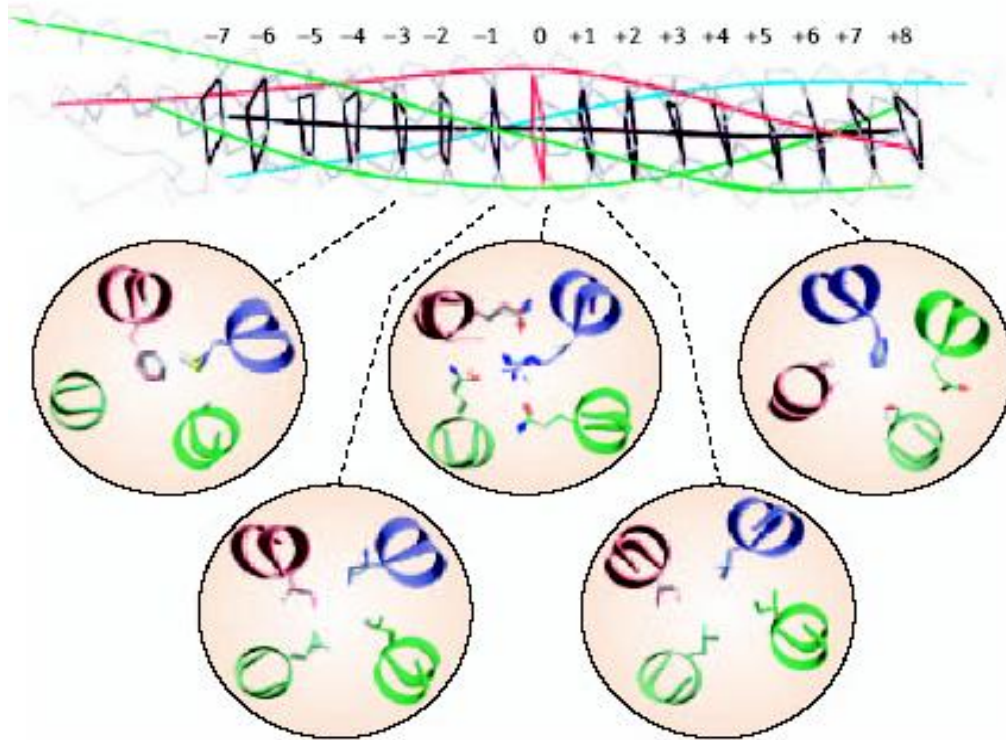
Figure 1.9. SNARE core complexes. A skeleton diagram indicates the 16 layers of interacting side chain (numbered) of the four SNARE helix-bundles. The interactions of the amino acids side chain from individual layers are exemplified in the circles. Figure is adopted from Jahn and Scheller (2006).

Eukaryotic cells contain many SNAREs. For instance, there are 25 members in *S. cerevisiae*. Each fusion event of intracellular membrane trafficking is driven by a specific set of SNARE proteins assembled into SNARE complexes (Jahn and Scheller, 2006) (Figure 1.10). It has been suggested that cognate SNARE pairing contributes to the specificity of membrane fusion. The distinct intracellular localization of many SNARE proteins might provide SNARE specificity. In *in vitro* experiments, non-cognate SNAREs have been shown to be able to form stable complexes (Fasshauer et al., 1999; Yang et al., 1999); nonetheless, the specificity of SNARE pairing *in vivo* can be restricted by localization.
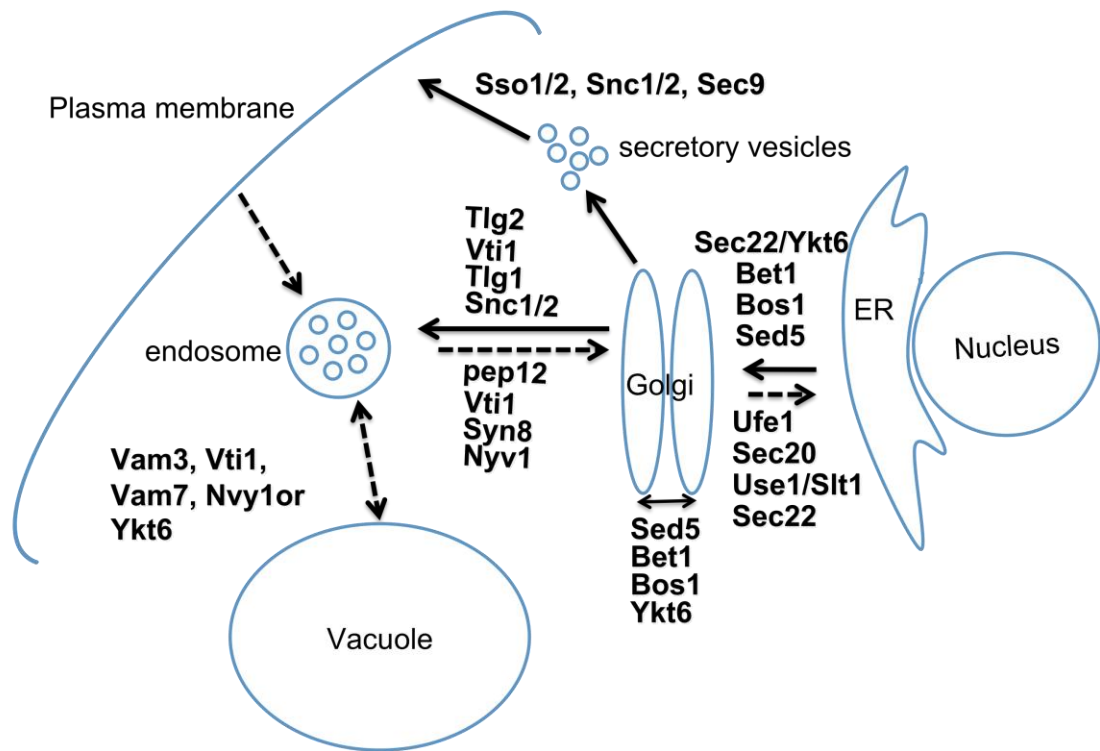
Figure 1.10. Distinct sets of SNARE complex are required for different fusion events in the secretory pathway of *S. cerevisiae*.

Alternatively, SNARE specificity could be due to the intrinsic binding specificity of SNARE proteins for each other. When different sets of v- and t- SNAREs were reconstituted into separate populations of liposomes to monitor the efficiency of membrane fusion, a considerable degree of specificity for functional SNARE assembly was observed (McNew et al., 2000). The intrinsic binding specificity could be determined by different binding energies of different combinations of SNARE proteins. In *Drosophila*, a single mutation in the helix bundle layer of syntaxin 1A which tightens the SNARE complex structure increases the rate of synaptic vesicle fusion and causes regulated synaptic vesicle fusion to resemble constitutive vesicle fusion (Lagow et al., 2007). This finding suggests that the binding energy of SNARE protein complexes can be adjusted by altering the interface layer of SNARE domains.

S. cerevisiae contains two members of the SNAP-25 family, Sec9 and Spo20 (Neiman, 1998). Although both proteins participate in the post-Golgi vesicle fusion and partner with the same SNARE proteins, each protein cannot execute the other's function (Neiman et al., 2000). A series of *SPO20/SEC9* chimeras was constructed to

19

define important domains for the functional specificity of the two gene products. Spo20 and Sec9 were divided into four parts: the N-terminal region covering the first 160 amino acids of Spo20 and 420 amino acids of Sec9, the first coiled-coil domain, the interhelical regions between the two coiled-coil domains, and the second coiled-coil domain (Neiman et al., 2000) (Figure 1.11). For Spo20, specificity resides in the N-terminal and interhelical regions. The N-terminal region of Spo20 confers sporulation specific function by regulating protein localization, in which it contains a nuclear targeting signal in the first 50 amino acids which sequesters Spo20 to the nucleus in vegetative cells, and an amphipathic helix which targets Spo20 to the prospore membrane (Nakanishi et al., 2004). It is unclear how the interhelical region of Spo20 confers its sporulation-specific function. For Sec9, specificity resides in the SNARE helices. The *SPO20/SEC9* chimera, *PSPS*, in which the SNARE domains of Spo20 are replaced with those of Sec9, can function in sporulating cells; however, when the SNARE domains of Sec9 are replaced with those of Spo20, the resulting chimera, *SPSP*, cannot substitute the function of Sec9 in vegetative cells (Neiman et al., 2000). These data suggest that in addition to their separate localization giving rise to the specificity, the SNARE domain of the two SNAP-25 family members might contribute to their distinct functions as well.
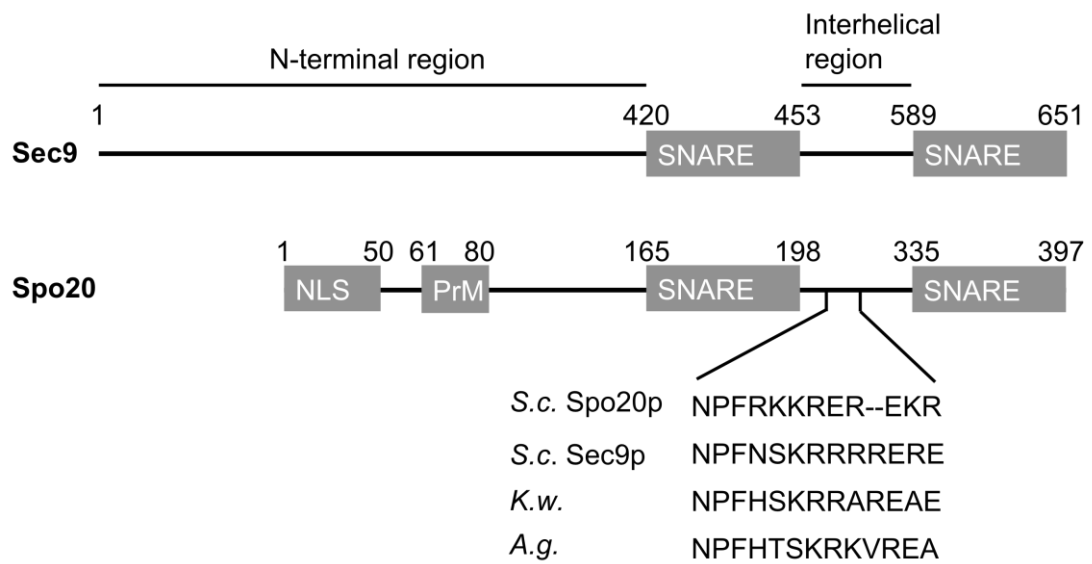
Figure 1.11. Domain diagrams of Sec9 and Spo20. Both Sec9 and Spo20 can be divided into the N-terminal region, the first SNARE domain, interhilical region, and the second SNARE domain. The N-terminal region of Spo20 contains a nuclear targeting signal (NLS) (amino-acids 1-50) and a prospore membrane targeting amphipathic helix (PrM) (amino-acids 61-80). Alignment of conserved residues in the interhelical region between Spo20 and other members of SNAP-25 in yeast are shown. *S.c.= S. cerevisiae*; *K.w.= Kluveromyces waltii*; *A.g.= Ashbya gossipii*.

Chapter 2

Binding Interactions Control SNARE Specificity *In Vivo*

Reformatting of article published in (Yang et al., 2008)
(Figure 2.2 is contributed by Dr. Hideki Nakanishi and Figure 2.8 is contributed by Dr. Song Liu and Dr. James A. McNew)

S. cerevisiae contains two SNAP-25 paralogues, Sec9 and Spo20, which mediate vesicle fusion at the plasma membrane and the prospore membrane, respectively. Fusion at the prospore membrane is sensitive to perturbation of the central ionic layer of the SNARE complex. Mutation of the central glutamine of the t-SNARE Sso1 impairs sporulation, but does not affect vegetative growth. Suppression of the sporulation defect of an *sso1* mutant requires expression of a chimeric form of Spo20 carrying the SNARE helices of Sec9. Mutation of two residues in one SNARE domain of Spo20 to match those in Sec9 created a form of Spo20 that restores sporulation in the presence of the *sso1* mutant and can replace *SEC9* in vegetative cells. This mutant form of Spo20 displayed enhanced activity in *in vitro* fusion assays, as well as tighter binding to Sso1 and Snc2. These results demonstrate that differences within the SNARE helices can discriminate between closely related SNAREs for function *in vivo*.

2.1 Introduction

Control of membrane fusion events is critical for the maintenance of an organized endomembrane system in eukaryotic cells. Fusion must be regulated so that carrier vesicles only fuse with the appropriate acceptor compartment. This control is exerted on several levels by a verity of regulatory proteins including SM proteins, Rab proteins and tethering complexes (McNew, 2008). Additionally, specific interactions between SNARE proteins are an important factor in the specificity of vesicle fusion (McNew et al., 2000; Sollner et al., 1993).

SNARE proteins are the core machinery of intracellular membrane fusion (Weber et al., 1998). They are characterized by a ~60 amino acid domain (the SNARE

domain) through which they form heteroligomers (Sutton et al., 1998; Weimbs et al., 1998). In addition, most SNARE proteins contain a C-terminal transmembrane domain adjacent to the SNARE domain. Interaction of a SNARE protein anchored in the vesicle membrane (a v-SNARE) with SNARE proteins in the target membrane (t-SNAREs) leads to the assembly of the SNARE domains into a parallel four helix bundle (Poirier et al., 1998; Sutton et al., 1998). Bundle formation drives the transmembrane domains of the SNAREs into close proximity and is proposed to provide the potential energy necessary to allow mixing and fusion of the lipid bilayers (Jahn and Scheller, 2006; Weber et al., 1998).

Discrete SNARE complexes control fusion at every level of the secretory pathway (Pelham, 1999). This has led to the suggestion that assembly of cognate SNAREs into exclusive complexes could be a central mechanism for the control of vesicle fusion in the cell (McNew et al., 2000; Sollner et al., 1993). Though isolated SNARE domains show little or no binding specificity *in vitro*, when full length SNAREs are reconstituted into synthetic liposomes, only specific combinations can mediate fusion of the artificial bilayers, suggesting that this could be the basis for *in vivo* control (McNew et al., 2000; Yang et al., 1999). However, many SNAREs have been found to participate in more than one fusion event *in vivo* (Parlati et al., 2000; Parlati et al., 2002; Paumet et al., 2001; Paumet et al., 2004), again raising the question of how the participation of an individual SNARE in a particular fusion event is regulated.

The process of sporulation in the budding yeast *S. cerevisiae* provides a useful model in which to address the question of SNARE specificity. During sporulation, fusion of post-Golgi vesicles with the plasma membrane stops, and instead these vesicles are directed to specific sites in the cytoplasm where they fuse to form new membrane compartments termed prospore membranes (Neiman, 1998). One prospore membrane envelops each of the four nuclei produced by meiosis, packaging the nuclei into four daughter cells or spores (Neiman, 2005).   In concert with this change in the target compartment of exocytic vesicles comes a change in one of the SNARE proteins required for their fusion (Neiman, 1998).

In vegetative cells, vesicles fusing with the plasma membrane use a SNARE complex that is composed of one of two redundant t-SNAREs Sso1 or Sso2, a second t-SNARE subunit, Sec9, and one of two redundant v-SNARE proteins Snc1 or Snc2

(Aalto et al., 1993; Brennwald et al., 1994; Protopopov et al., 1993). Sec9 is a member of the SNAP-25 subfamily of SNARE proteins, which differ from other SNAREs in that they lack a transmembrane domain but contains two SNARE helices (Brennwald et al., 1994; Oyler et al., 1989; Weimbs et al., 1998). Thus, a SNARE complex acting at the plasma membrane contains one helix from Sso1 or Sso2, one helix from Snc1 or Snc2, and two helices from Sec9. During sporulation, when exocytic vesicles fuse to generate a prospore membrane, the SNARE complex used is slightly differently. Sso1 is required for this fusion, but Sso2 does not function in this process (Jantti et al., 2002). An *sso1* single mutant, though normal for vegetative secretion, is completely blocked in fusion during sporulation. Direct evidence that Snc1 or Snc2 function at the prospore membrane has not been reported, but a role for these v-SNAREs has been inferred by their localization to the prospore membrane during sporulation (Neiman et al., 2000). Finally, the most notable difference is that the t-SNARE Sec9 is not required for fusion at the prospore membrane. Rather it is replaced by a second sporulation-specific SNAP-25 family member, the Spo20 protein (Neiman, 1998).

Sec9 and Spo20 are specialized for their sites of action. Ectopic expression of *SPO20* in vegetative cells cannot rescue the growth defect of a *sec9-4^{ts}* mutant at 37°C, nor can overexpression of *SEC9* during sporulation restore sporulation to a *spo20* mutant (Neiman, 1998). Chimera studies indicated that the basis of specificity is different for each protein. The ability of Spo20 to work at the prospore membrane requires a lipid-binding motif in its N-terminal domain that is not present in Sec9 (Nakanishi et al., 2004; Neiman, 1998). Targeting of Sec9 to the prospore membrane allows it to largely compensate for loss of *SPO20* (Nakanishi et al., 2006). By contrast, the ability of Sec9 to function at the plasma membrane is a property of its SNARE domains. Forms of Spo20 in which the SNARE domains are substituted with those of Sec9 can replace *SEC9* in vegetative cells (Neiman et al., 2000). Changes in genes involved in lipid metabolism were also found to promote the function of Spo20 in vegetative cells (Coluccio et al., 2004b). Finally, *in vitro* experiments comparing Sso1/Sec9-Snc2 and Sso1/Spo20-Snc2 complexes demonstrated that the Spo20-containing assemblies are less potent fusogens and that the stability of the assembled complexes is lower (Liu et al., 2007). These results suggest that the inability of Spo20 to function at the plasma membrane may be a function of it

forming complexes that provide insufficient binding energy to overcome a barrier to fusion at that compartment.

An assembled SNARE complex incorporates sixteen interfaces where the side chains from all four helices pack together (Sutton et al., 1998). The packing interactions are primarily hydrophobic contacts, except at the central or "zero layer" interface (Sutton et al., 1998). There, the interaction is mediated by polar binding between conserved glutamine and arginine side chains. Most SNARE complexes conform to a 3Q:1R rule, i.e., at the zero layer, three glutamine residues interact with one arginine (Fasshauer et al., 1998). In the yeast plasma membrane SNARE, Sso1/Sso2 and both helices from Sec9 contain a glutamine residue and Snc1/Snc2 provides the arginine residue. If the central layer glutamine in Sso1 is mutated to arginine, this mutant form of Sso1 is not functional; however function can be restored by coexpression of a form of Snc2 in which the arginine has been changed to glutamine (Katz and Brennwald, 2000). Such compensatory Q/R mutations also work in other SNARE complexes and have been used to demonsrate that specific pairs of SNARE proteins function together *in vivo* (Graf et al., 2005).

The interpretation of the Spo20 experiments described above assumes that the Snc1/Snc2 proteins function as the v-SNARE for fusion at the prospore membrane. To test this, we sought to use compensatory Q/R mutations in the SNARE domains of Sso1 and Snc2 to demonstrate a direct role of Snc2 during sporulation. We report here that strains carrying an Sso1^{Q224R} mutation failed to sporulate and that compensatory mutations in none of the *S. cerevisiae* R-SNAREs can rescue this sporulation defect. Sporulation is reduced by mutation of the central layer glutamine of Sso1 to any other residue, whereas vegetative growth is largely unaffected by these changes. The sensitivity of sporulation to changes in the Sso1 ionic layer residue, we show, is due to the presence of Spo20 in the prospore membrane SNARE complex. Coexpression of a Spo20 chimera carrying the Sec9 SNARE helices with the Snc2^{R52Q} allele rescues the sporulation defect of the *sso1*^{Q224R} mutant. Mutation of two residues located at binding interfaces in the SNARE domain of Spo20 to the corresponding residue in Sec9 allows Spo20 to function in concert with Sso1^{Q224R} and Snc2^{R52Q} proteins. This mutant form of Spo20 also shows enhanced ability to rescue *sec9-4*^{ts} in vegetative cells. *In vitro*, the mutant Spo20 forms tighter complexes with Sso1 and Snc2 and is a more efficient fusogen than the wild type protein. These results demonstrate that the

intrinsic binding energy of the SNARE domains can help control the specificity of vesicle fusion *in vivo*.

2.2 Materials and Methods

Yeast strains and genetics methods

Unless otherwise noted, standard media and genetic methods were used (Rose and Fink., 1990). The strains used in this chapter are listed in Table 1. Strain HI3 was constructed by PCR-mediated replacement (Longtine et al., 1998) of the *SSO1* gene in the haploid strains AN117-4B and AN117-16D (Neiman et al., 2000) and mating of the resulting haploids. Strain HI75 was constructed by mating the *sso1Δhis5*$^+$ derivative of AN117-4B to an *sso2Δkan*^{r} strain from the *S. cerevisiae* knockout collection (Winzeler et al., 1999). The resulting diploid was transformed with pRS316-SSO1 and then sporulated. Segregants lacking both *SSO1* and *SSO2* were then mated to generate HI75. To construct strain HJ3, a strain from the *S. cerevisiae* knockout collection carrying the *sso1Δkan*^{r} allele was first mated to AN117-4B. A haploid segregant from this cross was mated to strain AN1052 (Neiman et al., 2000), and this diploid was dissected and double mutant *sso1Δ spo20Δ* haploids were mated.

Plasmids

Plasmids used in this chapter are listed in Table 2.

pRS314-*SSO1* and pRS314-*sso1*^{Q224R} were constructed by digesting pRS316-SSO1 and pRS316-sso1^{Q224R} (Katz and Brennwald, 2000) with PvuII. These fragments were cotransformed into yeast with Kpn1–SacI-digested pRS314 (Sikorski and Hieter, 1989), and the reconstituted plasmids were recovered from yeast. To construct the other glutamine 224 substitutions, the *sso1*^{Q224R} gene was first cloned as a BamHI–HindIII fragment from pRS314-*sso1*^{Q224R} into similarly digested pUC119. Site-directed mutagenesis was then performed using oligonucleotides ANO377 and ANO378, which contain randomized nucleotides at codon 224. Sequencing of individual clones from the mutagenesis identified particular substitutions. All substitutions except lysine, glutamine, histidine, and aspartate were obtained in this

27

way. For lysine, glutamine, and histidine, the randomized oligos HNO961 and HNO962 were used. For aspartate, mutagenesis was performed using oligos HNO991 and HNO992. After specific mutations were identified by sequencing, the 3′ end of the *SSO1* gene carrying the glutamine 224 substitution was swapped into pRS314-*SSO1* as an NcoI–SalI fragment. To construct the pRS426 and pRS316 plasmids expressing the chimeras *PSPS*, *PSPP*, and *PPPS*, SacI–KpnI fragments carrying the *SPO20* promoter and the indicated chimera were isolated from the corresponding integrating plasmids (Neiman et al., 2000) and cloned into similarly digested pRS426 or pRS316, respectively (Christianson et al., 1992; Sikorski and Hieter, 1989). To construct pRS425–*snc2^{R52Q}* a BamHI–SalI fragment carrying the *snc2^{R52Q}* gene (Katz and Brennwald, 2000) was cloned into BamHI–SalI-digested pRS426.

To make pRS316-SEC9pr-*PSPP* and pRS316-SEC9pr-*PPPS*, SpeI–SacI fragments carrying the particular chimera were excised from pRS426-SPO20pr-*PSPP* or -*PPPS* and cloned into the backbone of SpeI–SacI-digested pRS316-SEC9pr-PSPS (Nakanishi et al., 2004). The plasmids pRS426-SPO20pr-*SPO20$^{C224L;S231N}$*, pRS426-SPO20pr-*SPO20$^{A378L;K385N}$*, and pRS426-SPO20pr-*SPO20$^{F357T;F361L}$* were created by site-directed mutagenesis of the plasmid pRS426-SPO20pr-*SPO20* (Nakanishi et al., 2004) using oligos HJO31 and HJO32, HJO33 and HJO34, and HJO35 and HJO36, respectively.

Integrating plasmids expressing Δ3-51*SPO20* and Δ3-51*SPO20$^{C224L;S231N}$* under the *SEC9* promoter were assembled by amplifying the genes from pRS426-SPO20pr-*SPO20* and pRS426-SPO20pr-*SPO20$^{C224L;S231N}$*, respectively, using oligos BBO14 and ANO168. The PCR products were digested with XhoI and SacI, and cloned into similarly digested pRS306-SEC9pr (Neiman et al., 2000). To make *SPO20$^{C224L;S231N,F357T,F361L,A378LK385N}$*, pRS306-SEC9pr-Δ3-51*SPO20$^{C224L;S231N}$* was used as template for site-directed mutagenesis using first primers HJO33 and HJO34, and then HJO35 and HJO36. To construct 2μ plasmids expressing the various *SPO20* mutants and *SPO20/SEC9* chimeras under *SEC9* promoter control, KpnI–SacI fragments containing *SEC9* promoter with indicated genes were cloned from the integrating and CEN plasmids into KpnI and SacI sites of pRS426.

To construct 3xHA tagged versions of the different SPO20 mutants, two complimentary oligos (HJO72 and HJO73) were synthesized that encode 3xHA

epitopes and anneal to leave XhoI-compatible ends. The oligos were phosphorylated with T4 polynucleotide kinase (Invitrogen) at 37℃ for 10 min, mixed, and then allowed to anneal. The annealed oligos were then ligated with XhoI-digested pRS306-SEC9pr-*SEC9* (Neiman et al., 2000). Site-directed mutagenesis was then performed using oligos HJO78 and HJO79 to restore an XhoI at the junction of 3xHA and *SEC9*. Finally, an XhoI–SacI fragment containing *SEC9* was replaced with the corresponding XhoI–SacI fragments from pRS306-*SEC9*pr-Δ3-51*SPO20*, -Δ3-51*SPO20* $^{C224L;S231N}$, or -Δ3-51*SPO20/SEC9*chimera plasmids.

Sporulation assays

Sporulation assays were performed as described previously (Neiman et al., 2000). For tests on solid medium, the strains to be tested were grown overnight on selective media, and then replica plated to sporulation medium. After 24 h, spore formation was quantified by direct observation in the light microscope.

For liquid sporulation and ether tests, 1.5 ml of overnight-cultured cells were pelleted, washed once in 1 ml 2% potassium acetate, and resuspended in 10 ml 2% potassium acetate. After 2 d of incubation at 30℃, the sporulation frequency was determined by observation under the light microscope; meanwhile, 5 μl of the culture was spotted onto a YPD plate. The plate was inverted over a paper filter soaked with 2 ml of ethyl ether for 30 min. After 30 min the paper filter was removed, and the plate was incubated at 30℃ overnight.

Growth assays

To assay the growth defect of the *spo20Δ sec9-4* mutant, cells were first cultured overnight at 25℃ in YPD. Thereafter, 10-fold serial-diluted cell cultures were spotted onto two identical plates selective for the plasmid. One plate was placed at 25℃, and the other at 37℃ to monitor the growth rate of the *spo20Δsec9-4* mutant.

Immunoprecipitations

The immunoprecipitation assays were modified from (Carr et al., 1999). Strain HI75 was transformed with *CEN* plasmids expressing the different *SSO1* genes and high copy plasmids expressing the different *SNC2* and *SPO20* alleles. 5 ml of overnight culture was diluted into 100 ml of selective medium and grown to mid-log phase. Cells were harvested and resuspended in 1 ml of ice-cold wash buffer (20 mM Tris, pH 7.5, 20 mM NaN$_3$, and 20 mM NaF). Washed cells were pelleted at 4℃, resuspended in 1 ml ice-cold IP buffer (50 mM Hepes, pH 7.4, 150 mM KCl, 1 mM EDTA, 1 mM DTT, and 0.5% NP-40), and treated with zymolyase (100 μg/ml) for 10 min. Cells were pelleted and resuspended in 500 μl ice-cold IP buffer with protease inhibitors. Cells were lysed by shaking with glass beads (0.5 mm) at 4℃ for 10 min. Lysed cells were pelleted for 10 min at 13,000 *g* and the supernatants were precleared by addition of protein G–Sepharose beads (GE Healthcare). The mixtures were rocked for 30 min at 4℃ and then centrifuged for 15 min at 13,000 *g* at 4℃ to pellet the beads, debris, and nonspecifically bound products. To precipitate the HA-tagged proteins, anti-HA monoclonal antibodies (clone HA-7; Sigma-Aldrich) were added to the precleared supernatants for 30 min before G–Sepharose beads were added, and the mixtures were incubated at 4℃ overnight. The beads and bound protein were pelleted for 10 s at 4,000 *g*, and washed five times with 1 ml ice-cold IP buffer. Proteins were eluted from the beads by boiling them in 2X SDS sample buffer (60 mM Tris-HCl, pH 6.8, 10% glycerol, 2% SDS, 0.05 mg/ml bromophenol blue, and 5% β-mercaptoethanol) for 5 min.

Proteins of interest were analyzed by Western blot. 3xHA-Δ3-51Spo20 species were separated by SDS-PAGE on 10% mini-gels, whereas Ssop and Sncp were resolved on 15% mini-gels. Proteins were transferred to PVDF membranes (Millipore). 3xHA-Δ3-51Spo20 species were visualized with chicken anti-HA antibodies (Aves Laboratories) to minimize the cross-reactivity from the mouse HA antibodies in the IP. Sso1 and Snc2 were detected by rabbit anti-Sso1 and rabbit anti-Snc2 (Sogaard et al., 1994), respectively. Peroxidase-conjugated secondary antibodies (anti–chicken or anti–rabbit) were used. The band intensities were determined using ImageJ and the ratios of Sso1 or Snc2 to the precipitated

3xHA-Δ3-51Spo20 protein were calculated to compare coprecipitation of Sso1 and Snc2 with the different 3xHA-Δ3-51Spo20 species.

Protein expression and purification

Sso1, Snc1, Sec9, and Spo20 were expressed and purified as previously described in detail (Liu et al., 2007). Spo20^{C224L,S231N} was expressed and purified from pET24a(+)-based plasmid pJM557 as done previously for Spo20.

The Spo20^{C224L,S231N} (147–397) fragment for pJM557 was amplified from pRS306*SEC9*pr::*Δ50spo20$^{C224L;S231N}$* using (CCGAATTCGACTATCCACAGTGG) and (GCACGCGTCTCGAGTCACCATCTTTTCCCG).

Liposome fusion assays

Liposome reconstitution and fusion assay were performed as described previously (Liu et al., 2007).

Melting temperature determination

The stability of Spo20^{C224L,S231N} ternary SNARE complex was determined by chemical denaturation using guanidine HCl as the denaturant. Changes in CD signal were performed using a spectrometer (model 62DS; Aviv) as described previously (Liu et al., 2007). The [GdnHCl]$_{1/2}$ of the Spo20^{C224L,S231N} ternary SNARE complex was determined by KaleidaGraph (Synergy Software) using nonlinear least squares analysis.

Image acquisition and processing

Images of yeast growth and Western blots were acquired on a scanner (model 2450; Epson) and figures were prepared using Microsoft PowerPoint and Adobe Photoshop 9.0.

Table 1 Strains used in chapter 2

Strain	Genotype	Source
HI3	*MATa/MATα ura3/ura3 trp1/trp1 leu2/leu2 his3/his3 lys2/lys2 arg4/ARG4 rme1ΔLEU2/ RME1 hoΔLYS2/hoΔLYS2 sso1Δhis5⁺/sso1Δhis5*	This study
HI75	*MATa/MATα ura3/ura3 trp1/trp1 leu2/leu2 his3/his3 met15/MET15 arg4/ARG4 sso1Δhis5⁺/ sso1Δhis5⁺ sso2Δkanᵣ/sso2Δkanᵣ⁺* pRS316-SSO1	This study
HJ3	*MATa/MATα ura3/ura3 trp1/trp1 leu2/leu2 his3/his3 sso1Δkanᵣ/sso1Δkanᵣ spo20Δhis5⁺/ spo20Δhis5⁺*	This study
AN211	*MATa/MATα ura3/ura3 trp1/trp1 leu2/leu2 his3/his3 lys2/LYS2 ade2/ADE2 s9-4/sec9-4 spo20Δhis5⁺/spo20Δhis5*	(Nakanishi et al., 2004)

32

Table 2 Plasmids used in chapter 2

Name	Source
pRS314	(Sikorski and Hieter, 1989)
pRS314-SSO1	This study
pRS314-$sso1^{Q224R}$	This study
pRS425	(Christianson et al., 1992)
pRS425-$snc2^{R52Q}$	This study
pRS426	(Christianson et al., 1992)
pRS426-SPO20	(Nakanishi et al., 2004)
pRS426-PSPS	This study
pRS426-PSPP	This study
pRS426-PPPS	This study
pRS426-$SPO20^{C224L,S231N}$	This study
pRS426-$SPO20^{F357T,F361L}$	This study
pRS426-$SPO20^{A378L,K385N}$	This study
pRS306-SEC9pr-SEC9	(Neiman et al., 2000)
pRS306-SEC9pr-Δ3-51SPO20	This study
pRS306-SEC9pr-Δ3-51PSPS	This study
pRS306-SEC9pr-Δ3-51$SPO20^{C224L,S231N}$	This study

Table 2 Plasmids used in chapter 2 (Continued)

Name	Source
pRS306-SEC9pr-Δ3-51$SPO20^{C224L,S231,F357T,F361L,A378L,K385N}$	This study
pRS316-SEC9pr-Δ3-51$PSPP$	This study
pRS316-SEC9pr-Δ3-51$PPPS$	This study
pRS426-SEC9pr-$SEC9$	This study
pRS426-SEC9pr-Δ3-51$SPO20$	This study
pRS426-SEC9pr-Δ3-51$PSPS$	This study
pRS426-SEC9pr-Δ3-51$SPO20^{C224L,S231N}$	This study
pRS426-SEC9pr-Δ3-51$PSPP$	This study
pRS426-SEC9pr-Δ3-51$PPPS$	This study
pRS426-SEC9pr-3xHA$SEC9$	This study
pRS426-SEC9pr-3xHAΔ3-51$SPO20$	This study
pRS426-SEC9pr-3xHAΔ3-51$PSPS$	This study
pRS426-SEC9pr-3xHAΔ3-51$SPO20^{C224L,S231N}$	This study
pRS426-SEC9pr-3xHAΔ3-51$SPO20^{F357T,F361L}$	This study
pRS426-SEC9pr-3xHAΔ3-51$PSPP$	This study
pRS426-SEC9pr-3xHAΔ3-51$PPPS$	This study

2.3 Results

Compensatory mutations in Snc2 cannot rescue the sporulation defect of a mutation in the Sso1 central ionic layer

Prospore membrane formation requires the t-SNAREs Sso1 and Spo20 (Jantti et al., 2002; Neiman, 1998). Though the v-SNAREs Snc1 and Snc2 localize to the prospore membrane (Neiman et al., 2000), direct evidence of their involvement in prospore membrane assembly has not been reported. Compensatory Q/R mutations in the central ionic layer of a t-SNARE and a v-SNARE have been used to demonstrate specific SNARE interactions *in vivo* (Graf et al., 2005; Katz and Brennwald, 2000). To examine the possible role of the Snc proteins during sporulation, we introduced a plasmid carrying the *sso1^{Q224R}* allele into strain HI3 (*sso1Δ/ sso1Δ*) alone or in combination with a plasmid carrying the *snc2^{R52Q}* allele. As expected, the *sso1^{Q224R}* allele did not rescue the sporulation defect of the *sso1Δ* (Figure 2.1). Neither *SNC2* nor *snc2^{R52Q}* were capable of restoring sporulation in this context (Figure 2.1). This failure of *snc2^{R52Q}* to rescue the sporulation defect raises the possibility that Snc2 does not participate in vesicle fusion at the prospore membrane. We therefore examined whether mutation of the central layer arginine to glutamine in any of the other *S. cerevisiae* R-SNAREs (Snc1, Ykt6, Sec22, Nyv1) could restore sporulation to the *sso1^{Q224R}* strain. As with *snc2^{R52Q}*, none of these mutant SNAREs could compensate for the *sso1^{Q224R}* mutation (H. Nakanishi, unpublished observations).

To ensure that *snc2^{R52Q}* was indeed capable of suppressing *sso1^{Q224R}* in our strains, we constructed a strain homozygous for deletion of *SSO1* and *SSO2* and kept alive by the *SSO1* gene on a centromeric plasmid (HI75). When the *sso1^{Q224R}* mutation was introduced into this strain, the plasmid bearing the wild-type gene could be lost only when the *snc2^{R52Q}* allele was also present. The resulting strain is viable because of the compensatory interaction between the two mutant SNAREs (Katz and Brennwald, 2000). However, as with the results in the *sso1Δ/ sso1Δ* strain, the presence of *snc2^{R52Q}* does not rescue the sporulation defect associated with *sso1^{Q224R}* (Figure 2.1). Taken together these results suggest either that no R-SNARE proteins are involved in fusion at the prospore membrane, and therefore they cannot

35

compensate for the *sso1*^{Q224R} mutation, or that fusion at the prospore membrane is particularly sensitive to the proper configuration of side chains at the central ionic layer in the SNARE complex.

Relevant Genotype	Gene expressed	% asci	Ether test
sso1ΔSSO2	none	< 0.2	
sso1ΔSSO2	*SSO1*	40.4	
sso1ΔSSO2	*sso1*^{Q224R}	< 0.2	
sso1ΔSSO2	*sso1*^{Q224R} *snc2*^{R52Q}	< 0.2	
sso1Δsso2Δ	*sso1*^{Q224R} *snc2*^{R52Q}	< 0.2	

Figure 2.1. Compensatory mutation of *SNC2* cannot rescue the sporulation defect of *sso1*^{Q224R}. Strains HI3 (*sso1Δ/sso1Δ*) or HI75 (*sso1Δ/sso1Δ sso2Δ/sso2Δ*) were transformed with the CEN plasmids expressing the indicated genes and sporulated in liquid culture. Sporulation was assessed by observation in the light microscope and by ether test. To determine percentage of sporulation, at least 500 cells were counted for each strain. For HI75, the plasmid carrying the wild-type *SSO1* was lost by growth on 5-FOA before cells were assayed.

Vegetative yeast cells are largely insensitive to mutation of the t-SNARE ionic layer

To further explore the role of the central ionic layer in Sso1 function, codon 224 was mutated and alleles bearing all possible amino acid replacements of the glutamine were constructed. Each of these $sso1^{Q224X}$ alleles was introduced on a plasmid into strain HI75 ($sso1\Delta/\ sso1\Delta\ sso2\Delta/\ sso2\Delta$ p$SSO1$) and the transformants were then transferred to plates containing 5-fluoroorotic acid (5-FOA) to select for loss of the wild- type $SSO1$-containing plasmid. Like $sso1^{Q224R}$,$sso1^{Q224P}$ failed to grow on 5-FOA indicating that a proline substitution at this position also interferes with Sso1p function. Though arginine cannot function, lysine is weakly tolerated at this position as cells containing $sso1^{Q224K}$ as their only source of Sso protein were viable, but slow growing at elevated temperature (Figure 2.2). The phenotype of $sso1^{Q224K}$ may be due to the presence of the positively charged side chain because, as with $sso1^{Q224R}$, coexpression of $snc2^{R52Q}$ suppressed the slow growth of $sso1^{Q224K}$ (H. Nakanishi, unpublished observations). However, other than these three mutations, all other amino acids at position 224 were well tolerated. As judged by colony size, strains carrying these $sso1^{Q224X}$ alleles as their sole form SSO grew as well as those carrying $SSO1$ even at low or high temperatures (Figure 2.2; data not shown). Thus, despite the strong evolutionary conservation of ionic layer glutamine, the yeast plasma membrane SNARE can tolerate a wide variety of residues at this position.
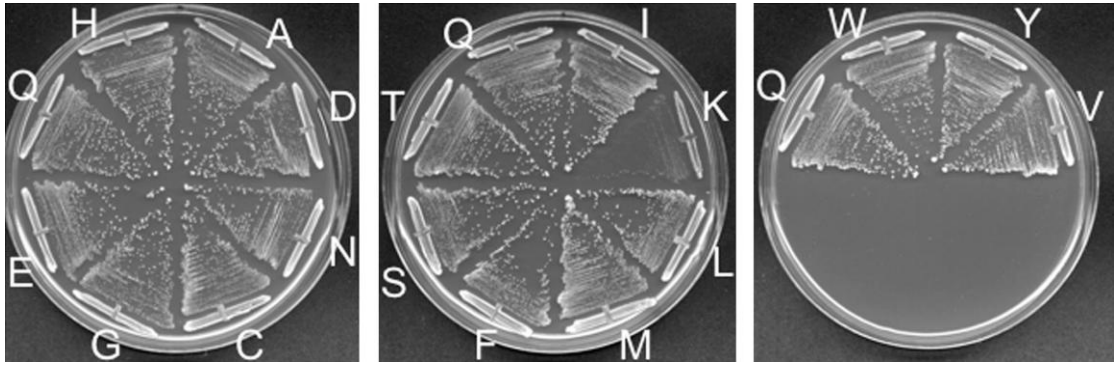
Figure 2.2. Mutation of Sso1Q224 is well tolerated in vegetative growth. Strain HI75 (*sso1Δ/sso1Δ sso2Δ/sso2Δ*) was transformed with CEN plasmids carrying all possible amino acid substitutions at position 224 of Sso1 and the plasmid carrying the wild-type *SSO1* was lost by plasmid shuffle, leaving the mutant as the sole form of Sso protein in the cell. Transformants carrying substitutions that could support growth (all except arginine and proline) were streaked out on YPD plates and incubated at 37℃. Letters indicate the amino acid present at position at 224 of Sso1 in each strain.

Sporulation is sensitive to perturbation of Sso1^{Q224}

The strains carrying the various $sso1^{Q224X}$ alleles as their only *SSO* were then examined for their ability to sporulate. Unlike growth rate, sporulation was sensitive to changes at this position (Figure 2.3). All of the mutations caused a reduction in sporulation efficiency, varying from a two- to fourfold to several hundred-fold with small or polar amino acids better tolerated than large hydrophobic or positively charged side chains. Substitution of a lysine, which causes slow growth, led to a loss of sporulation, as did the arginine and proline mutations (examined in the *sso1* single mutant strain) that cannot support vegetative growth. Substitution of leucine or tryptophan had no effect on growth, yet these mutants displayed strong sporulation defects. Thus, mutations such as $sso1^{Q224W}$ behave as sporulation-specific alleles of *SSO1*; they are as effective as wild type in supporting vegetative growth but unable to support sporulation. These results suggest that the inability of $snc2^{R52Q}$ to rescue the sporulation defect of $sso1^{Q224R}$ might be caused by the sensitivity of sporulation to changes in the ionic layer residue of Sso1, rather than an indication that Snc2 does not function at the prospore membrane.
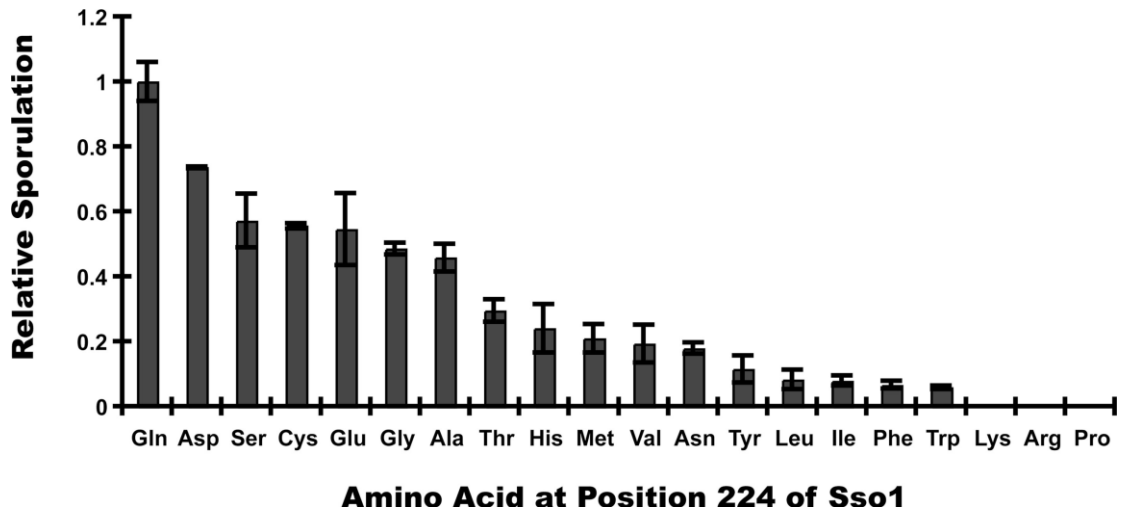
Figure 2.3. Sporulation is sensitive to mutation of Sso1Q224. Strains HI3 (*sso1Δ/sso1Δ*) (for Sso1Q224R, Q224P, and Q224K) or HI75 (*sso1Δ/sso1Δ sso2Δ/sso2Δ*) (all other substitutions) expressing an *SSO1* gene with the indicated amino acid substitution from a CEN plasmid were sporulated, and the percentage of sporulation in the culture was measured. At least 500 cells were counted for each strain. Sporulation efficiency is shown relative to HI75 carrying the wild-type *SSO1*. Error bars indicate one standard deviation.

The combination of Snc2^{R52Q} and Sec9 helices can rescue the sporulation defect of sso1^{Q224R}

One possible explanation for the observation that *snc2*^{R52Q} can only rescue *sso1*^{Q224R} during vegetative growth is that one or both of these mutant proteins is mislocalized during sporulation. However, examination of GFP-tagged forms of the proteins revealed that both display an SPB-associated fluorescence in *sso1* mutant cells indistinguishable from wild-type Snc2 protein and consistent with localization to prospore membrane precursor vesicles (data not shown).

An alternative possibility is the existence of sporulation-specific proteins whose interaction with Sso1 and/or Snc2 is sensitive to the mutations. As Sec9 works with these proteins in vegetative cells and Spo20 replaces it during sporulation, Spo20 would be a candidate for such a factor (Brennwald et al., 1994; Neiman, 1998). To test the possibility that the switch to Spo20 during sporulation is the basis for the *sso1*^{Q224X} phenotypes, we examined the ability of chimeras in which the helices of Spo20 are replaced with those of Sec9 (*PSPS*) to rescue the *sso1*^{Q224R} sporulation defect. Strain HJ3 (*sso1Δ/ sso1Δ spo20Δ/spo20Δ*) carrying p*sso1*^{Q224R} was transformed with either an empty vector, or one carrying *snc2*^{R52Q}, as well as high copy plasmids expressing either wild type *SPO20* or the *PSPS* chimera. Expression of *snc2*^{R52Q} or *SPO20* alone did not increase the frequency of sporulation and expression of *PSPS* resulted in only a modest improvement. Similarly, co-overexpression of *snc2*^{R52Q} and *SPO20* had no effect. However, coexpression of both *snc2*^{R52Q} and the *PSPS* chimera resulted in sporulation at levels comparable to the same strain carrying *SSO1* and *SPO20* plasmids (Figure 2.4). This result demonstrates that *snc2*^{R52Q} can contribute to suppression of *sso1*^{Q224R} indicating that Snc2 does participate in fusion at the prospore membrane. Moreover, in the context of the rearranged central layer, the partner SNARE for Sso1/Snc2 must contain the Sec9 helical domains for sporulation to occur. Spo20 cannot support membrane assembly under these circumstances. Sensitivity of Spo20-containing complexes to perturbations of the ionic layer may also explain the sporulation-specific nature of other *sso1*^{Q224X} mutations.

To more precisely define the differences between Sec9 and Spo20 in their ability to mediate fusion in the context of *sso1*^{Q224R}/ *snc2*^{R52Q}, the ability of chimeras

41

replacing only one of the two Spo20 helices with that of Sec9 was examined. A swap of the first Spo20 helix (*PSPP*) was as effective at rescuing sporulation as the *PSPS* chimera. A swap of only the second helix (*PPPS*) increased sporulation, but to a much lesser extent than the first helix (Figure 2.4). These results suggest that differences in the first helical domains of Spo20 and Sec9 are largely responsible for their differing phenotypes in this assay.

Ionic Layer Configuration	Genes Expressed	% asci	Ether Test
a	*SSO1 SPO20*	21.4	
b	*sso1^{Q224R} SPO20*	0.1	
a	*SSO1 PSPS*	20	
b	*sso1^{Q224R} PSPS*	4.65	
c	*sso1^{Q224R} snc2^{R52Q} SPO20*	0.55	
	SSO1 snc2^{R52Q} PSPS	17.6	
c	*sso1^{Q224R} snc2^{R52Q} PSPS*	11.8	
c	*sso1^{Q224R} snc2^{R52Q} PPPS*	6.2	
c	*sso1^{Q224R} snc2^{R52Q} PSPP*	14.3	

a Sso1 / Snc2 (Q Q / R Q) Spo20   **b** Sso1 / Snc2 (R Q / R Q) Spo20   **c** Sso1 / Snc2 (R Q / Q Q) Spo20

Figure 2.4. Co-expression of *snc2^{R52Q}* and a chimeric *SPO20* rescues the sporulation defect of *sso1^{Q224R}*. Strain HJ3 (*sso1Δ/sso1Δ spo20Δ/spo20Δ*) was transformed with plasmids carrying the indicated genes and sporulated in liquid culture. *SSO1* alleles were expressed from CEN plasmids; *SNC2* and *SPO20* alleles were expressed from high copy plasmids. Sporulation was assessed by observation in the light microscope or by ether test. To determine percentage of sporulation, at least 500 cells were counted for each strain; percentages represent the average of four experiments. "a", "b", and "c" illustrate the arrangement of side chain residues at the ionic layer in the different strains.

Mutation of two interface residues allows Spo20 to function with the altered Sso1/Snc2

In vitro, Sso1/Snc2/Spo20 complexes have a lower melting temperature than Sso1/Snc2/Sec9 complexes, suggesting that Spo20 binds less tightly to these other SNAREs then does Sec9 (Liu et al., 2007). Packing interactions between side chains of amino acids located at interfaces on the SNARE helices determine how tightly the SNAREs in a given complex bind to each other. We aligned the interface residues of Spo20 and Sec9 to look for possible sub-optimal residues in Spo20 (Figure 2.5). As criteria to identify such residues we looked for differences in the size and/or chemical properties of the side chains. In the first helix, only two positions stood out, a cysteine at the +3 layer of Spo20 that is leucine in Sec9, and a serine at +5 that is an asparagine in Sec9. In the second helix, four differences of note were found; phenylalanines at the -2 and -1 layers that are threonine and leucine, respectively, in Sec9, an alanine in the +4 layer (leucine in Sec9) and a lysine residue at the +6 position (asparagine in Sec9). These six residues were mutated in pairs in the context of an otherwise wild type *SPO20* sequence. The resulting mutants, $SPO20^{C224L,S231N}$, $SPO20^{F357L,F361T}$, and $SPO20^{A378L,K385N}$ were all capable of rescuing the sporulation defect of a *spo20* mutant, indicating that the mutants encode functional proteins (data not shown). They were then tested for their ability to rescue the sporulation defects of HJ3 (*sso1Δ/ sso1Δ spo20Δ/spo20Δ*) expressing the $sso1^{Q224R}$ and $sso1^{Q224R}$ alleles (Figure 2.5).

When sporulation was assessed on solid medium, the differences between the *PSPP* and *PPPS* chimeras were more pronounced than in liquid sporulation (Figure 2.4). Consistent with the relative ability of different chimeras to promote sporulation, the alterations in the second helix, $SPO20^{F357L,F361T}$ and $SPO20^{A378L,K385N}$ had little effect on suppression, though $SPO20^{F357L,F361T}$ did display a reproducible, slight improvement in sporulation efficiency. By contrast, $SPO20^{C224L,S231N}$ allowed sporulation at a level comparable to the *PSPP* chimera, indicating that these two residues are primarily responsible for the ability of this chimera to function in conjunction with $sso1^{Q224R}$ and $snc2^{R52Q}$.
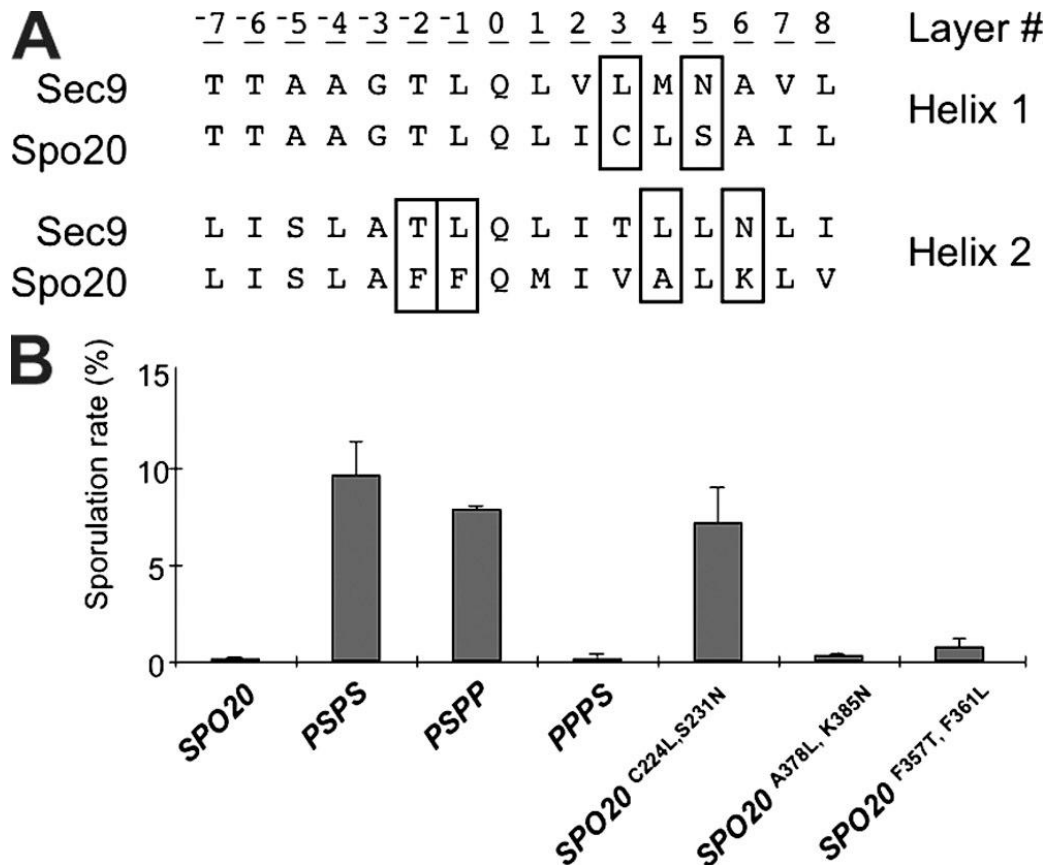
Figure 2.5 Mutation of two interface residues in the Spo20 SNARE helix allows it to function with *sso1^{Q224R}*. (A) Alignment of the interface residues in the SNARE domains of Spo20 and Sec9. Residues chosen for mutation are in blocks. (B) Sporulation of *sso1^{Q224R}* *snc2^{R52Q}* strains expressing different forms of *SPO20*. Strain HJ3 (*sso1Δ/sso1Δ spo20Δ/spo20Δ*) was transformed with plasmids carrying *sso1^{Q224R}* and *snc2^{R52Q}* as well as the indicated form of *SPO20*. The *sso1^{Q224R}* allele was expressed from a CEN plasmid; *snc2^{R52Q}* and the *SPO20* alleles were expressed from high copy plasmids. These strains were sporulated and sporulation efficiency measured in the light microscope. At least 500 cells were scored for each strain. Results are the average of three experiments. Error bars indicate one standard deviation.

$SPO20^{C224L,S231N}$ can rescue *sec9-4ts*

Ectopic expression of *SPO20* cannot rescue the temperature sensitive growth defect of a *sec9-4* mutant, though a chimeric form of Spo20 carrying the Sec9 helical regions can rescue *sec9-4* (Neiman et al., 2000). This suggests that the inability of Spo20 to function at the plasma membrane is tied directly to its SNARE domain. We examined whether the $SPO20^{C224L,S231N}$ allele affects the ability of Spo20 to compensate for loss of *SEC9*. These experiments were performed with proteins lacking the inhibitory domain (amino acids 3-51) present in the amino terminus of Spo20 (Neiman et al., 2000). As previously reported, Δ3-51*SPO20* cannot rescue *sec9-4*, even when present on a high copy plasmid, though Δ3-51*PSPS* was capable of rescuing growth at high temperature. The Δ3-51$SPO20^{C224L,S231N}$ allele also rescued growth of this strain at 37℃ when present in high copy, though neither $SPO20^{C224L,S231N}$ nor the *PSPP* chimera could rescue when expressed from centromeric plasmids (Figure 2.6). These results again suggest that the $SPO20^{C224L,S231N}$ mutations increase the strength of Spo20/Sso/Snc interactions, though not to the same degree as complete replacement with the Sec9 helices. All the constructs used in these experiments included an amino terminal 3XHA tag. Western blotting with anti-HA antibodies indicated that all the *SPO20* forms were present in comparable amounts (data not shown). Therefore, the results reflect differences in the ability of the different forms to promote vesicle fusion, not differences in protein stability.
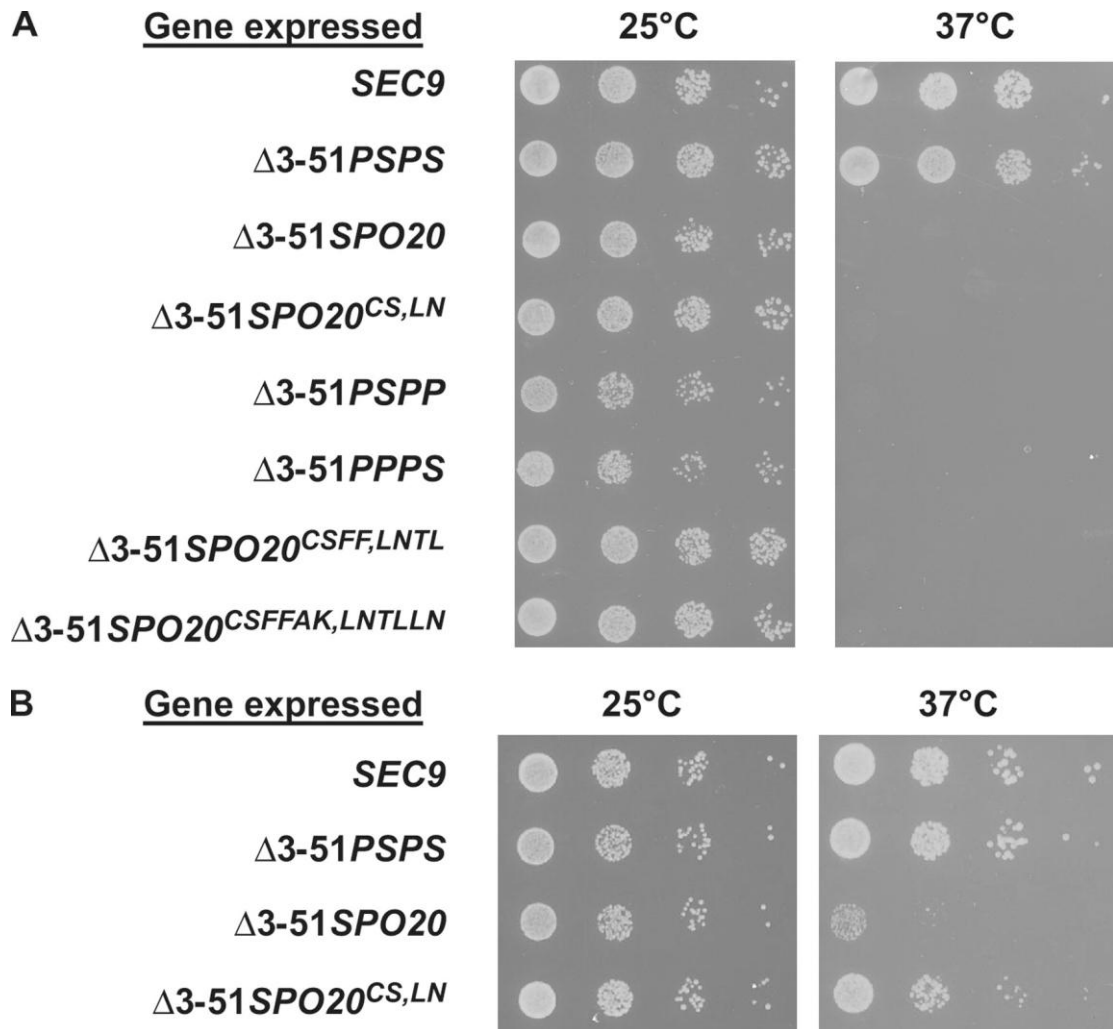
Figure 2.6. $SPO20^{C224L,S231N}$ **can rescue the growth defect of** *sec9-4*. (A) Strain AN211 (*sec9-4*) was transformed with integrating or centromeric (for *PSPP* and *PPPS*) plasmids expressing the indicated genes. Cells were grown to saturation in rich medium and 10-fold serial dilutions were spotted onto selective plates incubated at permissive (25℃) or restrictive (37℃) temperature. $SPO20^{CS,LN}$ is $SPO20^{C224L, S231N}$; $SPO20^{CSFF,LNTL}$ is $SPO20^{C224L,S231N,F357T,F361L}$; $SPO20^{CSFFAK,LNTLLN}$ is $SPO20^{C224L,S231N,F357T,F361L,A378K,K385N}$. (B) A similar growth assay in strain AN211 (*sec9-4*) using high copy plasmids to express the indicated genes.

Mutation of Spo20 increases association with Sso1 and Snc2 *in vivo*

If alteration of the SNARE helices of Spo20 increases its affinity for its partner SNAREs, this should be reflected in increased binding of the protein to Sso1 and Snc2. To address this possibility, HA-tagged Δ3-51Spo20, Spo20 ^{C224L,S231N}, or PSPS were expressed in combination with either wild-type Sso1 ^{Q224R} and Snc2 ^{R52Q} or Sso1 and Snc2 in an *sso1 sso2* strain. Lysates were made from each strain and the Spo20 proteins immunoprecipitated using anti-HA antibodies. Immunoprecipitates were then blotted with anti-HA, anti-Sso1, or anti-Snc2 antibodies to examine association of the three SNARE proteins (Figure 2.7). In the presence of both the wild-type and mutant Sso1 and Snc2 proteins the same pattern was seen; the PSPS chimera precipitated significantly more Sso1 and Snc2 than Spo20 ^{C224L,S231N}, which in turn brought down slightly more Sso1 and Snc2 than the wild-type Spo20. Though these immunoprecipitations do not provide a direct measure of affinity, the increased association of PSPS and Spo20 ^{C224L,S231N} with both forms of Sso1 and Snc2 are consistent with the idea that they bind more avidly than wild-type Spo20. Interestingly, all three forms of Spo20 exhibited greater association with Sso1 ^{Q224R} and Snc2 ^{R52Q} proteins than with the wild-type SNAREs. Because the amount of SNAREs in complex reflects both the rates of assembly and disassembly, we suggest that the general increase in the amount of SNARE complex seen with Sso1 ^{Q224R} /Snc2 ^{R52Q} might reflect a role for the central ionic layer in complex disassembly, as suggested previously (Scales et al., 2001).
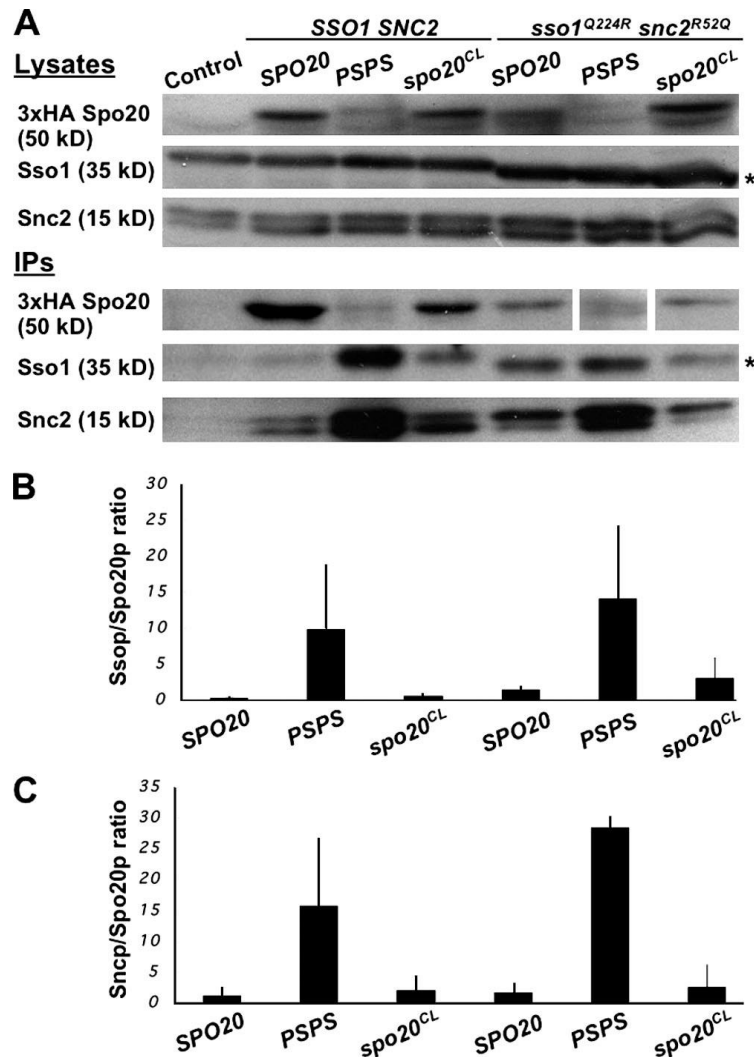
Figure 2.7. Mutation of the Spo20 helices increases binding of Sso1 and Snc2. Strain HI75 (*sso1Δ sso2Δ*) was transformed with high copy plasmids expressing 3xHA tagged forms of Δ3-51Spo20, Δ3-51Spo20$^{C224L, S231N}$, or Δ3-51PSPS chimera. Additionally, these cells carried a CEN plasmid expressing either *SSO1* or *SSO1^{Q224R}* and high copy plasmids expressing *SNC2* or *SNC2^{R52Q}*, respectively. These strains were grown to mid-log in selective medium, lysed, and the HA-tagged Spo20 proteins immunoprecipitated. (A) (top) Western blots of cell lysates from each strain probed with anti-HA, anti-Sso1, or anti-Snc2 antibodies. 3X-HA indicates bands corresponding to the different Spo20 mutants; (bottom) Western blots of anti-HA immunoprecipitates from the same lysates. The band corresponding to Δ3-51PSPS in the Sso1^{Q224R}/Snc^{R52Q} strain is shown from a longer exposure of the same blot. Asterisks indicate Sso1^{Q224R}, which displays slightly increased mobility compared with the wild-type Sso1. (B) Quantitation of the coprecipitation of Sso1 proteins with the different forms of Spo20. Amounts are expressed as the ratio of Sso1 to Spo20 protein based on relative intensity of bands on the anti-HA and anti-Sso1 blots. Values shown are the average of three experiments. Bars indicate one standard deviation. (C) Quantitation of the coprecipitation of Snc2 proteins with the different forms of Spo20. Amounts are expressed as the ratio of Snc2 to Spo20 protein based on relative intensity of bands on the anti-HA and anti-Snc2 blots. Values shown are the average of three experiments. Bars indicate one standard deviation.

49

$SPO20^{C224L,S231N}$ improves function of the SNARE complex *in vitro*

Studies of Sec9- and Spo20-containing SNARE complexes in an *in vitro* liposome fusion system indicate that, in a given lipid composition, Spo20-containing complexes are less fusogenic than Sec9 complexes (Liu et al., 2007). Moreover, this lesser activity correlates with decreased SNARE complex stability (measured as a lower melting temperature) of the Spo20 complexes compared with Sec9 complexes. The behavior of the $SPO20^{C224L,S231N}$ mutant in the genetic tests and immnoprecipitations described above suggests that these mutations might increase the binding energy of the Spo20-containing complexes. To test this directly, the recombinant SNARE domain (amino acids 147-397) of $Spo20^{C224L,S231N}$ was purified from *Escherichia coli* and tested with the Sso1 and Snc2 proteins in a liposome fusion assay. Using liposomes containing 85% POPC (palmitoyl oleoyl phosphatidylcholine) and 15% DOPS (dioleoyl phosphatidylserine), Sso1/Sec9-Snc2 complexes promote liposome fusion at a greater rate than the Sso1/Spo20-Snc2 SNAREs (Figure 2.8A). By contrast, Sso1/$Spo20^{C224L,S231N}$-Snc2 mediates fusion at a rate comparable to the Sec9 complexes. Thus, parallel to the *in vivo* results, $Spo20^{C224L,S231N}$ promotes more efficient fusion than Spo20 *in vitro*.

To determine if the increased fusion activity was reflected in increased binding energy, the stability of the $Spo20^{C224L,S231N}$-containing complexes was examined. We previously reported that Sec9-containing complexes are significantly more stable than Spo20 complexes during equilibrium unfolding reactions with chemical denaturants where the concentrations of Guanidinium-HCL required to disrupt 50% of the ternary SNARE complex was reduced (2.1M for Sec9 vs. 0.9M for Spo20) (Liu et al., 2007). When the $Spo20^{C224L,S231N}$-containing SNAREs were examined, a concentration of 1.1M Guanidinium-HCL disrupted 50% of these ternary complexes, indicating that they were more stable than those with Spo20, though still well below the stability of Sec9 complexes (Figure 2.8B). This moderate improvement in stability of the $Spo20^{C224L,S231N}$-containing complexes consistent with the slight increase in binding of $Spo20^{C224L,S231N}$ to Sso1 and Snc2 seen in the immunoprecipitation experiments (Figure 2.7). Together with the liposome fusion data, this result suggests that modest changes in affinity can have strong effects on the fusogenic properties of the SNAREs. For the neuronal SNARE SNAP-25 it has similarly been found that mutation of

interface residues can result in large differences in function while only modestly altering stability of the SNARE complex (Sorensen et al., 2006).
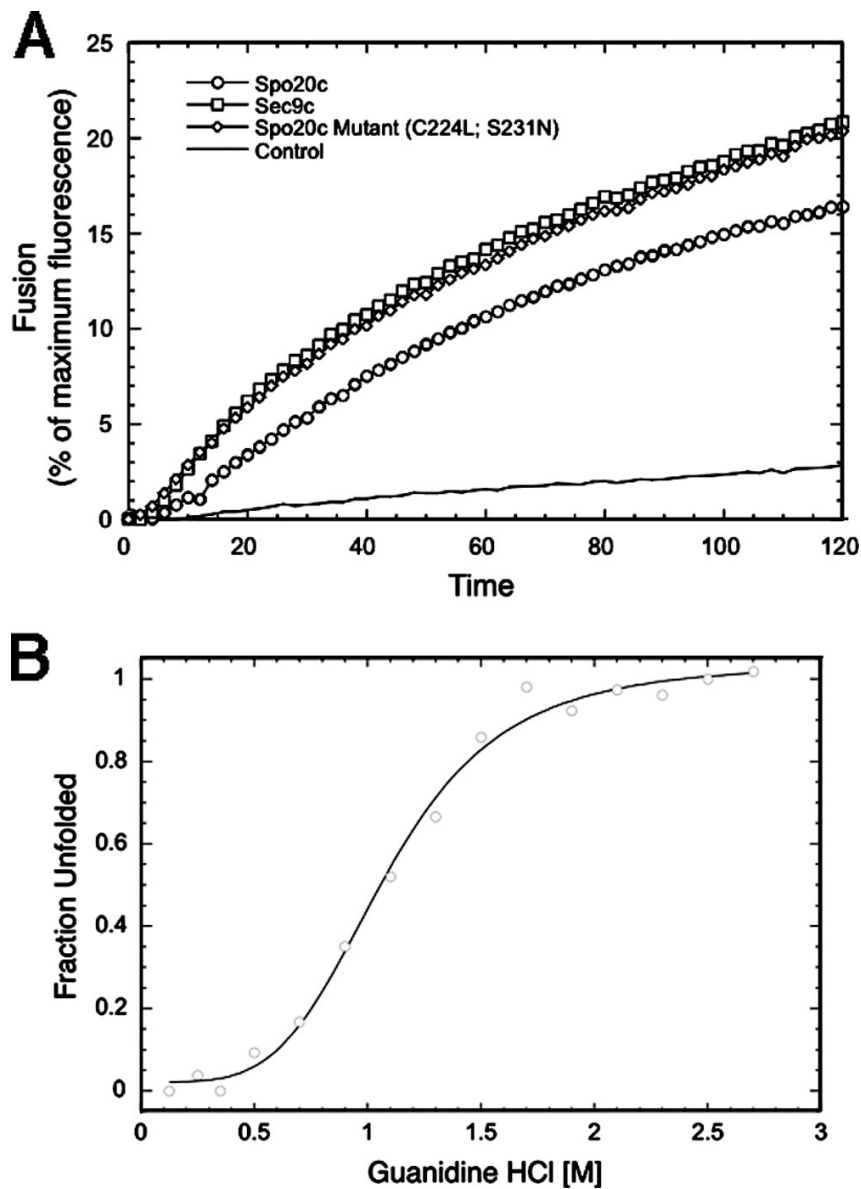
Figure 2.8. Spo20^{C224L,S231N} is a more efficient fusogen in vitro. (A) Liposome fusion assay. Liposomes containing Sso1 and the SNARE domains of Sec9, Spo20, or Spo20^{C224L,S231N} were mixed with Snc2-containing liposomes and fusion assayed by fluorescence. (B) Stability of Sso1/Snc2/ Spo20^{C224L,S231N} complexes in increasing concentrations of Guanidinium-HCl.

2.4 Discussion

The use of compensatory mutations in the central ionic layer of the SNARE domain has proven to be an effective means to demonstrate the participation of different SNARE proteins in the same complex *in vivo* (Graf et al., 2005). Here, we attempted to use this technique to demonstrate a role for the Snc1/2 proteins in fusion at the prospore membrane. A compensatory mutation in *SNC2* could only rescue the sporulation defect of *sso1*^{Q224R} when expressed in concert with forms of Spo20 carrying the Sec9 SNARE helices. Similar results were obtained using a compensatory mutation in *SNC1* (unpublished data). These results demonstrate, first, that the Snc1 and Snc2 proteins indeed function as the R-SNARE subunits of the prospore membrane SNARE complex and, second, that placement of the central layer arginine in different helices is not functionally equivalent. In this instance, swapping the glutamine and arginine between the Sso1 and Snc2 helices creates a SNARE bundle that is more sensitive to the composition of other interface layers in the complex. When Spo20 is the partner, the binding energies at other interfaces are insufficient to overcome the weaker central layer interactions.

During the course of this work, a crystal structure of the SNARE complex containing the Sso1, Snc2, and Sec9 helical domains was published (Strop et al., 2008). When this structure is used to model in the Spo20 cysteine and serine side chains at the +3 and +5 interface layers, the Spo20 residues result in an apparent loss of packing interactions between the side chains (unpublished data), consistent with our results indicating that the Sec9 residues at these positions improve stability of the SNARE complex. Mutational analysis of interface residues in SNAP-25 revealed that interactions in the N-terminal half of the SNARE domain are important for promoting priming or docking of the vesicle, whereas interactions in the C-terminal half of the SNARE helix are critical to drive membrane fusion (Sorensen et al., 2006). In this regard, it is noteworthy that the critical interfaces differentiating the ability of Spo20 and Sec9 to promote fusion at the plasma membrane lie in the C-terminal domain, suggesting that fusion and not docking is the affected step. Again, this is consistent with the results we observe in the liposome fusion assay.

Role of the central ionic layer

Our results raise questions about the function of the central ionic layer present in all SNARE complexes. We found that vegetative secretion was remarkably insensitive to mutation of the glutamine found at this layer in Sso1. Mutation to proline, which would likely disrupt the SNARE helix, or to arginine or lysine, which would introduce positive charges that clash with the arginine on the Snc2 helix, reduced or eliminated function. However, any other amino acid at this position was well tolerated. This is quite surprising in light of the strong conservation of this glutamine in all syntaxin-family SNARE proteins (Bock et al., 2001). Our results with Spo20 suggest one possible explanation for this apparent paradox. The sensitivity of Spo20-containing complexes to alteration of glutamine 224 would provide selective pressure for its maintenance in Sso1. It may be that other SNARE complexes more closely resemble Spo20- than Sec9-containing SNAREs and are sensitive to perturbation of the central ionic layer.

The ability of mutant forms of Sso1 to function well also raises the question of the conservation not just of the glutamine residue, but also of the ionic layer. The ionic layer has been shown to be important for efficient disassembly of the neuronal SNARE complex *in vitro* (Scales et al., 2001), and our immunoprecipitation data are consistent with this idea. However, the lack of growth phenotype of the $SSO1^{Q224}$ mutations suggests that disassembly must still occur with reasonable efficiency in the mutants. Another suggested explanation is that the ionic layer allows the multiple helices to assemble in the appropriate register (Fasshauer et al., 1998). Examination of the interface residues in defined SNARE complexes reveals that interfaces with one or two polar residues are not uncommon. However a charged residue or more than two polar residues is quite rare (A. M. Neiman, unpublished data). In our experiments, three of the four helices still contain polar or charged residues (two glutamines and an arginine). Therefore, this may still provide sufficient information to assemble the complex in register. Though mutation of all the central ionic layers to hydrophobic residues did not disrupt assembly of the neuronal SNARE complex *in vitro* (Scales et al., 2001), it would be interesting to determine if combining additional ionic layer changes with $SSO1^{Q224}$ changes in the yeast SNARE would result in a much more severe fusion defect.

Control of SNARE specificity *in vivo*

The switch from Sec9- to Spo20-dependent fusion during sporulation provides an excellent system to explore the mechanisms by which a change in a single SNARE subunit can alter the target specificity of a particular class of vesicle. Our results here, along with those previously reported (Nakanishi et al., 2004), allow us to answer this question. The specificity of Sec9 and Spo20 for their respective membranes is reinforced in three ways. First, there is transcriptional control. In wild-type cells *SPO20* is transcribed only during sporulation and so cannot function in constitutive secretion (Neiman, 1998). The second mechanism is control of intracellular localization. Efficient targeting of Sec9 to the prospore membrane, either by fusing it to the Spo20 lipid binding motif or to an integral membrane protein (Nakanishi et al., 2006; Neiman et al., 2000), allows Sec9 to restore some degree of sporulation to *spo20* cells. Finally, as we show here, SNARE specificity can be controlled by the strength of the binding interactions between the SNAREs themselves. As the binding energy required for a given fusion event will depend on the potential energy barrier to fusion of the two membranes involved, this form of regulation is linked to the lipid composition of the membranes.

Control of localization and strength of binding are likely to be general mechanisms contributing to SNARE specificity. In liposome binding experiments, the R-SNARE Sec22 is capable of mediating fusion in concert with Sso1 and Sec9 (McNew et al., 2000). This result has been suggested to indicate the existence of a direct ER-to-plasma membrane secretion step in yeast, as found in mammalian cells (Becker et al., 2005). Alternatively, it may be that, though Sec22 is capable of forming productive complexes with Sso1 and Sec9, it does not do so because its localization as a v-SNARE is limited to the cis Golgi- and ER- directed vesicles that do not dock with the plasma membrane *in vivo*. Consistent with this idea, overexpression of a Sec22[R157Q] mutant cannot rescue sporulation of the Sso1[Q224R] mutant even in the presence of the PSPS chimera (unpublished data), suggesting that Sec22 cannot participate in prospore membrane fusion events *in vivo*.

A recent study revealed that a suboptimal interface at the +7 layer in the neuronal *syx-1A* gene is important for allowing calcium-mediated regulation of secretion (Lagow et al., 2007). Mutation of the threonine residue at this position in

syx-1A to the corresponding isoleucine residue in syx-2 led to constitutive fusion. Thus, as with Spo20 and Sec9, in the neuronal SNARE, tuning of the strength of binding interactions is important for allowing proper regulation of vesicle transport.

Finally, Spo20 and Sec9 provide a useful model to trace the evolution of novel SNARE complexes. During the evolution of *Saccharomyces*, a whole genome duplication occurred that ultimately gave rise to many related gene pairs in the *S. cerevisiae* genome (Wolfe and Shields, 1997). Sec9 and Spo20 arose from this duplication event. In yeasts that diverged from the *S. cerevisiae* lineage prior to the duplication, such as *Schizosaccharomyces pombe*, a single Sec9/Spo20 related gene participates in fusion at both the plasma membrane and the prospore membrane (Nakamura et al., 2005). Thus, in the *S. cerevisiae* lineage, the duplication event allowed the two paralogues to become specialized for action at distinct compartments where the ancestral protein functioned at both membranes. Similar patterns are likely at work in the expansions of particular SNARE families seen in plant and mammalian genomes (Bock et al., 2001; Sanderfoot et al., 2000).

Chapter 3

A Guanine Nucleotide Exchange Factor Is a Component of the Meiotic SPB in *Schizosaccharomyces pombe*

Reformatting of article published in (Yang and Neiman, 2010)

Spore morphogenesis in yeast is driven by the formation of membrane compartments that initiate growth at the spindle poles during meiosis II and grow to encapsulate daughter nuclei. Vesicle docking complexes, called Meiosis II outer plaques (MOPs), form on each Meiosis II spindle pole body (SPB) and serve as sites of membrane nucleation. How the MOP stimulates membrane assembly is not known. Here, we report that SpSpo13, a component of the MOP in *Schizosaccharomyces pombe*, shares homology with the guanine nucleotide exchange factor (GEF) domain of the *Saccharomyces cerevisiae* Sec2 protein. ScSec2 acts as a GEF for the small Rab GTPase ScSec4, which regulates vesicle trafficking from the late-Golgi to the plasma membrane. A chimeric protein in which the ScSec2-GEF domain is replaced with SpSpo13 is capable of supporting the growth of a *sec2Δ* mutant. SpSpo13 binds preferentially to the nucleotide-free form of ScSec4 and facilitates nucleotide exchange *in vitro*. *In vivo*, a *Spspo13* mutant defective in GEF activity fails to support membrane assembly. *In vitro* specificity experiments suggest that SpYpt2 is the physiological substrate of SpSpo13. These results demonstrate that stimulation of Rab-GTPase activity is a property of the *S. pombe* MOP essential for the initiation of membrane formation.

3.1 Introduction

Formation of ascospores by yeast cells is an unusual cell division event in which daughter cells are formed by *de novo* synthesis of new plasma membranes around daughter nuclei, providing an excellent model system by which to study the generation of novel intracellular membrane compartments (Neiman, 1998; Neiman, 2005). In response to nitrogen starvation, the fission yeast *Schizosaccharomyces*

pombe exits the mitotic cell cycle, mates to form diploid cells, and enters meiosis. During Meiosis II, four newly formed membrane compartments, termed forespore membranes (FSMs), appear in the cytosol (Shimoda, 2004). As meiosis is completed each of the four haploid nuclei produced by meiosis is engulfed within a forespore membrane. Capture of a nucleus and associated cytoplasm by an FSM gives rise to a nascent spore, with the forespore membrane now serving as the plasma membrane of the spore.

Real-time videomicroscopy of FSM formation in *S. pombe*, and of the analogous prospore membrane in *Saccharomyces cerevisiae*, has revealed that membrane formation can be dissected into three distinct stages: 1) membrane initiation at the spindle pole pody (SPB), 2) expansion to engulf a daughter nucleus, and 3) closure to complete cytokinesis (Diamond et al., 2009; Nakamura et al., 2008). Notably, assembly of FSMs always starts at SPBs. In yeast, SPBs, which are functional analogues of centrosomes in higher cells, have distinct nuclear and cytoplasmic faces, called the inner and outer plaques, respectively (Jaspersen and Winey, 2004). In dividing cells, the inner and outer plaques serve as microtubule-organizing centers. However, at the beginning of Meiosis II, there is a protein exchange on the outer plaques, which are now called Meiosis II outer plaques (MOPs) (Neiman, 2005; Shimoda, 2004). In *S. pombe*, MOPs appear as multilayered disk-shaped structures in the electron microscope (Hirata and Shimoda, 1994). The assembly of the MOP changes the function of the outer plaque from microtubule nucleation to membrane nucleation (Neiman, 2005; Shimoda, 2004). Nascent FSMs are assembled on the outermost surface of the MOPs and the membranes remain in contact with the MOPs until very late in FSM development (Hirata and Shimoda, 1994; Nakamura et al., 2008).

In *S. cerevisiae*, genetic and cell biological studies have demonstrated that the prospore membrane compartment is derived from the coalescence of post-Golgi secretory vesicles (Neiman, 1998; Neiman, 2005). This is likely true for the *S. pombe* FSM as well, as mutations in genes encoding SNARE proteins that mediate fusion at the plasma membrane in vegetative cells disrupt FSM assembly (Nakamura-Kubo et al., 2003; Nakamura et al., 2005; Nakase et al., 2001). In both *S. pombe* and *S. cerevisiae*, deletion of the genes for individual MOP components leads to failure of the structure to assemble and a complete block to membrane formation,

indicating that the MOP is essential for vesicle coalescence (Bajgier et al., 2001; Knop and Strasser, 2000; Nakase et al., 2008; Nickas et al., 2003). In mutants that fail to properly form MOPs, the precursor vesicles are dispersed from the spindle poles. This differentiates MOP mutants from mutants in proteins such as SNAREs that are involved directly in membrane fusion. In SNARE mutants, precursor vesicles accumulate on and around the MOP surface (Nakanishi et al., 2006). These results, and the direct association of precursor vesicles with the MOP, suggest that the MOP functions as a vesicle tethering complex and promotes SNARE-mediated membrane fusion. How the MOP stimulates fusion of the FSM precursor vesicles is not understood.

Docking or tethering complexes function upstream of SNARE-mediated fusion in a variety of other vesicle fusion events, and often function in association with Rab GTPases (Pfeffer, 1999). For example, association of secretory vesicles with the plasma membrane is mediated by a tethering complex termed the exocyst and the exocyst is an effector of the Rab GTPase ScSec4 (Guo et al., 1999; TerBush et al., 1996). Rab GTPases are important regulators of vesicle traffic (Stenmark, 2009). A Rab GTPase cycles between its guanosine triphosphate (GTP)-bound and guanosine diphosphate (GDP)-bound forms (Segev, 2001; Stenmark, 2009). A Rab protein in its GTP-bound form is switched on to bind to effectors. The exchange of GDP with GTP in a Rab GTPase is facilitated by a guanine nucleotide exchange factor (GEF), and the GEF activity directs where a Rab protein executes its function (Cai et al., 2008; Jones et al., 2000; Ortiz et al., 2002).

In *S. cerevisiae* Sec4, the protein is activated by the GEF ScSec2. ScSec2 itself is localized to secretory vesicles, thus the GEF activity of ScSec2 serves to activate ScSec4 on the surface of the vesicles, promoting ScSec4-mediated interaction of the vesicle with the exocyst complex (Guo et al., 1999; Nair et al., 1990; Walch-Solimena et al., 1997). The exchange activity of ScSec2 resides in an NH_2-terminal coiled-coil domain (amino acids 1-160), to which ScSec4 binds (Dong et al., 2007; Walch-Solimena et al., 1997). In addition to the GEF domain, the remaining 599 amino acids of the ScSec2 protein are required for its proper association with secretory vesicles (Elkind et al., 2000; Ortiz et al., 2002). Mutants impaired in ScSec2 localization display growth defects due to a failure of polarized delivery of ScSec4-containing vesicles (Walch-Solimena et al., 1997); however, overexpression

of only the GEF domain is sufficient to complement the growth defect of a *sec2* deletion (Dong et al., 2007; Nair et al., 1990).

In *S. pombe*, the MOP is composed of three sporulation-specific proteins: SpSpo15, SpSpo2, and SpSpo13 (Nakase et al., 2008). Localization of SpSpo13 is dependent on the other two MOP components, and SpSpo13 is thought to be located at the membrane-proximal surface of the MOP (Nakase et al., 2008). Here, we report that SpSpo13 has homology to the ScSec2 GEF domain. SpSpo13 can replace the GEF domain of ScSec2 *in vivo* and the SpSpo13 protein can bind to ScSec4 and stimulate GDP release *in vitro*. A point mutation that impairs SpSpo13 GEF activity leads to a failure of FSM assembly. GDP release assays using different *S. pombe* Ypt proteins suggest that SpYpt2 is the physiological substrate of SpSpo13. These results provide the first description of a biochemical activity associated with the MOP and provide insight into how this docking complex functions to regulate the initiation of FSM formation.

3.2 Materials and Methods

Yeast strain construction

The strains used in this study are listed in Table 3. HJ79 was constructed as follows. First, a *sec2Δ* heterozygous diploid, HJ75, was constructed by deleting *SEC2* in AN120 by polymerase chain reaction (PCR) (Longtine et al., 1998) using pFA6a-His3MX6 as a template and HJO105 and HJO106 as primers. Second, pRS416-*TEFpr-ScSEC2* was transformed into HJ75, and the resulting transformants were sporulated and dissected. An Ura$^+$ His$^+$ segregant was selected and named HJ79.

ANP3 is an *S. pombe* segregant from a cross between GP46 (a gift from Gerry Smith, Fred Hutchinson Cancer Research Center, Seattle, WA) and B82 (a gift from Chikashi Shimoda, Osaka City University, Osaka, Japan). HJP1 was obtained as a segregant from a cross of ANP3 and GP1327 (a gift from Gerry Smith).

Plasmids

The plasmids used in this study are listed in Table 4. To make plasmids pRS416TEF-*ScSEC2* and pRS414TEF-*ScSEC2*, full-length *ScSEC2* was amplified by PCR using *S. cerevisiae* genomic DNA from strain AN120 as a template and HJO97 and HJO98 as primers. The PCR products were purified, digested with EcoRI and XhoI, and cloned into similarly digested pRS416TEF or pRS414TEF (Mumberg et al., 1995). *ScSEC2$^{1-160}$* and *ScSEC2$^{161-759}$* were similarly amplified by PCR from strain AN120 using oligos HJO97 and HJO99, and HJO104 and HJO98, respectively. The EcoRI- and XhoI-digested PCR products were cloned into similarly digested pRS414TEF to get pRS414TEF-*ScSEC2$^{1-160}$* and pRS414TEF-*ScSEC2$^{161-759}$*.

The *Spspo13$^+$* coding region was amplified by PCR using *S. pombe* genomic DNA as a template and HJO116 and HJO134 as oligos. Because the genomic DNA of *Spspo13$^+$* contains an intron after the fifth codon, HJO116 was designed to add these codons to the 5′ end second exon and thereby remove the intron.

The *Spspo13+* coding region was then digested with EcoRI and XhoI, and cloned into similarly digested pRS414TEF to get pRS414TEF-*Spspo13+*.

To construct the chimeric plasmid, pRS414TEF-*Spspo13+-ScSEC2^{161-759}*, the coding region of *Spspo13+*, without the stop codon, was PCR amplified from *S. pombe* genomic DNA using HJO116 and HJO117 as oligos. A BamHI-EcoRI–digested PCR fragment was then cloned into similarly digested pRS414TEF-*ScSEC2^{161-759}*.

Plasmid pJRU-MCS2 (Moreno et al., 2000) was used as the vector backbone for plasmids used in *S. pombe*. The *Spspo13+* promoter (−500 upstream of first ATG) was amplified from *S. pombe* genomic DNA by oligos HJO178 and HJO179. The PCR products was purified, digested with XhoI and PstI, and cloned into similarly digested pJRU-MCS2 to create pJRU-MCS2-P*_{SpSpo13}*. To make pJRU-MCS2-P*_{SpSpo13}-Spspo13+*, the *Spspo13+* coding region was PCR amplified using *S. pombe* genomic DNA as a template and HJO176 and HJO145 as oligos. A KpnI-SacI–digested PCR fragment was cloned into similarly digested pJRU-MCS2-P*_{SpSpo13}*.

The plasmid pJRU-MCS2-P*_{SpSpo13}-Spspo13+*-mRFP was constructed in three steps. First, a PCR fragment containing the monomeric red fluorescent protein (mRFP) gene was amplified using pTi mRFP as a template (Gao et al., 2005) and YSO33 and HNO944 as primers and cloned as a HindIII-XhoI fragment into pRS424*TEF* (Mumberg et al., 1995). Next, the mRFP fragment from this construct was isolated as an EcoRI-XhoI fragment and used to replace the *ScSEC2* coding region of pRS414TEF-*Spspo13+-ScSEC2^{161-759}*, creating pRS414TEF-*Spspo13+-mRFP*. Finally,*Spspo13-mRFP* was PCR amplified from pRS414TEF-*Spspo13+*-mRFP by using HJO176 and HJO188 as oligos. This PCR product was KpnI-SacI digested and cloned into pJRU-MCS2-P*_{SpSpo13}*.

pJRU-MCS2-*SpSpo13pr-Spspo13-F77A* was created by site-directed mutagenesis of the plasmid pJRU-MCS2-*SpSpo13pr-Spspo13+* using oligos HJO182 and HJO183 (QuikChange kit; Stratagene, La Jolla, CA). The same oligos were used for site-directed mutagenesis of pJRU-MCS2-*SpSpo13pr-Spspo13+*-mRFP to make pJRU-MCS2-*SpSpo13pr- Spspo13^{F77A}* -mRFP. The *Spspo13* gene was fully sequenced after mutagenesis to ensure that no other mutations were introduced during the procedure (sequencing performed at the Stony Brook DNA Sequencing Facility).

To make plasmids expressing glutathione transferase (GST)-tagged $ScSEC2^{1-160}$, an EcoRI-XhoI fragment of pRS414-*TEFpr-ScSEC2$^{1-160}$* containing Sc*SEC2$^{1-160}$* was cloned into pGEX5X-1 (GE Healthcare, Little Chalfont, Buckinghamshire, United Kingdom). To make plasmids expressing GST-tagged *Spspo13^{+}*, the *Spspo13^{+}* gene was first PCR amplified using pRS414-*TEFpr-Spspo13^{+}* as a template and HJO137 and HJO134 as oligos. The PCR product was then cloned into pGEX3X (GE Healthcare) as a BamHI-EcoRI fragment. The plasmid expressing GST-tagged *Spspo13^{F77A}* was constructed by site-directed mutagenesis of the plasmid pGEX3X-*Spspo13^{+}* using oligos HJO182 and HJO183. To construct plasmids expressing 6XHis-tagged *ScSEC4* or *ScYPT1*, *ScSEC4* and *ScYPT1* were PCR amplified using *S. cerevisiae* genomic DNA as a template and using oligos HJO150 and HJO151, HJO152 and HJO153, respectively. The PCR products were purified, digested with XhoI and BamHI, and cloned into similarly digested plasmid pET15b (Novagen, Madison, WI).

S. pombe sporulation assays

Freshly transformed *S. pombe* cells were grown on selective medium at 32°C for 2 d. The cells were then patched onto an SPA plate (1%, wt/vol glucose, 7.3 mM KH_2PO_4, 1 ml of 1000× vitamin stock, and 3%, wt/vol Difco Bacto Agar [Difco, Detroit, MI]) to induce mating and sporulation. Sporulation was assayed by observation in the light microscope after 15–18 h incubation on the SPA plate at room temperature.

Fluorescence microscopy

Freshly transformed *S. pombe* cells were cultured in 3 ml of EMM2 (3 g/l potassium hydrogen phthalate, 2.2 g/l sodium phosphate dibasic, 5 g/l ammonium chloride, 20 g/l dextrose, 2.1 g/l minimal salts, 0.2 g/l vitamins, and 3 mg/l trace elements), with selective supplements (75 µg/ml adenine and 225 µg/ml histidine) for 24 h. The cells were precipitated, washed twice with 1 ml EMM-N sporulation

medium (3 g/l potassium hydrogen phthalate, 2.2 g/l sodium phosphate dibasic, 20 g/l dextrose, 2.1 g/l minimals, 0.2 g/l vitamins, and 3 mg/l trace elements). The cells were induced to enter meiosis by incubating in 3 ml of EMM-N at room temperature. After 9-h incubation in the EMM-N, aliquots of cells were examined in an Axioplan2 microscope (Carl Zeiss, Thornwood, NY). Fluorescence images were obtained by using Axiovision release 4.7.

Recombinant protein preparation

All recombinant proteins were expressed in *Escherichia coli* (*BL21*) and induced at room temperature by adding 0.5 mM isopropyl β-d-thiogalactoside for 4 h. The 6XHis-tagged Rab proteins were purified using nickel-nitrilotriacetic acid Superflow columns under native conditions (QIAGEN, Valencia, CA). To stabilize nucleotide-binding protein, 0.1 mM GDP was included in the lysis buffer (50 mM NaH_2PO_4, 300 mM NaCl, 10 mM imidazole, pH 8.0), wash buffer (50 mM NaH_2PO_4, 300 mM NaCl, 20 mM imidazole, pH 8.0) and elution buffer (50 mM NaH_2PO_4, 300 mM NaCl, and 250 mM imidazole, pH 8.0). After elution, samples were concentrated by centrifugation in a Microcon YM-10 centrifugal filter unit (Millipore, Billerica, MA) and kept in storage buffer (20 mM Tris, pH 8.0, 100 mM KCl, 1 mM dithiothreitol [DTT], 0.1 mM GDP, 100 μM phenylmethylsulfonyl fluoride [PMSF], and 20% glycerol) at −20°C.

GST fusion proteins were purified as described previously (Nakanishi et al., 2004). After elution and concentration, samples were kept in storage buffer (20 mM Tris, pH 8.0, 100 μM PMSF, and 20% glycerol) at −20°C.

GST pull-down assay

GST pull-down assays were modified from Ortiz et al., (2002). For binding experiments with the nucleotide-bound form of Rab proteins, 0.8 μg of 6XHis-ScSec4 or 6XHis-ScYpt1 was preloaded with GDP or guanosine 5′-(β,γ-imido)triphosphate (GppNHp) in $MgCl_2$binding buffer (1× phosphate-buffered saline [PBS], 5 mM $MgCl_2$, 1 mg/ml bovine serum albumin [BSA], and 1 mM DTT) for 30 min at room

temperature. The GST fusion proteins immobilized on glutathione-Sepharose beads (30 μl of beads) were incubated with the preloaded Rab proteins (0.3 μg) in the MgCl$_2$ binding buffer for 60 min at room temperature. After the binding reactions, the glutathione-Sepharose beads were washed five times with PBS buffer containing MgCl$_2$ and resuspended in 2× SDS sample buffer (60 mM Tris-HCl, pH 6.8, 10% glycerol, 2% SDS, 0.05 mg/ml bromphenol blue, and 5% β-mercaptoethanol). Pull-down products were separated by SDS-polyacrylamide gel electrophoresis and analyzed by Western blot. 6XHis-ScSec4 and 6XHis-ScYpt1 were first detected by rabbit anti-histidine antibody (Santa Cruz Biotechnology, Santa Cruz, CA), and then goat anti-rabbit peroxidase-conjugated secondary antibody was used (GE Healthcare). GST fusion proteins were detected by goat horseradish peroxidase-conjugated anti-GST antibody (Abcam, Cambridge, MA).

For binding experiments with the nucleotide-free form of the Rab proteins, 6XHis-ScSec4 and 6XHis-ScYpt1 were not preloaded with nucleotides but were incubated with GST fusion proteins immobilized on beads in EDTA binding buffer (1× PBS, 5 mM EDTA, 1 mg/ml BSA, and 1 mM DTT). The resins were washed with PBS buffer containing EDTA.

Nucleotide exchange assays

Purified 6XHis-tagged Rab proteins were incubated in loading buffer (50 mM Tris, pH 8.0, 100 mM KCl, 1 mM EDTA, and 1 mM DTT) containing a twofold molar excess of GDP (Jena Bioscience, Jena, Germany) or *N*-methylanthraniloyl (mant)-GDP (Invitrogen, Carlsbad, CA) for 30 min at room temperature. To terminate the loading reaction, MgCl$_2$was added to a final concentration of 20 mM, and free GDP or free mant-GDP was removed by centrifugation in a Microcon YM-10 filter unit (Millipore). 6XHis-Rab bound to GDP or mant-GDP was then concentrated in buffers containing 50 mM Tris, pH 8.0, 100 mM KCl, and 6 mM MgCl$_2$.
For the GTP loading assay, 100 nM mant-GppNHp (Invitrogen) was added to reaction buffer (10% glycerol, 50 μg/ml BSA, 50 mM Tris, pH 8.0, 100 mM KCl, 1 mM DTT, and 6 mM MgCl$_2$) and allowed to equilibrate for 300 s in a thermostated cuvette (15℃). To initiate the reaction, 6XHis-ScSec4 preloaded with GDP was added to the

mixture to a final concentration of 400 nM. To test GEF activity, purified GST, GST-ScSec2, or GST-SpSpo13 was premixed with 6XHis-ScSec4-GDP and then added to the mixture at the concentrations indicated. Fluorescence emission was monitored every 5 s for a total of 1500 s by using a fluorimeter (FP-6200; Jasco, Tokyo, Japan) with the following settings: $\lambda_{ex} = 290$ nm, $\lambda_{em} = 460$ nm, and slits = 5/5.

For GDP release assay, 6XHis-ScSec4 was loaded with mant-GDP as describe above and added to the reaction buffer containing an excess of GppNHp (final concentration, 20 μM) (Jena Bioscience). The dissociation of mant-GDP was first monitored without a GEF protein by using the fluorimeter with the same settings as described in GTP loading studies. At the indicated time point, purified GST-ScSec2, GST-SpSpo13, or GST-SpSpo13^{F77A}, or EDTA, was added to the mixture at desired concentrations, and the fluorescence emission was then monitored for another 1300 s.

Table 3 Strains used in chapter 3

Name	Genotype	Source
S.cerevisiae		
AN120	*MATa/MATα ARG4/arg4-NspI his3SK/his3SK hoΔ::LYS2/hoΔ::LYS2 leu2/leu2 lys2/lys2 RME1/rme1Δ::LEU2 trp1::hisG/trp1::hisG ura3/ura3*	(Neiman *et al.*, 2000)
HJ75	*MATa/MATα ARG4/arg4-NspI his3SK/his3SK ho::LYS2/ho::LYS2 leu2/leu2 lys2/lys2 RME1/rme1::LEU2 trp1::hisG/trp1::hisG ura3/ura3 sec2Δhis5+/SEC2*	This study
HJ79	*MATa arg4-NspI his3SK ho::LYS2 leu2 lys2 rme1::LEU2 trp1::hisG ura3 sec2Δhis5+*	This study
HJ75-4	*MATα arg4-NspI his3SK ho::LYS2 leu2 lys2 RME1 trp1::hisG ura3 sec2Δhis5+pRS416-TEFpr-ScSEC2*	This study
S. pombe		
GP46	*h+ ade6-M375 ura4-294*	(Virgin et al., 1995)
B82	*h90 spo13-B82 ade6-M210*	(Bresch et al., 1968)
ANP3	*h90 spo13-B82 ura4-294*	This study
GP1327	*h90 ade6-52 ura4-294 leu1-32*	(Lin and Smith, 1995)
HJP1	*h90 spo13-B82 ura4-294 leu1-32*	This study
FY12476	*h90 spo13::ura4+ ura4 leu1 sid4GFP::kanR*	(http://yeast.lab.nig.ac.jp/nig/)

Table 4 Plasmids used in chapter 3

Plasmid	Selected Features	Source
pRS416TEF	*CEN, ARSH4, URA3*	(Mumberg et al., 1995)
pRS414TEF	*CEN, ARSH4, TRP1*	(Mumberg et al., 1995)
pRS416TEF-*ScSEC2*	*CEN, ARSH4, URA3*	This study
pRS414TEF-*ScSEC2*	*CEN, ARSH4, URA3*	This study
pRS414TEF-*ScSEC2*	*CEN, ARSH4, TRP1*	This study
pRS414TEF-*ScSEC2*$^{1-160}$	*CEN, ARSH4, TRP1*	This study
pRS414TEF-*ScSEC2*$^{161-759}$	*CEN, ARSH4, TRP1*	This study
pRS414TEF-*Spspo13*$^+$	*CEN, ARSH4, TRP1*	This study
pRS414TEF-*Spspo13*$^+$ -*ScSEC2*$^{161-759}$	*CEN, ARSH4, TRP1*	This study
pRS425TEF-*Spypt2*$^+$	2 micron, *LEU2*	This study
pGP564-*ScSEC4*	2 micron, *LEU2*	(Jones et al., 2008)
pGP564-*ScYPT1*	2 micron, *LEU2*	(Jones et al., 2008)
pGP564-*ScYPT31*	2 micron, *LEU2*	(Jones et al., 2008)
pJRU-MCS2	Exp, *ars1, ura4*$^+$	(Moreno et al., 2000)
pJRU-MCS2-P$_{Spspo13}$-*Spspo13*$^+$	Exp, *ars1, ura4*$^+$	This study
pJRU-MCS2-P$_{Spspo13}$-*Spspo13*^{F77A}	Exp, *ars1, ura4*$^+$	This study
pJRU-MCS2-P$_{Spspo13}$-*Spspo13*$^+$ -mRFP1	Exp, *ars1, ura4*$^+$	This study
pJRU-MCS2-P$_{Spspo13}$-*Spspo13*^{F77A} -mRFP1	Exp, *ars1, ura4*$^+$	This study

Table 4 Plasmids used in chapter 3 (Continued)

Plasmid	Selected Features	Source
FY532 (pREP41-GFP-*psy1*[+])	Exp, *ars1*, *LEU2*	(Nakamura et al., 2001)
pET15b	*His-tag*, *Amp*[R]	Novagen
pET15b-*ScSEC4*	*His-tag*, *Amp*[R]	This study
pET15b-*ScYPT1*	*His-tag*, *Amp*[R]	This study
pET15b-*Spypt1*^{+}	*His-tag*, *Amp*[R]	This study
pET15b-*Spypt2*^{+}	*His-tag*, *Amp*[R]	This study
pET15b-*Spypt3*^{+}	*His-tag*, *Amp*[R]	This study
pGEX5X-1	*GST*, *Amp*[R]	Amersham Biosciences
pGEX5X-1-*ScSEC2*[1-160]	*GST*, *Amp*[R]	This study
pGEX3X-*Spspo13*^{+}	*GST*, *Amp*[R]	This study
pGEX3X-*Spspo13*[F79A]	*GST*, *Amp*[R]	This study

3.3 Results

The MOP component SpSpo13 has homology to ScSec2 GEF domain

Spspo13⁺ encodes a protein of 138 amino acids predicted to form a coiled-coil structure (Nakase et al., 2008). Iterative blast searches with the full-length SpSpo13 revealed a strong patch of conservation between SpSpo13 and the ScSec2 protein of budding yeast. Full-length SpSpo13 shares 24% identity and 43% similarity with the N-terminal 160 amino acids that contain the GEF activity of ScSec2 (Figure 3.1). The crystal structure of this domain of ScSec2 has been solved in complex with ScSec4 (Dong et al., 2007; Sato et al., 2007). The residues of ScSec2 that contact ScSec4 are highly conserved in SpSpo13 (Figure 3.1). This sequence homology suggests that SpSpo13 might have GEF activity similar to ScSec2.

SpSpo13⁺ can substitute for the *ScSEC2* GEF domain

If SpSpo13 has GEF activity, it might be able to substitute for ScSec2 in activating ScSec4 in *S. cerevisiae*. Sc*SEC2* is an essential gene in budding yeast (Nair et al., 1990). The N-terminal GEF domain is sufficient to support the essential function of ScSec2, and the remaining C-terminal region seems to be required for proper polarized localization of ScSec2 (Elkind et al., 2000; Ortiz et al., 2002). To examine whether*SpSpo13⁺* can provide GEF function, *Spspo13⁺*/ *ScSEC2* chimeras were constructed and tested for ability to rescue the growth of a *sec2Δ* strain.

Using a plasmid shuffle approach, we showed that the *ScSEC2* GEF domain alone (*ScSEC2^{1-160}*) was sufficient to restore the growth of the *sec2Δ* mutant at a level comparable with expression of full-length *ScSEC2* gene, in agreement with an earlier report (Ortiz et al., 2002). In contrast, the *ScSEC2* C-terminal region (*ScSEC2^{161-759}*) failed to rescue the growth defect of the *sec2Δ* mutant (Figure 3.2).

Although *Spspo13⁺* alone did not suppress the *sec2Δ* growth defect, the *Spspo13⁺-ScSEC2^{161-759}* fusion did restore growth (Figure 2), indicating that this fusion gene encodes a functional protein that can substitute for ScSec2. This result

indicates that SpSpo13 has GEF activity capable of activating ScSec4 in *S. cerevisiae*.

A

ScSec2	31	LEEQLNKSLKTIASQKAAIENYNQLKEDYN
SpSpo13	1	--MMSNSQISKLFSSISNKENSNENALKES

ScSec2	61	TLKRELSDRDDEVKRLREDIAKENELRTKA
SpSpo13	29	TNKQLNNANTLAITHLKEQLSREVQRREEL

ScSec2	91	EEEADKLNKEVEDLTASLFDEANNMVADAR
SpSpo13	59	EGLLEQSQKEMEDLSVSLFTEANEMVAKAR

ScSec2	121	KEKYAIEILNKRLTEQLREKDTLLDTLTLQ
SpSpo13	89	QDTEVLKRELDYLRAKEKGRIGKLRSIQTA

ScSec2	151	LKN--LKKVMHSLDNESTV-
SpSpo13	119	VRTSIEARKLLSYSNESNYH

B
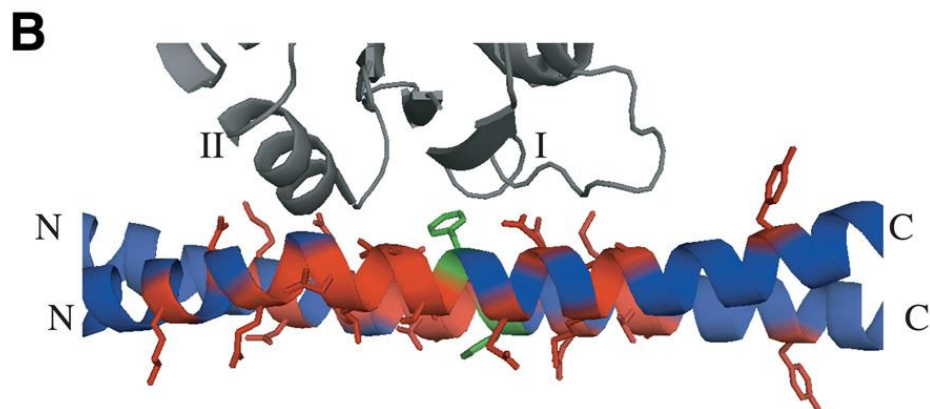
Figure 3.1. SpSpo13 is homologous to the ScSec2 GEF domain. (A) Sequence alignment of ScSec2 GEF domain with SpSpo13. Identical residues are highlighted in yellow, and conservative changes are shaded gray. ScSec2 residues that are found in a close contact with ScSec4 in the cocrystal structure are in red (Dong *et al.*, 2007). SpSpo13 residues that are conserved in the ScSec4 binding surface are in green. Phe77 of SpSpo13 that was mutated to alanine is indicated in green. (B) View of the cocrystal structure of ScSec2 GEF domain and ScSec4 (PDB 2OCY; Dong *et al.*, 2007). ScSec4 is in gray, above and the ScSec2 dimer is below. The switch I and II regions of ScSec4 are labeled. The side chains of the ScSec2 residues highlighted in A are shown in red, except for Phe109 in green.
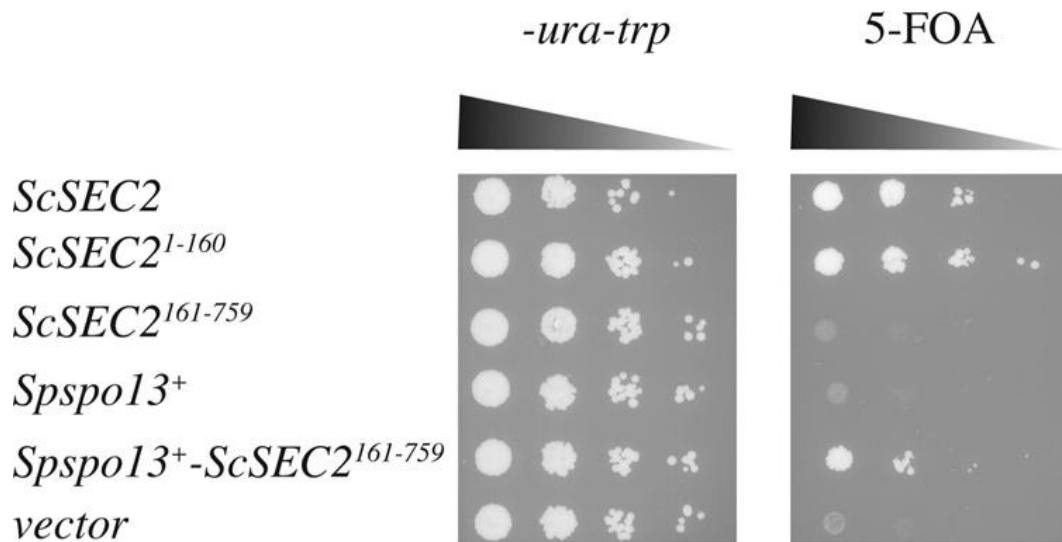
Figure 3.2. A *Spspo13⁺-ScSec2* chimera rescues the growth defect of a *sec2Δ*. Strain HJ79 (*sec2Δ*; *pCEN-URA3-ScSEC2*) was transformed with *CEN-TRP1*-plasmids carrying the indicated genes. Numbers indicate amino acids. The transformed strains were grown in nonselective medium overnight, and 10-fold serial dilutions of the overnight culture were spotted onto a synthetic plate lacking tryptophan and uracil or onto a plate containing 5-fluoroorotic acid (5-FOA). The plates were photographed after 2-d incubation at 30℃.

SpSpo13 binds preferentially to the nucleotide-free form of ScSec4

To test directly whether SpSpo13 can bind to ScSec4, glutathione transferase-tagged-SpSpo13 (GST-SpSpo13) was prepared from *E. coli*. The predicted molecular mass of the GST-SpSpo13 fusion protein is ~44 kDa, and a band that ran a little above the 37-kDa marker was confirmed as GST-SpSpo13 by Western blot analysis using anti-GST antibodies (Figure 3.3A). GEFs preferentially bind to the nucleotide-free form of their target GTPase (Bos et al., 2007). GST-SpSpo13 attached to glutathione-Sepharose beads was therefore incubated with three different forms of recombinant hexahistidine-tagged ScSec4 (6XHis-ScSec4): the GDP-bound form, GppNHp (a nonhydrolysable analogue of GTP)-bound form, or the nucleotide-free form. Binding of ScSec2 GEF domain GST-ScSec2$^{1-160}$ was performed as a positive control in the binding assay.

GST-SpSpo13 preferentially bound to the nucleotide-free form of ScSec4 compared with the GDP- or GppNHp-bound form, whereas GST-ScSec2$^{1-160}$ displayed binding to both the GDP-bound and nucleotide-free forms. The interaction of GST-SpSpo13 and ScSec4 was specific because GST alone did not bind to any conformations of ScSec4, and GST-SpSpo13 did not bind to another Rab GTPase, ScYpt1 (Figure 3.3B). These binding characteristics of GST-SpSpo13 support the idea that SpSpo13 is a guanine nucleotide exchange protein.
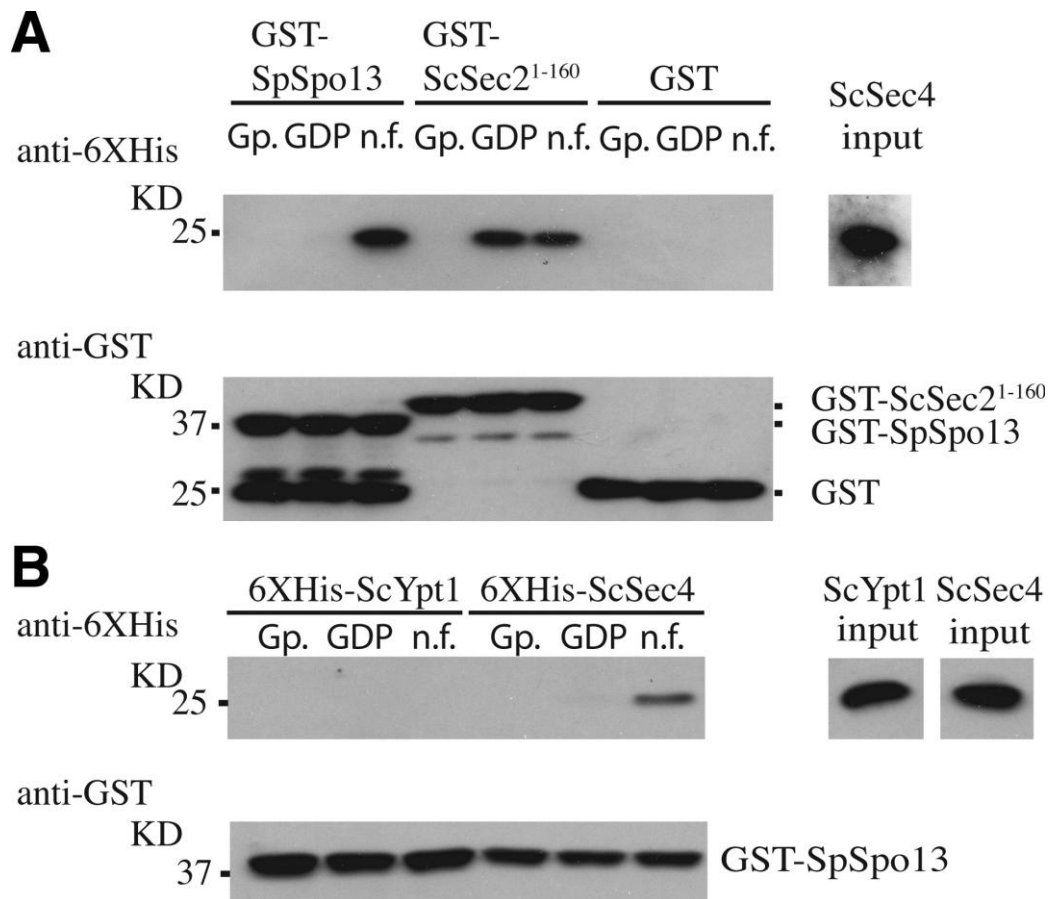
Figure 3.3. SpSpo13 binds preferentially to the nucleotide free form of ScSec4.
GST-pull down assays. (A) 6XHis-ScSec4 bound to GppNHp (Gp.), GDP, or in its
nucleotide-free (n.f.) form was mixed with the indicated GST fusion. After precipitation
of the GST fusion proteins, the resulting pellets were analyzed by Western blot using
anti-6XHis antibodies to detect precipitated 6XHis-ScSec4 (top) or with anti-GST
antibodies to detect SpSpo13 and ScSec2$^{1-160}$. (B) GST-SpSpo13 immobilized on
Sepharose beads was mixed with different derivatives of 6XHis-ScYpt1 or
6XHis-ScSec4 and analyzed as described in A. Input (right) represents 10% of Rab
proteins used per binding reaction.

SpSpo13 has guanine nucleotide exchange activity toward ScSec4 *in vitro*

To confirm that SpSpo13 can act as a GEF, a real time fluorescent nucleotide exchange assay that monitored the level of ScSec4 activation was performed (Rojas et al., 2003). In this assay, ScSec4 was preloaded with GDP and added to buffer containing a limited amount of mant-GppNHp. Binding of the mant-GppNHp, a fluorescent nonhydrolysable analogue of GTP, to ScSec4 is detected by monitoring a fluorescence resonance energy transfer (FRET) interaction between a tryptophan residue on ScSec4 and the fluorophore. Although little FRET was detected with buffer containing only the fluorophore, an increase of fluorescence intensity was observed when ScSec4-GDP alone was added (Figure 3.4A). The fluorescence intensity increased linearly over the time course after ScSec4 was added, probably due to the high intrinsic GDP-release rate of ScSec4 (Ortiz et al., 2002). Notably, when ScSec4 was premixed with GST- SpSpo13 and added to the buffer containing mant-GppNHp, the increase in fluorescence intensity during first 200 s was dramatically higher, and the fluorescence intensity soon reached an asymptotic value (Figure 3.4A). Similar results were seen when ScSec4 was premixed with the known GEF, GST-ScSec2[1-160] (Figure 3.4A). In contrast, the initial rate of ScSec4 activation did not rapidly increase when ScSec4 premixed with GST.

This assay establishes that SpSpo13 can stimulate GTP binding by ScSec4 but, because of the low concentration of mant-GppNHp present in the buffer, is not informative about the kinetics of GDP release (Rojas et al., 2003). To examine these kinetics, the displacement of mant-GDP from ScSec4 in a solution containing a large excess of GppNHp was examined. In the reverse of the mant-GppNHp loading assay, release of mant-GDP from ScSec4 was monitored by a decrease of FRET (Figure 3.4B). Addition of GST-ScSec2[1-160] to buffer containing the mant-GDP loaded ScSec4 triggered a swift drop of fluorescence intensity to a basal level, indicating that GST-ScSec2[1-160] efficiently facilitates mant-GDP dissociation. Addition of GST-SpSpo13 to the preloaded ScSec4 also stimulated a drop in fluorescence intensity but at a much slower rate (Figure 3.4B), indicating that SpSpo13 facilitates mant-GDP release of ScSec4 with slower kinetics than GST-ScSec2[1-160]. These data demonstrate that SpSpo13 can act as a GEF for ScSec4 *in vitro*, though not as efficiently as its natural GEF, ScSec2. This result is consistent with our finding

that *Spspo13⁺-ScSEC2^{161-759}* rescues the growth of a *sec2Δ* mutant less well than the native *ScSEC2 in vivo* (Figure 3.2).
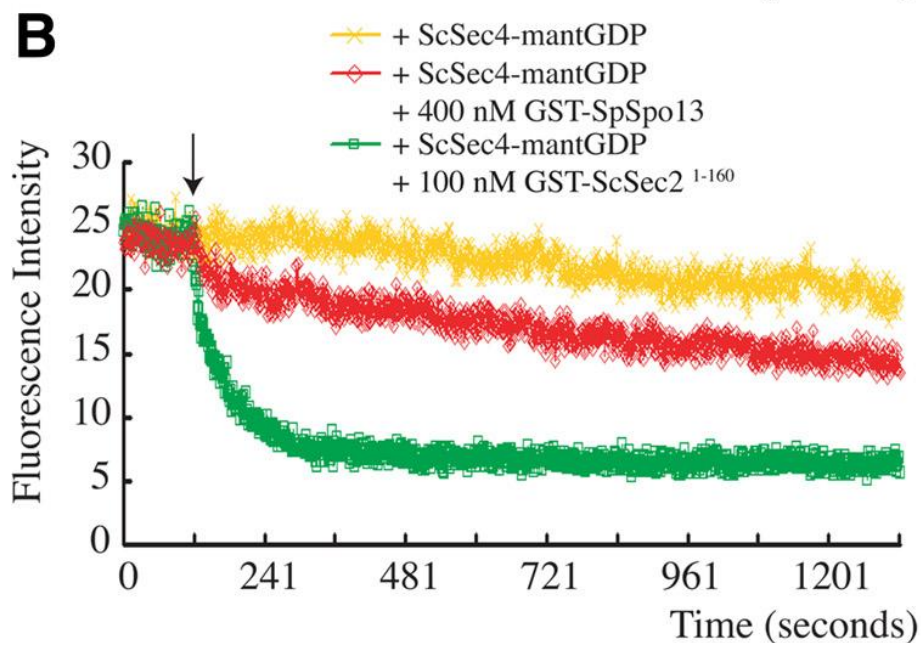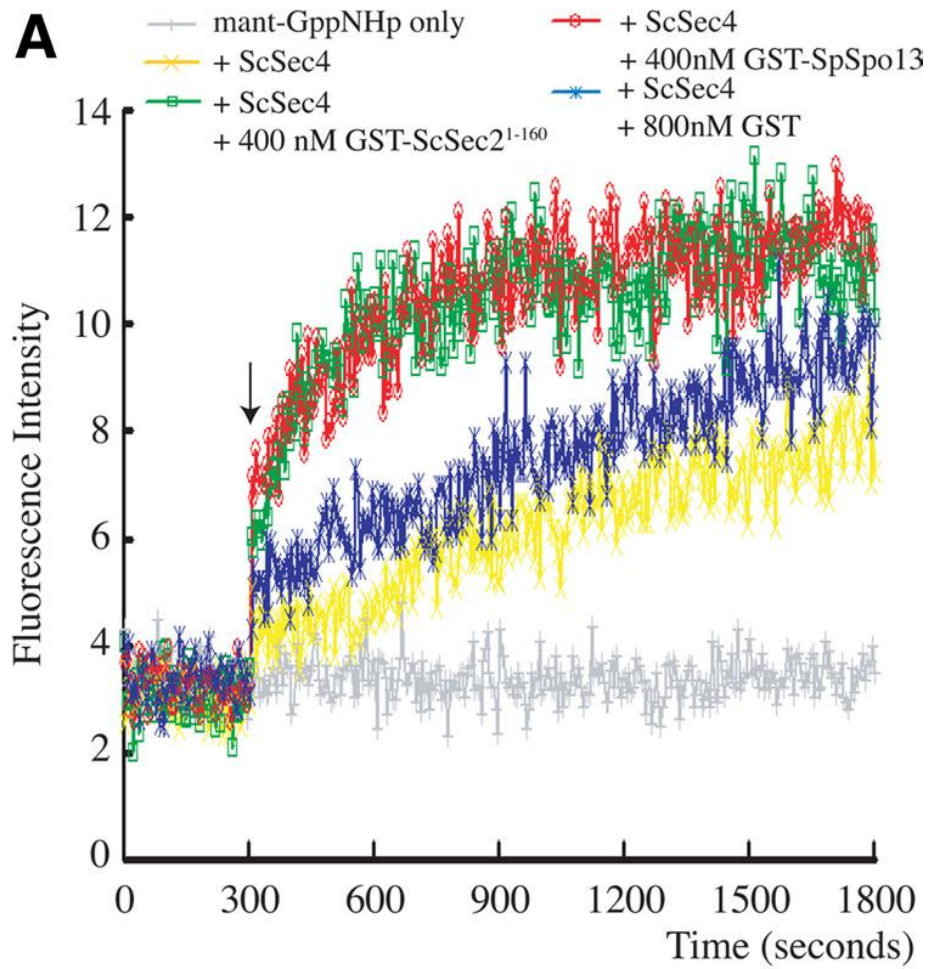
Figure 3.4. SpSpo13 facilitates nucleotide exchange on ScSec4. (Continues to next page)

(Continues from last page) (A) SpSpo13 stimulates GTP binding. ScSec4 was preloaded with GDP. At t = 300 s (indicated by arrow), ScSec4 alone, ScSec4 mixed with GST, ScSec4 mixed with GST-ScSec2$^{1-160}$, or ScSec4 mixed with GST-SpSpo13 was added to buffer containing the fluorescent GTP analogue mant-GppNHp. We used 400 nM ScSec4-GDP per reaction. Binding of the analogue to ScSec4 was monitored by following the fluorescence signal created by a FRET interaction between ScSec4 and the mant-GppNHp. The gray line indicates the basal level of fluorescence signal from the fluorophore under these conditions. (B) SpSpo13 stimulates GDP release. 6XHis-ScSec4 preloaded with the fluorescent GDP analogue mant-GDP was incubated in buffer containing GppNHp. We used 400 nM ScSec4-mant-GDP per reaction. At the time indicated by the arrow, buffer, GST-ScSec2$^{1-160}$, or GST-SpSpo13 was added to the reaction mixture. Release of GDP was monitored by a loss of fluorescent signal from the ScSec4-mant-GDP FRET interaction. The gray line indicates the basal level of fluorescence signal from the fluorophore under these conditions.

A mutation in *Spspo13⁺* that impairs GEF activity blocks FSM formation

Within the ScSec4 binding site of ScSec2, Phe109 of ScSec2 is a critical residue for its GEF activity and binding affinity for ScSec4 (Sato et al., 2007) (Figure 3.1). We reasoned that if SpSpo13 acts on an *S. pombe* Rab in a similar way to ScSec2 on ScSec4, then the corresponding residue of SpSpo13, Phe77, should be essential for SpSpo13 GEF activity. Therefore, Phe77 of SpSpo13 was mutated to alanine, and the resulting mutant protein was tested in the GST-pull-down and GEF assays. The pull-down assay revealed that GST-SpSpo13^{F77A} still bound to the nucleotide-free form of ScSec4 but at a lower level than wild-type GST-SpSpo13 (Figure 3.5A). In the GEF assay, adding GST-SpSpo13^{F77A} did not stimulate mant-GDP dissociation, indicating that the mutant protein has lost GEF activity *in vitro* (Figure 3.5B). Moreover, expression of a *Spspo13^{F77A}-ScSEC2$^{161-759}$* fusion gene in a *sec2Δ* mutant does not support cell growth in *S. cerevisiae* (data not shown), suggesting that the mutant protein lacks GEF activity *in vivo* as well.

To examine the effect of the F77A mutant on sporulation and FSM formation in *S. pombe*, plasmids carrying *Spspo13⁺* or *Spspo13^{F77A}* were expressed in a *spo13-B82* mutant. The *spo13-B82* allele has a nonsense mutation at the 53rd residue and fails to form FSMs or spores (Nakase et al., 2008). Introduction of the wild-type *Spspo13⁺* restored sporulation to this strain; however expression of *Spspo13^{F77A}* did not (Figure 3.6A). SpSpo13 and SpSpo13^{F77A} were next tagged with mRFP and expressed in sporulating cells under the native *spo13* promoter. Sid4-GFP was used as a marker for the SPB (Chang and Gould, 2000). Spo13-mRFP was visible at the SPB, beginning with cells in Meiosis I and persisted at the SPB throughout Meiosis II, as reported previously (Nakase et al., 2008) (Figure 3.6B). The localization of SpSpo13^{F77A}-mRFP was indistinguishable from the wild-type protein (Figure 3.6C), indicating that the mutant protein is expressed and properly localized. To more closely examine the *Spspo13^{F77A}* defect, FSM assembly was visualized using GFP-Psy1, which encodes a SNARE protein and localizes at FSM during Meiosis II (Maeda et al., 2009), and SpSpo13 was detected again by tagging with mRFP. Growing FSMs were observed adjacent to each of the SPBs in 100% of the cells expressing wild-type *Spspo13⁺* (n = 20), but no FSMs were formed in cells expressing *Spspo13^{F77A}* (Figure 3.7) (n = 20). The GEF activity of SpSpo13 is therefore required

for FSM assembly in *S. pombe*.
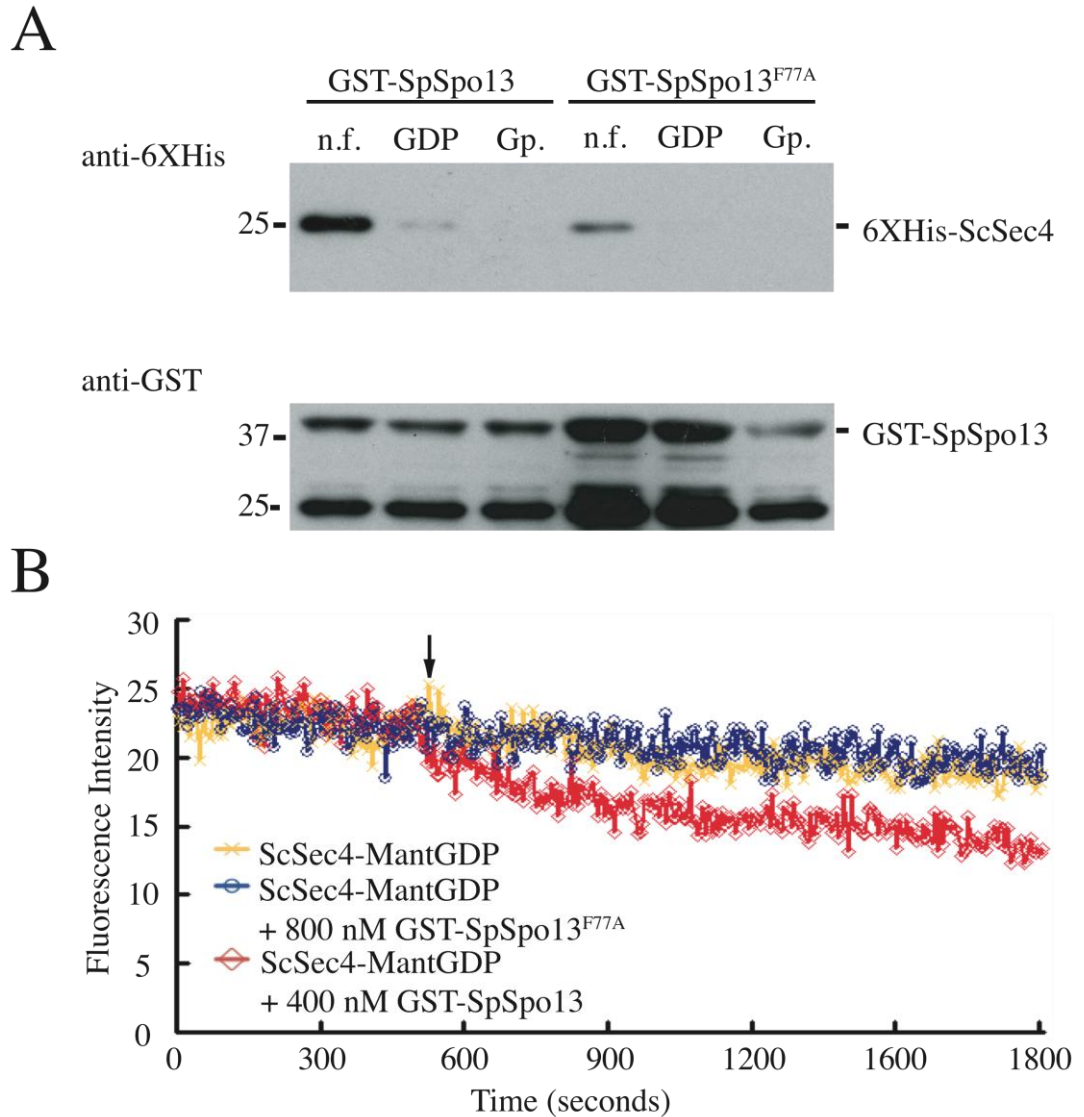
Figure 3.5. Mutation of conserved residue in SpSpo13 leads to the loss of GEF activity in vitro and a FSM assembly defect in vivo. (A) GST-SpSpo13 displays reduced binding to ScSec4. GST-SpSpo13 or GST-SpSpo13[F77A] immobilized on glutathione-Sepharose beads was mixed with the nucleotide-free (n.f.), GDP-bound, or GppNHp-bound (Gp.) forms of 6XHis-ScSec4. The mixtures were centrifuged, and the resulting pellets analyzed by Western blot. Top, blot probed with anti-6XHis antibodies. Bottom, same samples probed with anti-GST antibodies. (B) GDP release assay. 6XHis-ScSec4 preloaded with the fluorescent GDP analogue mant-GDP was incubated in buffer containing GppNHp. At the time indicated by the arrow, buffer (yellow line), 400 nm GST-SpSpo13 (red line), or 800 nM GST-SpSpo13[F77A] (blue line) was added to the reaction mixture. Release of GDP was monitored by a loss of fluorescent signal from the ScSec4-mant-GDP FRET interaction.

A

+ *Spspo13*^{+}   + *Spspo13*[F77A]

30%   0%   5μm

B

| Sid4-GFP | Spspo13 -mRFP1 | Merge |

MI

MII

2μm

C

| Sid4-GFP | Spspo13[F77A] -mRFP1 | Merge |

MI

MII

2μm
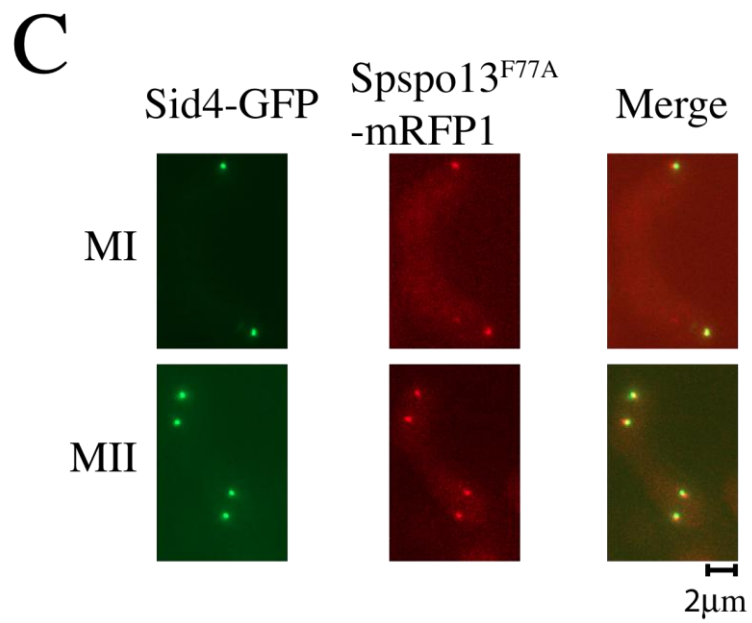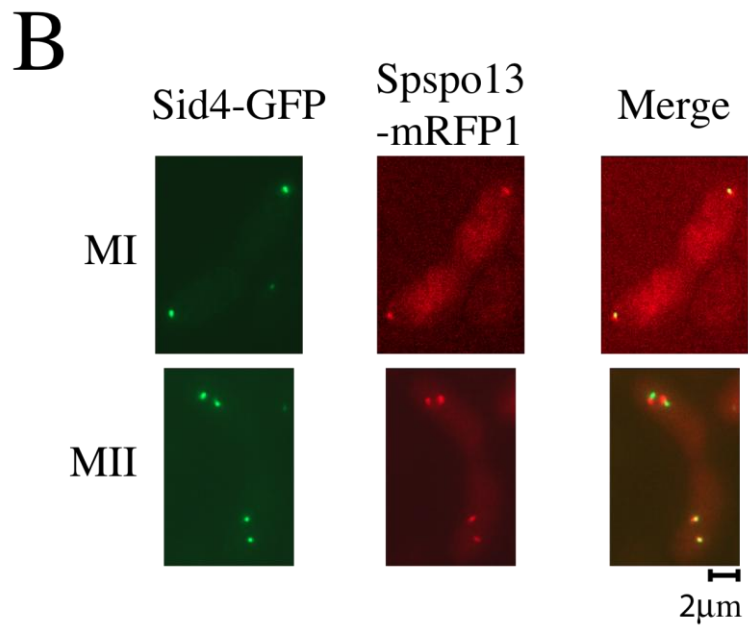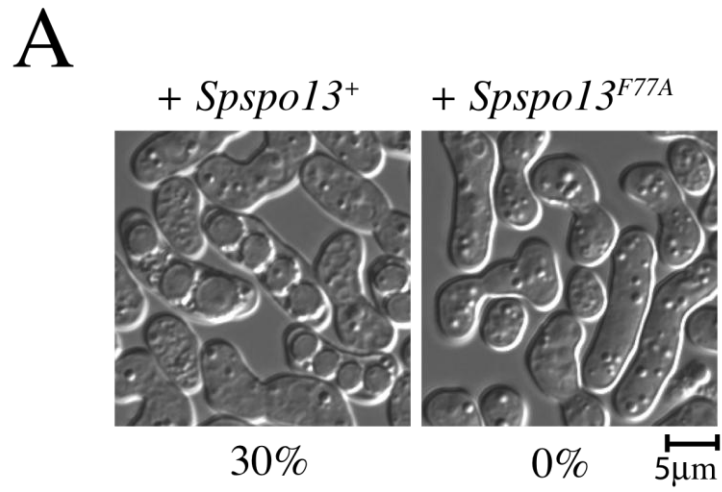
Figure 3.6. SpSpo13^{F77A} fails to support spore formation but localizes properly to the SPB. (A) *spo13-F77A* cells fail to sporulate. Strain ANP3 (*h90*, *spo13-B82*) was transformed with plasmids carrying *Spspo13$^+$* or *Spspo13-F77A* and incubated on sporulation medium. Sporulation was assessed by light microscopy. The sporulation frequency for each strain, measured as the percentages of asci out of 200 total zygotes, is shown. (B and C) SpSpo13^{F77A}-mRFP and SpSpo13-mRFP localize to the meiotic SPB. Strain FY12476 (*h90 spo13::ura4$^+$ ura4 leu1 sid4GFP::kanR*) was transformed with plasmids carrying *Spspo13$^+$*-mRFP or SpSpo13^{F77A}-mRFP, sporulated, and examined by fluorescence microscopy.

$Spspo13^+$ $Spspo13^{F77A}$

mRFP1

Psy1-GFP

Merge

2µm
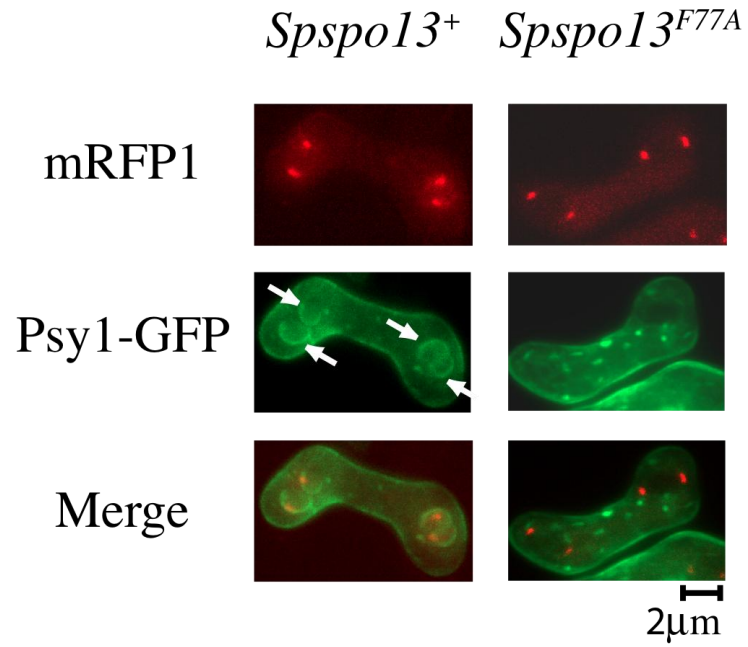
Figure 3.7. Loss of GEF activity in SpSpo13 leads to an FSM assembly defect in vivo. *Spspo13^{F77A}* cells do not form FSMs. Strain HJP1 (*h90, spo13-B82*) was cotransformed with plasmids carrying GFP-Psy1 and *Spspo13^+*-mRFP or *Spspo13^{F77A}*-mRFP, sporulated, and examined by fluorescence microscopy. Arrows indicate FSMs.

SpYpt2 is the probable *in vivo* target of SpSpo13

SpYpt2 is the *S. pombe* Rab most closely related to ScSec4 and, like ScSec4 has been shown to function in exocytosis (Craighead et al., 1993). Given the homology of ScSec4 and SpYpt2, the activity of SpSpo13 on ScSec4, and that ScSec4 has been shown to be required for prospore membrane formation during sporulation in *S. cerevisiae* (Neiman, 1998), SpYpt2 was a strong candidate to be the physiological target of SpSpo13. A 6XHis-tagged version of SpYpt2 was purified from *E. coli*, and the ability of SpSpo13 to stimulate GDP release was examined (Figure 3.8A). Similar to what was observed with ScSec4 as a substrate (Figure 3.4B), SpSpo13 stimulated GDP release, although not as efficiently as ScSec2. Thus, SpSpo13 can act on SpYpt2. To examine the specificity of SpSpo13, two other *S. pombe* Rab proteins, SpYpt1 and SpYpt3, were also purified and examined. Addition of 6 mM EDTA to the reaction was used as a control for GDP release in these experiments (Figure 3.8B). SpSpo13 failed to stimulate release of GDP from either SpYpt1 or SpYpt3, indicating specificity of SpYpt2 *in vitro*.

Deletion of *Spypt2*$^+$ is lethal (Craighead et al., 1993), and overexpression of *Spypt2*$^+$ did not rescue the spore formation defect of the *Spspo13*^{F77A} mutant (Yang, unpublished observations). Therefore, to look for evidence of *in vivo* interaction between SpSpo13 and SpYpt2, we used the *sec2Δ* rescue assay. SpSpo13 expression was unable to rescue the growth defect of a *sec2Δ* mutant (Figure 3.2). Similarly, overexpression of *ScSEC4*, *ScYPT1*, *Spypt2*$^+$, or *ScYPT31* did not restore growth to the mutant. However, coexpression of *Spspo13*$^+$ with *Spypt2*$^+$ or with *ScSEC4* allowed rescue of the *sec2Δ* mutant (Figure 3.8C). In particular, coexpression of *Spspo13*$^+$ and *Spypt2*$^+$ completely rescued the growth defect. This result indicates that SpSpo13 can interact with SpYpt2 *in vivo* as well as *in vitro*.
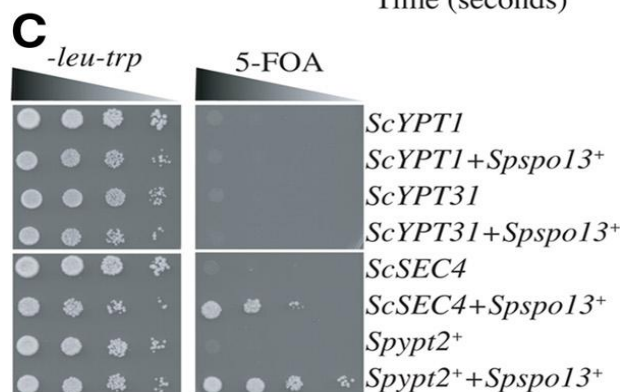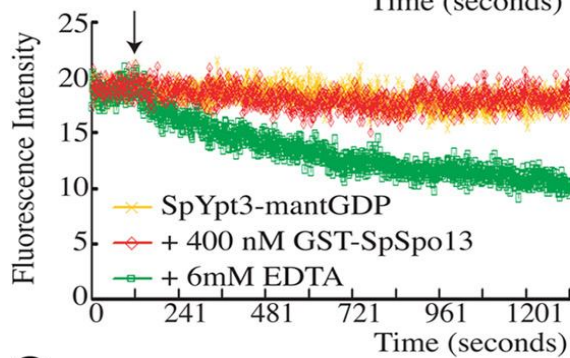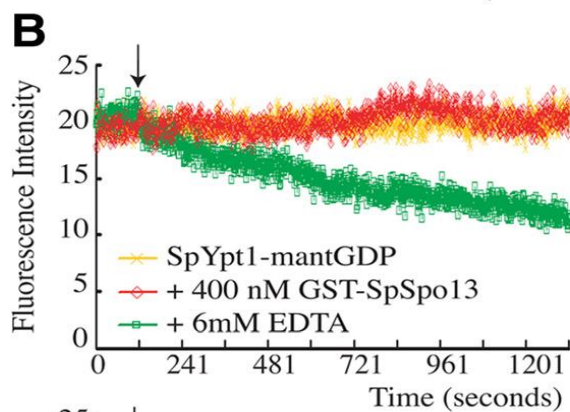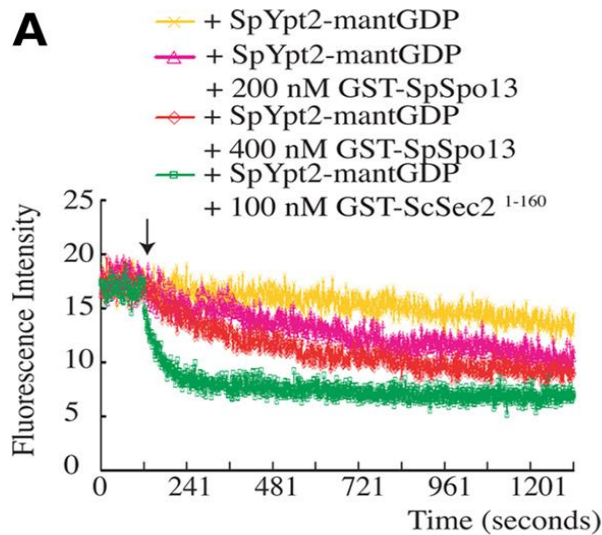
Figure 3.8. SpSpo13 specifically facilitates nucleotide exchange by SpYpt2. (A) SpSpo13 stimulates GDP release by SpYpt2. 400 nM SpYpt2-mant-GDP was used per reaction. At the time point indicated by the arrow, GST-ScSec2$^{1-160}$ or GST-SpSpo13 was added to the reaction mixture at the indicated concentrations.

(B) SpSpo13 cannot stimulate GDP release by SpYpt1 or SpYpt3. We used 400 nM SpYpt1-mant-GDP or 400 nM SpYpt3 per reaction. At the time point indicated by the arrow, 400 nM GST-SpSpo13 or 6 mM EDTA was added to the reaction mixture. (C) SpSpo13 genetically interacts with SpYpt2 *in vivo*.

Strain HJ75-4 was cotransformed with a *CEN-TRP1*-plasmid carrying *Spspo13$^+$* and *2µ-LEU2*-plasmids carrying indicated *YPT* genes. The transformed strains were grown in nonselective media overnight, and 10-fold serial dilutions of the overnight culture were spotted onto a synthetic plate lacking tryptophan and leucine or onto a plate containing 5-fluoroorotic acid (5-FOA). The plates were photographed after 2-d incubation at 30℃.

3.3 Discussion

We report here that a SPB component in *S. pombe*, SpSpo13, has homology to the GEF domain of ScSec2 and can function to stimulate nucleotide exchange both *in vitro* and *in vivo*. A mutation of SpSpo13 that impairs GEF activity blocks FSM assembly, indicating that the GEF activity is required for MOP-mediated membrane formation. Several lines of evidence suggest that SpYpt2 is the physiological Rab target of SpSpo13: 1) SpYpt2 is the homologue of ScSec4, which is required for prospore membrane formation in *S. cerevisiae* (Neiman, 1998); 2) SpSpo13 can act as a GEF for ScSec4 both *in vivo* and *in vitro* and 3) interact with SpYpt2 when coexpressed in *S. cerevisiae*; and 4) SpSpo13 specifically stimulates GDP release from SpYpt2 and not other *S. pombe* Rab proteins *in vitro*.

In *S. cerevisiae*, vesicles attach to the MOP before fusion (Nakanishi et al., 2006), suggesting that the MOP functions as a vesicle docking complex upstream of SNARE-mediated membrane fusion. In this light, our finding that the *S. pombe* MOP contains a GEF activity provides a strong parallel to other vesicle tethering complexes (Stenmark, 2009). For example, the TRAPP-I and TRAPP-II complexes involved in endoplasmic reticulum-to-Golgi trafficking and intra-Golgi trafficking, contain GEF activity directed toward Ypt1, and possibly Ypt31/Ypt32 (Cai et al., 2008; Jones et al., 2000). Similarly, the Vps-C/HOPS complex involved in endosome–vacuole trafficking acts as a Ypt7-directed GEF (Wurmser et al., 2000). Stimulation of Rab activity may be a common mechanism by which tethering complexes promote the downstream events of vesicle fusion.

The fact that SpSpo13 is a component of the SPB also highlights a difference between the function of SpSpo13 and ScSec2. In addition to the GEF domain, ScSec2 has additional domains that target it to the vesicle and interact with the exocyst complex (Elkind et al., 2000; Ortiz et al., 2002). ScSec2 is therefore thought to associate with transport vesicles and travel with them to the site of membrane fusion (Walch-Solimena et al., 1997). By contrast, SpSpo13 is already localized to the future site of membrane fusion, the SPB, in meiosis I before precursor vesicles arrive. This leaves open the question of how the vesicles interact with SpSpo13. It may be that other components of the SPB initially interact with the vesicles and this serves to recruit them for SpSpo13 action.

In vitro, the GEF activity of SpSpo13 is not strong relative to the GEF domain of ScSec2, even when assayed on SpYpt2. It may be that the GST-SpSpo13 fusion protein does not fold properly *in vitro*. Alternatively, other SPB proteins missing from the *in vitro* reactions may be necessary to stimulate greater GEF activity of SpSpo13 *in vivo*.

It should be noted that, in addition to SpSpo13, the *S. pombe* genome also contains an open reading frame (ORF) that seems to be a *bona fide* homologue of ScSec2, SPAC23C4.10. As with ScSec2, the predicted protein is large and contains an N-terminal GEF domain. Examination of other sequenced fungal genomes revealed the presence of two ScSec2/SpSpo13 related ORFs in many species. In the ascomycetes, such as *Aspergillus*, that contain both ORFs, one is shorter and more closely related to SpSpo13 and the other ORF is longer and more closely related to ScSec2. In the more distantly related basidiomycetes, such as *Coprinus* or *Cryptococcus*, one short and one long ORF are also present, although they are not obviously more closely related to SpSpo13 or ScSec2. Thus, in most fungi there seem to be two ScSec2/SpSpo13-related ORFs. However, in the Saccharomycotina, the lineage leading to budding yeasts, the shorter ORF has been lost and only the longer ScSec2-like ORF is present (Figure 3.9 and Figure 3.10).

Although no characterization of any of these genes has been reported, this observation raises the possibility that SPB-associated GEF activity is a conserved mechanism driving localized membrane formation during ascosporogenesis. In both *S. pombe* and *S. cerevisiae*, the MOP is essential for membrane formation. It is somewhat surprising therefore that there is no primary sequence homology between any of the *S. pombe* or *S. cerevisiae* MOP components so far identified. One interesting question is whether the *S. cerevisiae* MOP also contains a GEF activity, perhaps in a subunit structurally unrelated to SpSpo13/ScSec2. Alternatively, ScSec2 may provide the GEF activity at the MOP during *S. cerevisiae* meiosis. A temperature-sensitive *sec2* allele, *sec2-59*, sporulates well at restrictive temperature (Neiman, unpublished observations). However, this allele carries a stop codon that leaves the GEF domain intact (Nair et al., 1990; Walch-Solimena et al., 1997). Testing the possible role of ScSec2 in sporulation in *S. cerevisiae* will require the isolation of an allele with conditional GEF activity.

The issue of how activation of ScSec4 leads to FSM precursor vesicle fusion

remains to be determined. During exocytosis at the plasma membrane in *S. cerevisiae*, activated ScSec4 promotes fusion, in part, by mediating the interaction of the vesicle with the exocyst tethering complex (Guo et al., 1999). Presumably, SpYpt2 functions similarly in exocytosis in *S. pombe*. That activation of the SpYpt2 in FSM formation occurs in the context of a distinct tethering complex, the MOP, raises the question of whether or not the exocyst is required for coalescence of FSM precursor vesicles. If the MOP substitutes for the role of the exocyst in tethering the two membranes, then the Rab protein involved must promote fusion through some other route, perhaps by interaction with other factors that impinge on the assembly of SNARE complexes such as Sec1-family or tomosyn-family proteins (Aalto et al., 1997; Grosshans et al., 2006a; Wiederkehr et al., 2004).

Finally, these results highlight an intriguing parallel between FSM formation and ciliogenesis in animal cells. During ciliogenesis a membrane cap initially forms on one of the centrioles. This membrane expands as the centriole migrates to the cell periphery and will eventually fuse with the plasma membrane and form the sheath of the cilium (Sorokin, 1962). Transport to this ciliary membrane requires Rab8, a member of the same Rab subfamily as Sec4 (Nachury et al., 2007; Yoshimura et al., 2007), and a centriole/basal body localized GEF, Rabin8, which is a Sec2/Spo13 family member (Nachury et al., 2007). Thus, in higher cells and in yeast, membrane organization by the microtubule organizing center uses orthologous Rabs and Rab-GEFs.

	SpSpo13 homolog	ScSec2 homolog
Saccharomyces cerevisiae	N	Y
Kluyveromyces lactis	N	Y
Debarryomyces hansenii	N	Y
Yarrowia Lipolytica	N	Y
Aspergillus nidulans	Y	Y
Coccidioides immitis	Y	Y
Magnaporthe grisei	Y	Y
Neurospora crassa	Y	Y
Schizosaccharomyces pombe	Y	Y
Cryptococcus neoformans	Y*	Y*
Coprinus cinerus	Y*	Y*
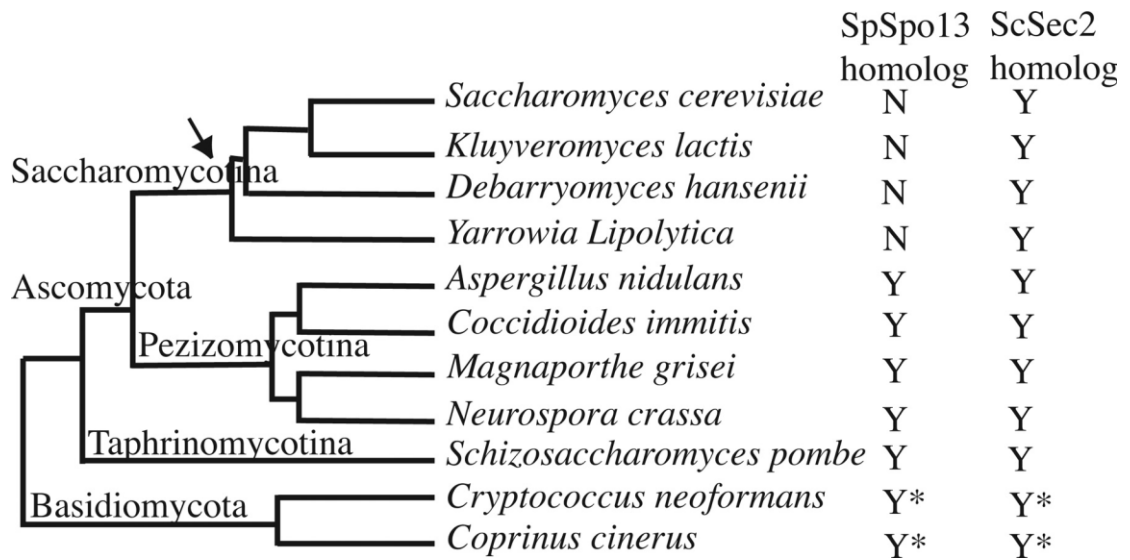
Figure 3.9. Phylogenetic distribution of SpSpo13/ScSec2 related proteins within representative fungi. Fungal tree is based on Fitzpatrick *et al.* (2006) . Arrow indicates loss of an apparent SpSpo13 homologue in the Saccharomycotina lineage. Asterisks indicate that the two ORFs present in *Cryptococcus cinerus* and *Cryptococcus neoformans*, although one ORF is short and one ORF is long, do not obviously correspond to SpSpo13 and ScSec2, respectively.

```
S. pombe        Spo13        67  KEMEDLSVSLFTEANEMVAKARQDTEVLKRELDYLRAKEKGRIGKLRSIQTAVR  (total 138aa)
N. crassa       EAA32074    271  REIEELSVTLFSEANEMVASERRARAKLEERVKTLEKRDEQKKERLEMLEGAVR  (total 376aa)
C. immitis      EER25262    204  SELEDLTTQLFSQANEMVAQERKARAKLEERVELLERRDGEKRRRLDRLEKAVA  (total 279aa)
M. grisea       EDJ94906    253  REVEELSASLFEEANEMVATERRARAKLEERVDILEKRDVEKKRRLERLELAVG  (total 318aa)
A. nidulans     XP_680621   217  TELEELTAQLFSQANEMVAQERKARARLEERVAVLERRDIEKRNRLERLEKAME  (total 280aa)
S. cerevisiae   Sec2         99  KEVEDLTASLFDEANNMVADARKEKYAIEIL                         (total 742aa)
K. lactis       XP_45229     92  QEIEDLTASLFDEANNMVADARKEQNAVEIL                         (total 658aa)
D. hansenii     XP_459929    96  AEVEDLTASLFNEANEMVSNASREAYNFKVK                         (total 647aa)
Y. lypolytica   XP_505944    97  EEMQELSAELFDEANNMVSDARRDAAKEVAE                         (total 661aa)
A. nidulans     XP_662363   193  QELETLTAALFEEANKMVAAAKLEREAVEKK                         (total 605aa)
N. crassa       EAA36306    103  QELENLTAALFEEANKMVISAKEEARIEQEI                         (total 642aa)
M. grisea       EDK01615    160  QELEELSTQLFEEAQKMVIAAKEDAQKEQEI                         (total 669aa)
S. pombe        NP_593182   109  NELEDLTSSLFEEANRMVANARKETVASEKR                         (total 527aa)
C. immitis      XP_001246665 196 QELADLTAALFEEANKMVAAAKKEREAVEKR                         (total 705aa)
C. cinerus      EAU89437    163  KDLDDLSASLFDQANTMVAEARFAQHLSEQK                         (total 1145aa)
C. cinerus      EAU90994    177  DELESLSQALFEEANKMVAQERMKLAETEEE                         (total 451aa)
C. neoformans   XP_569677    94  AELESLSQALFEEANKMVADERKRRAEMEEN                         (total 300aa)
C. neoformans   XP_567458   217  NEVDDLTAKLFDQANTMVATERMSRAQAEAR                         (total 990aa)
            Consensus            EI  LS  LF  AN MVA  R
                                 V   T           I  K
                                 L               S
                                 M
```

Figure 3.10. Alignments of the Sec2 GEF domains from the fungal Sec2/Spo13familymembers noted in Figure3.9. For each protein in species, the GenBank accession number of the protein, and its total length are shown. Amongst the presumptive Spo13 orthologs, the homologous domain extends to the C-terminal side of the GEF homology (upper five sequences).

Chapter 4

Discussion and Perspectives

The generation of prospore membranes in *S. cerevisiae* requires vesicle targeting to the SPBs, followed by vesicle docking at the MOPs, and finally membrane fusion. In Chapter 2, I presented data that shows Spo20 has a weaker affinity to Sso1 and Snc1/2 as compared to Sec9. This difference in binding affinity between Spo20 and Sec9 is attributed to their distinctive interacting side chains of the SNARE domains and supports *in vivo* models that Sec9 cannot be replaced by Spo20 to execute fusion activity at the plasma membrane. Prior to SNARE-mediated membrane fusion at the prospore membranes, the precursor vesicles are targeted to the SPBs where the MOP provides the tethering site for the incoming vesicles. It is not clear how the MOP mediates vesicle tethering in *S. cerevisiae*, but our current study (Chapter 3) begins to reveal the mechanism for vesicle docking on the MOP. Our data show that a MOP component of *S. pombe*, SpSpo13, has homology to the Sec2 GEF domain and can stimulate nucleotide exchange in Sec4/SpYpt2. A mutation of SpSpo13 that impairs GEF activity blocks FSM assembly. We suggest that the GEF activity of the *S. pombe* MOP facilitates vesicle docking by activating SpYpt2 (Figure 4.1)
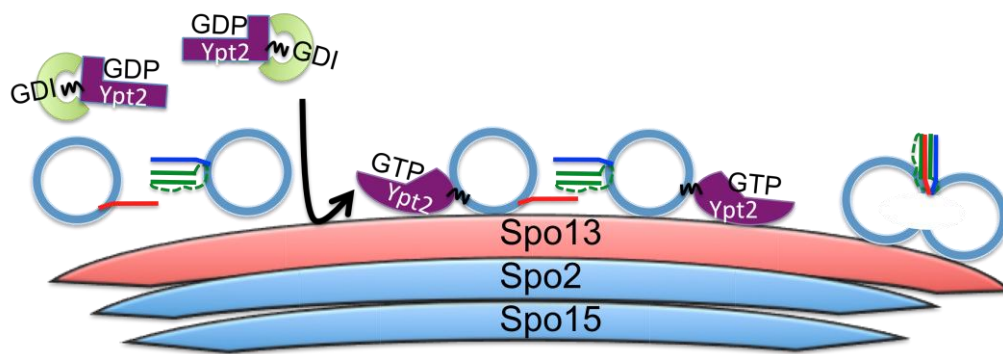
Figure 4.1. Model of initiation of FSM assembly in *S. pombe*. Spo13, Spo2 and Spo15 constitute the MOP, where Spo13 has GEF activity toward Ypt2. (A) Golgi-derived vesicles are targeted nearby the MOP by unknown mechanism. (B) Spo13 activates Ypt2 in its GTP-bound conformation. Ypt2-GTP now is associated with the vesicles facilitates vesicle docking to the MOP. Vesicle docking may promote the SNARE pairing. (C) The SNARE complex assembly drives the vesicle fusion to form FSM.

93

SNARE specificity correlates with lipid composition

We interpret our data in chapter 2 to indicate that Spo20-containing SNARE complexes cannot generate sufficient energy to facilitate fusion at the plasma membrane, but are energetic enough to drive fusion at the prospore membrane. This suggestion infers that the energy barrier to fusion at the plasma membrane is different from the prospore membrane. The barrier to fusion is affected by the lipid composition of the membrane. Cone-shaped lipids, such as phosphatidic acids (PA) and diacylglycerol, can decrease the energy barrier for membrane fusion while inverted cone-shaped lipids like lysophospatidic acid, have the opposite effect (Kooijman et al., 2003; Kooijman et al., 2005). Interestingly, an elevated level of PA in the plasma membrane permits function of SNAREs containing the Spo20 helices in vegetative cells even though the PA targeting sequence of Spo20 is not required for fusion in this particular case (Coluccio et al., 2004b). It is possible that increased PA in the lipid bilayer lowers the energy barrier of fusion and allows the Spo20-containing SNARE complex to function.

Other than PA, phosphatidylinositol-4,5-bisphosphate [$PI(4,5)P_2$] is also enriched at the prospore membrane (Nakanishi et al., 2004; Rudge et al., 2004). It is reported that Sso1/2 binds to $PI(4,5)P_2$ through the Habc domain (Mendonsa and Engebrecht, 2009). Like other syntaxin homologs, Sso1/2 contains a conserved Habc domain in its amino terminus and adopts a fusion-inactive closed conformation by self-interaction between its Habc and SNARE domains (Munson and Hughson, 2002). Binding of the Habc domain to $PI(4,5)P_2$ might facilitate opening of the closed conformation of Sso1/2 and allow the formation of the SNARE complex. Interestingly, the Sso1 Habc domain exhibits a greater binding affinity toward $PI(4,5)P_2$ than the Sso2 Habc domain (Mendonsa and Engebrecht, 2009). Sso1 and Sso2 are functionally redundant for fusion at the plasma membrane; nonetheless, only Sso1 is required for fusion at the prospore membrane (Jantti et al., 2002). The differential ability to bind phosphorylated phosphoinositides might differentiate fusion activity of Sso1 from Sso2 at the prospore membranes. Consistent with this idea, the amount of $PI(4,5)P_2$ at the prospore membranes is much less than at the plasma membrane in sporulating cells (Nakanishi et al., 2004; Rudge et al., 2004), suggesting that only Sso1, but not Sso2, is activated at the prospore membranes where

PI(4,5)P$_2$ becomes the limiting factor.

MOP as a tethering complex contains a Rab GEF activity

Our finding that the *S. pombe* MOP contains a GEF activity is consistent with the observation that tethering complexes often contain GEF activity (Stenmark, 2009). It has been suggested that the local GEF activity in a tethering complex consolidates the Rab-effector interactions. This might be true for the MOP as well. We observed that in cells expressing *Spspo13*^{+}, most of the MOPs are decorated by Psy1-GFP positive vesicles, whereas in the *Spspo13*[F77A] mutant these GFP labeled precursor vesicles are not associated with the MOPs (Figure 3.7). This indicates that Spspo13 is required for vesicle docking on the MOPs. However, the identities of the hypothetical SpYpt2 effectors, in the context of MOP mediated vesicle tethering/docking, remain unknown. One candidate might be the MOP itself, which can be tested by binding assays between SpYpt2-GTP and the other MOP components, SpSpo2 and SpSpo15.

Another candidate is the exocyst complex, which is required for secretory vesicle fusion and consists of eight subunits, Sec3, Sec5, Sec6, Sec8, Sec10, Sec15, Exo70, and Exo84. Although a role for the exocyst in FSM assembly in *S. pombe* hasn't been addressed, the exocyst components of *S. cerevisiae*, Sec8, Sec3, Exo70, and Sec15 are found to be associated with the SPB during sporulation (Mathieson et al., 2010). Interestingly, the localization of Sec3 and Sec8 to the SPB requires vesicle docking to the MOP; moreover, a mutant of the MOP component, *mpc54-47,* that shows defects in vesicle docking displays a reduced level of Sec4 recruitment (Mathieson et al., 2010). We speculate that in *S. cerevisiae*, activated Sec4 promotes vesicle docking to the MOP by binding to the exocyst.

However, a Rab GEF activity of the MOP is the missing piece in this model of prospore membrane initiation. Since there is no paralogue of Sec2 in the genome of *S. cerevisiae*, it is possible that Sec2 itself is associated with the MOP during sporulation. A temperature sensitive mutant of *SEC2*, *sec2-59* sporulates well (unpublished observations by Neiman A.M.); nonetheless, the GEF domain (amino acids 1-160) and the Ypt31/32 or Sec15 binding region (amino acids 160-374) remain intact in this mutant. It will be interesting to know if Sec2 is localized to the MOP. In vegetative

cells of *S. cerevisiae*, Sec2 is recruited to the post-Golgi vesicles by the preexisting Rab GTPase, Ypt31/32, and subsequently activate the second Rab, Sec4 (Ortiz et al., 2002). Accordingly, similar Rab cascades might apply to vesicle trafficking to the SPBs, and Sec2 might associate with the precursor vesicles through Ypt31/32.

Alternatively, in parallel with the case in *S. pombe* that SpSpo13 is a resident of the MOP, Sec2 localization to the MOP might be independent of the vesicle association. Notably, in mammalian cells, the Sec15 homolog interacts with Nud1 homology domain of Centriolin, which is required for the secretory-vesicle-mediated abscission during cytokinesis (Gromley et al., 2005). Nud1 is a constitutive component of the outer plaques of SPBs where it serves as a scaffold protein to anchor the γ-tubulin receptor, Spc72 and components of the mitotic exit network to the SPBs (Adams and Kilmartin, 1999; Gruneberg et al., 2000). Although there is no direct evidence of Nud1 involvement in prospore membrane formation, the homolog of Nud1 in *S. pombe*, SpCdc11, is required for proper FSM assembly (Krapp et al., 2006). It is possible that Sec15 recruits Sec2 to the SPBs by interacting with Nud1.

A Model for initiation of prospore membrane formation

In Figure 4.2, I propose a model for prospore membrane initiation. In this model, the MOP is associated with a GEF activity (Sec2) that converts Sec4 into a GTP-bound conformation. Sec4-GTP subsequently tags the precursor vesicles and promotes vesicle docking to the MOP by binding to the exocyst. The existence of a physical linker between the MOP and the precursor vesicle is still unknown. After docking, the vesicles, enriched with $PI(4,5)P_2$ and PA, are fused with each other by the Spo20-containing SNARE complex formation.

Different phosphoinositides contribute to membrane identity by recruiting specific proteins and facilitate vesicle tethering/docking (Grosshans et al., 2006b). *SPO14* encodes a phospholipase D that catalyzes hydrolysis of phosphatidylcholine to PA, which is essential for fusion at the prospore membranes (Nakanishi et al., 2006). A *spo14Δ* mutant displays a fusion defect similar to the *sso1Δ* mutant, in which vesicles dock to the MOP but do not fuse with each other (Nakanishi et al., 2006). One function of Spo14-generated PA is to recruit Spo20 to the prospore membranes;

however, independent targeting of Spo20 to the prospore membrane cannot rescue the sporulation defect of the *spo14Δ* mutant (Nakanishi et al., 2006). It has been suggested that Spo14 or Spo14-generated PA might have additional unknown functions. Interestingly, the precursor vesicles appear to have less contact with the MOPs in the *spo14Δ* mutant compared to the *sso1Δ* mutant (Figure 4.3) (Nakanishi et al., 2006). This might simply be due to the difference in the physical properties of the vesicles (with PA or without PA), or, alternatively, PA may facilitate vesicle docking to the MOP.

Spo14 is relocated from the cytoplasmic pool to the prospore membranes during sporulation (Rudge et al., 1998). The localization of Spo14 to the prospore membranes is essential for prospore membrane formation and requires the first 313 amino acids of the N terminus (Rudge et al., 1998; Rudge et al., 2002). The relocalization is independent of the N-terminal pleckstrin homology (PH) domain, although the PH domain is required for Spo14 activity (Rudge et al., 1998; Sciorra et al., 2002). It is not clear how Spo14 localizes to the prospore membrane. Spo20$^{51-91}$-GFP binds to PA and moves from the plasma membrane to the prospore membranes during sporulation due to an increased activity of Spo14 at the prospore membranes (Nakanishi et al., 2004). It is worth noting that the signal of Spo20$^{51-91}$-GFP to the precursor vesicles at the SPBs is greatly reduced in the *mpc54-47* mutant compared to the wild-type cell (Mathieson et al., 2010), suggesting Spo14 is not fully functional at the prospore membranes prior to the vesicle docking. Interestingly, Sec4 recruitment is also defective in the *mpc54-47* mutant (Mathieson et al., 2010). It is possible that Sec4-GTP recruits Spo14 to the prospore membranes by binding to its N-terminal region. It would be interesting to know if Spo14 localization relies on vesicle docking and Sec4-GTP.

How does Sec4-mediated vesicle docking communicate with SNARE-mediated membrane fusion? The Sec4 effector, Sec15, was found to co-immuoprecipitate with Sec1 (Knop et al., 2005). Sec1/Munc-18 (SM) proteins that bind to syntaxins and assembled ternary SNARE complex are essential for activation of SNARE complex assembly (Shen et al., 2007). The yeast Sec1 only binds to the SNARE complex but not individual SNARE proteins (Togneri et al., 2006). Sec1 forms a stable complex with Mso1, which is required for fusion at the prospore membranes (Knop et al., 2005; Weber et al., 2010). Intriguingly, Mso1 selectively interacts with Sso1 rather than

Sso2 (Weber et al., 2010); coincidentally, only Sso1 but not Sso2 is essential for the prospore membrane formation. Another effector of Sec4-GTP, Sro7/Sro77, binds directly to Sec9 to regulate SNARE assembly (Grosshans et al., 2006a; Hattendorf et al., 2007). This raises the possibility that Sro7/Sro77 binds to Spo20 during the prospore membrane formation. While it is not fully understood how Sro7/Sro77 and the interaction of Sec1 and Mso1 regulate SNARE complex assembly, initiation of the prospore membrane formation can offer a good model system to tackle such questions.
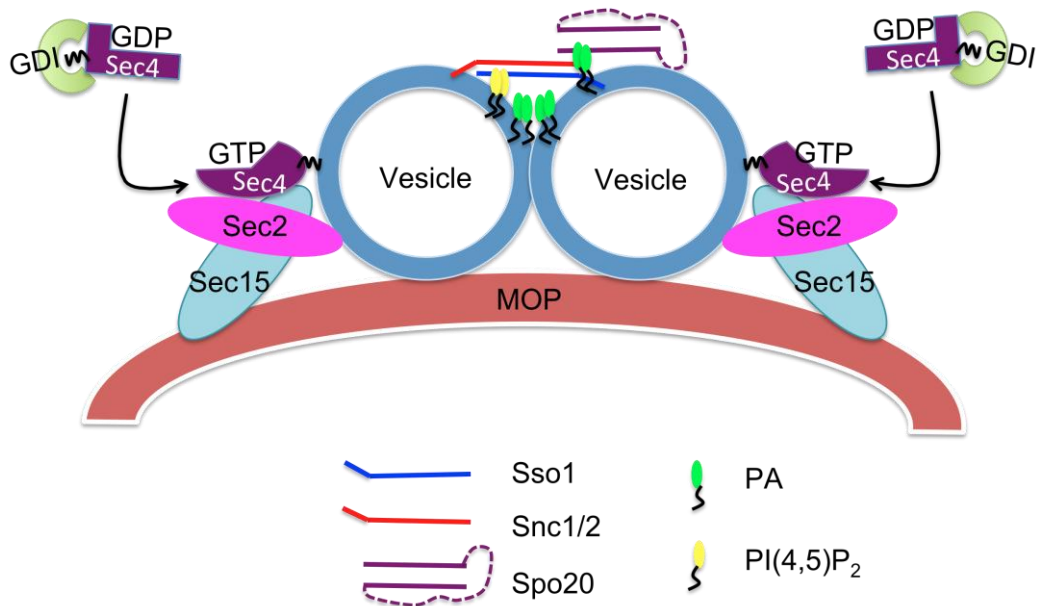
Figure 4.2. Model of prospore membrane formation in *S. cerevisiae*.
Sec2 binds to Sec15, which is localized to the MOP. Subsequently, Sec4-GTP that is activated by Sec2 facilitates vesicle docking by binding to Sec15. Sec15 might bridge other exocyst components to further help vesicle docking (not shown). Following vesicle docking, Sso1, Snc1/2 and Spo20 are assembled into a SNARE complex to drive the membrane fusion. The precursor vesicles are enriched with PA and $PI(4,5)P_2$. PA is not only required for Spo20 targeting to the vesicles but a lipid fusogen. $PI(4,5)P_2$ interacts with the N-terminus of Sso1 is essential for the membrane fusion.
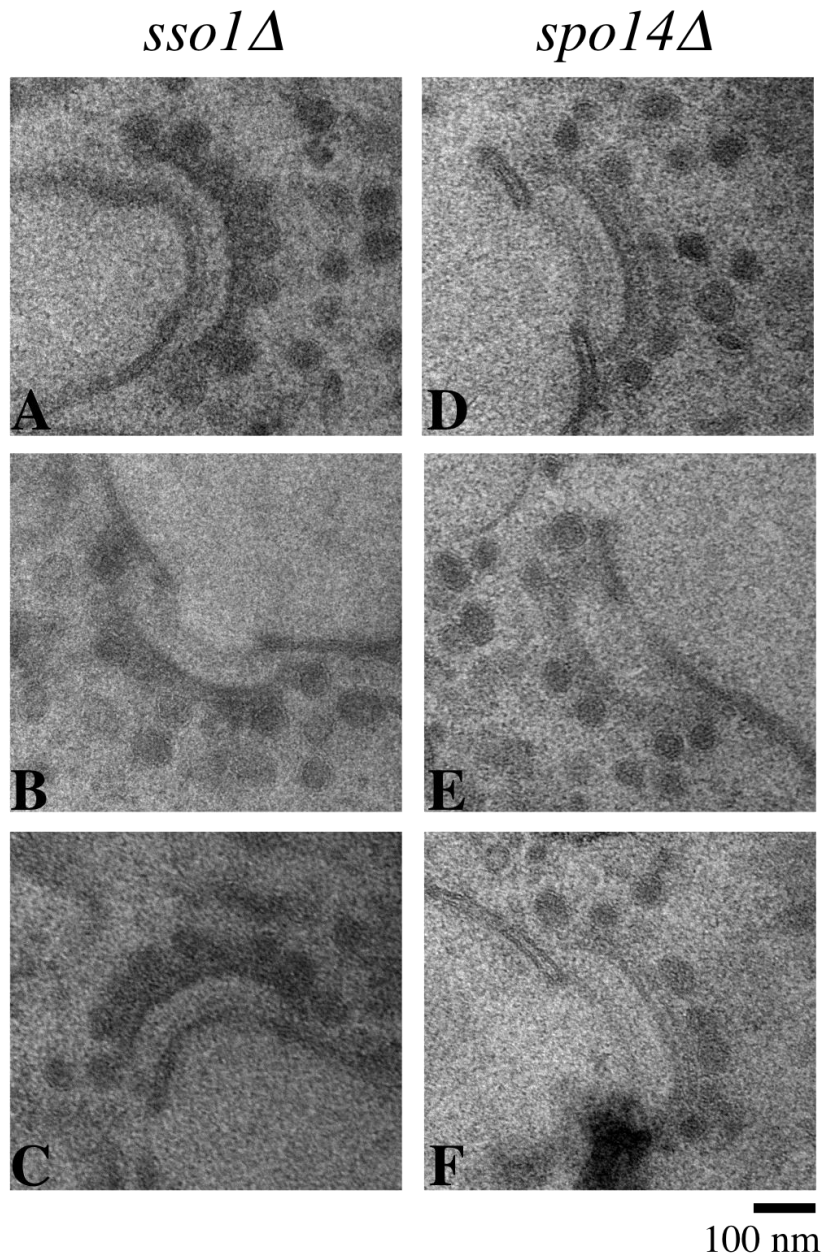
Figure 4.3. Vesicles docked to the MOP accumulate in *sso1Δ* and *spo14Δ* mutants. Electron micrographs of three represented *sso1Δ* cells (A-C) and three represented *spo14Δ* cells (D-F).

Initiation of the prospore membrane formation is equivalent to primary cilium formation

The phenomenon of prospore membrane initiation at the SPBs is analogous to the process of ciliogenesis as it begins at basal bodies in human cells (Figure 4.4 A and B)(Moens and Rapport, 1971; Sorokin, 1962). A basal body or centriole is a cylindrical structure composed of microtubules in bundles that is always found in a pair (Figure 4.4 C)(Hoyer-Fender, 2010). In a proliferating cell, centrioles recruit the pericentriolar matrix to constitute the centrosome next to the nucleus, and are essential for formation of mitotic spindles. In a centrosome from the proliferating cells, the two centrioles differ in structure where only the mature one (mother centriole) has distal and sub-distal appendages connected to the cylinder (Figure 4.4 C) (Hoyer-Fender, 2010). In a quiescent cell (cells in G1/G0 stage), the centrioles migrate to the cell surface and the mother centriole, i.e. the basal body, nucleates a cilium.

We propose that the ability to act as a membrane nucleation site is an evolutionary conserved feature of microtubule organizing centers. When examining the phylogeny of eukaryotes, the centriole is a conserved feature among species having cilia or flagella formation (Marshall, 2009). Even in the Kingdom Fungi, centrioles are present in flagellate zoospores of the Phyla Chytridiomycota and Blastocladiomycota (Stajich et al., 2009). Interestingly, with evolution time forward, the flagellum is lost in the other Phyla of the Fungi; meanwhile, the centriole is replaced by the SPB (Stajich et al., 2009) (figure 4.5). The SPBs among the different Fungi are diversified in morphology when examined by an electron microscope; however, they all are attached to the nucleus and have electron-dense plaques at the nuclear site and the cytoplasmic site (Celio et al., 2006) (Figure 4.5). Although the SPB is no longer a cylinder made of bundles of microtubules as the centriole, it keeps the ability to recruit γ-tubulin and serve as the microtubule-organizing center in the Fungi. Given that FSM assembly in *S. pombe* and prospore membrane formation in *S. cerevisiae* both require the cytoplasmic plaques of SPBs, we propose that the SPBs also preserve the ability of nucleating membranes. Lack of flagellum among these species might be due to an inability of pushing membranes outward from the cell surface. Our hypothesis predicts that the cytoplasmic plaques of SPBs in other fungi

serve as membrane nucleation sites as well. Consistent with this idea, a membranous cap was found associated with the cytoplasmic plaque of the SPB in the clade of Pucciniomycotina (Celio et al., 2006) (Figure 4.5).

Our finding that the SPB contains a GEF activity toward SpYpt2/Sec4 to promote FSM assembly is reminiscent of the fact that Rabin8, an ortholog of Sec2, and Rab8a, a Sec4 orthologue, are localized to basal bodies and required for primary cilium formation (Nachury et al., 2007; Yoshimura et al., 2007). Therefore, we believe that even though the SPB and the centriole have evolved into divergent ultrastructures and diversified protein compositions, they might recruit the same machineries to facilitate membrane formation.

A

scv

sheath

jct

Basal body

B

PrM

OP

N

M

C

Distal appendages

Sub-distal appendages

Mother centriole

Daughter centriole
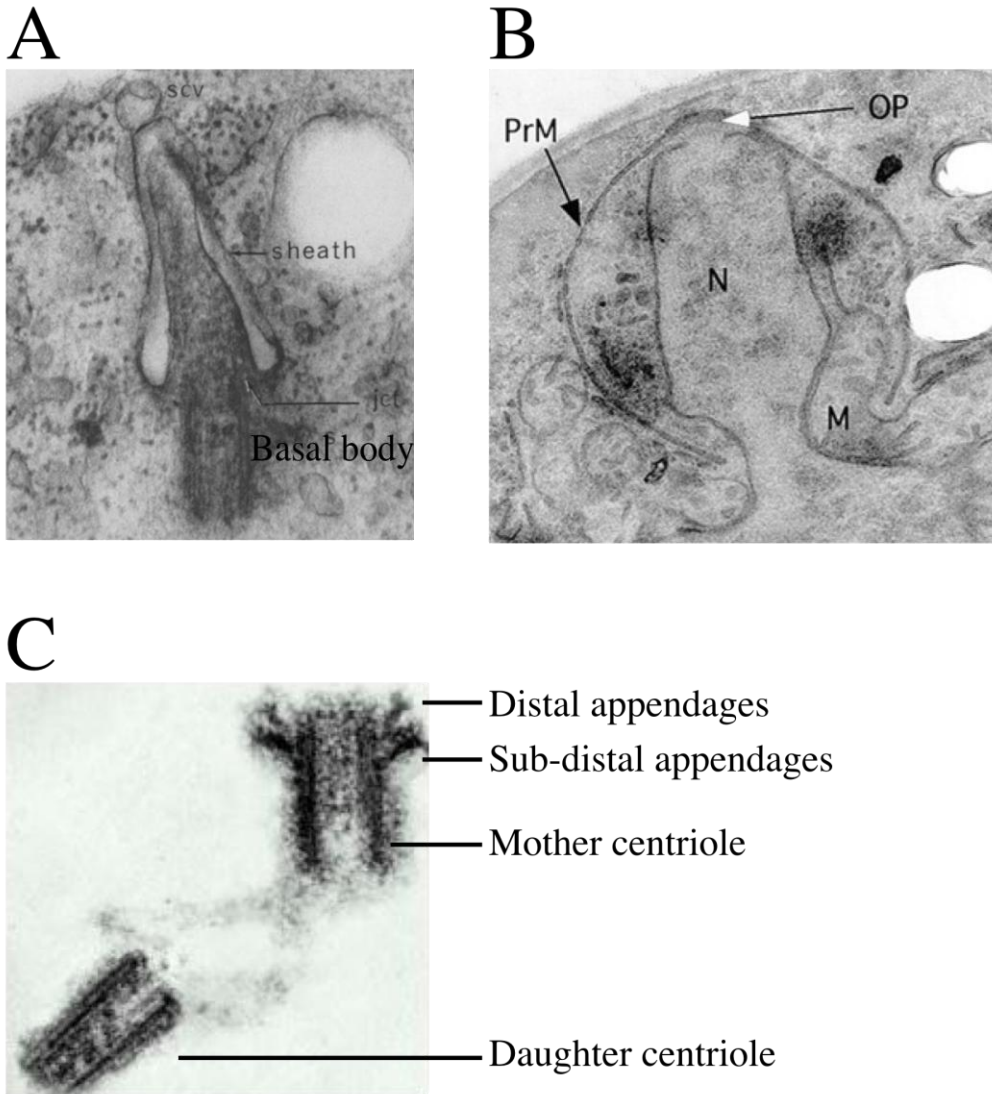
Figure 4.4. Centriole and SPB are membrane nucleation sites.
(A) Cilium formation. Initiation of cilium formation involves a membrane sheath growing on top of the basal body. The figure is reproduced from Sorokin (1962).
(B) Prospore membrane (PrM) formation. PrM is initiated at the outer plaque (OP) of the SPB. N= Nucleus; M= Mitochondria. The Figure is reproduced from Neiman (1998)
(C) Electron micrograph of a centriole pair. Centrioles are cylindrical-shaped. The mother centriole has distal and sub-distal appendages at the distal end, while the daughter centriole doesn't have appendage structures. Only is the mother centriole able to form a cilium. The figure is reproduced from Molecular Biology of the Cell, 4th edition.

103
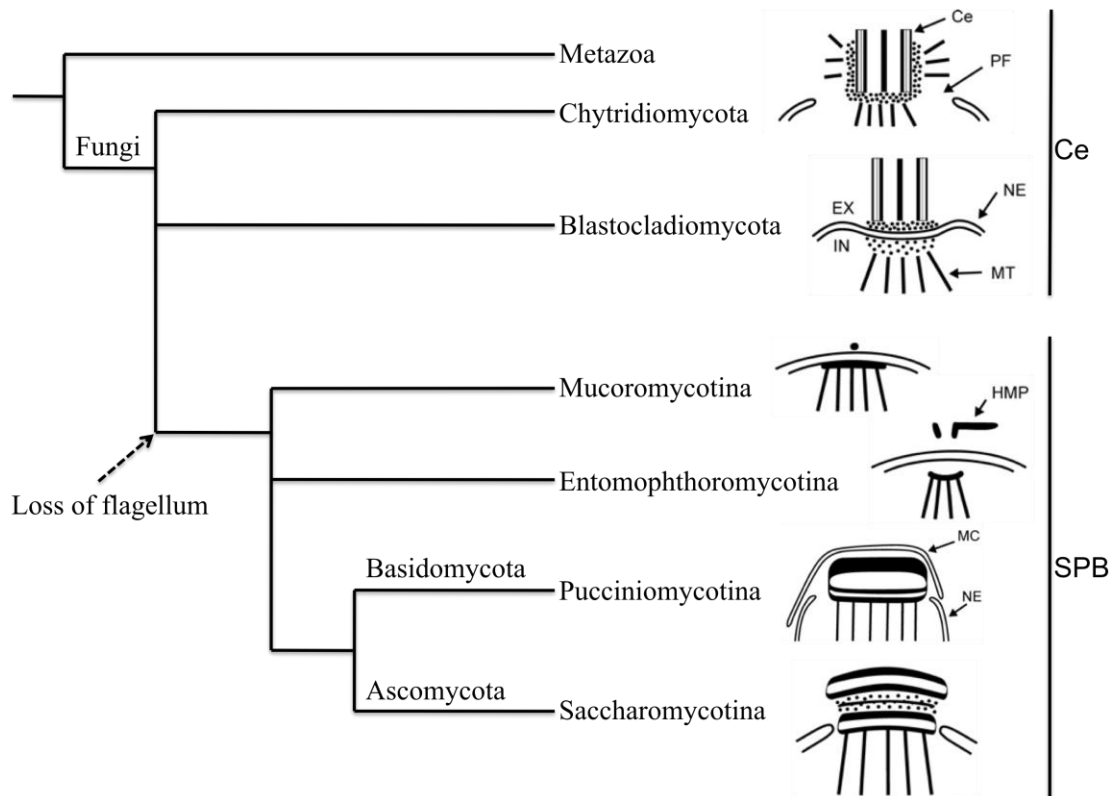
Figure 4.5. Phylogenetic tree of the Fungi. Dashed-arrow indicates the loss of flagellum in fungal form. This loss is associated with replacements of the centrioles by the SPBs. Different forms of the microtubule-organizing centers used in each phylum are depicted according to the electron microscope images (Celio et al., 2006). The SPBs appear to be plaques or disk-shaped. Ce= Centriole; PF= Polar fenestra; NE= Nuclear envelope; MT= Microtubule; EX= Extranuclear component; IN= Intranuclear component; HMP= Half-middle piece; MC= Membranous cap.

In our model, the MOP recruits the exocyst to facilitate vesicle docking during prospore membrane formation (Figure 4.2). This model might be able to apply to cilium formation as well. In fact, the proteins of the exocyst complex, Sec6, Sec8, and Sec10 are localized to the primary cilium in Madin-Darby canine kidney (MDCK) epithelial cells (Rogers et al., 2004). Furthermore, knockdown of *SEC10* gene expression leads to decreased primary ciliogenesis in the cells (Zuo et al., 2009). The exocyst might be recruited to the cilium by the centriole-associated proteins Centriolin, which is related to the SPB outer plaque component, Nud1/SpCdc11. It has been reported that Centriolin can interact with Sec15 through its Nud1-homology region (Gromley et al., 2005). Intriguingly, Centriolin is associated with two different parts of the centriole. Localization of Centriolin at the proximal region of the centriole is involved in microtubule anchoring (Szebenyi et al., 2007). Centriolin is also associated with the sub-distal appendage of basal bodies (mother centrioles) (Gromley et al., 2003; Ishikawa et al., 2005). Although a direct role of Centriolin in cilia formation hasn't been addressed, recruitment of Centriolin to the sub-distal appendage is disrupted in an Outer dense fiber 2 (Odf2)-knockout mouse cell line (Ishikawa et al., 2005). Odf2 is a scaffold protein that is specifically localized to the distal and sub-distal appendages of mother centrioles (Nakagawa et al., 2001). Strikingly, the Odf2-deficient cells are defective in generation of primary cilia, but are normal with cell cycle progression, centrosomal function, and microtubule nucleation (Ishikawa et al., 2005), suggesting that the distal and sub-distal appendages are specifically required for cilia formation. It is likely that Centriolin at the sub-distal appendage recruits the exocyst to the basal bodies and facilitates the initial docking of basal bodies to membranes.

Primary cilia are found in almost all cell types in the human body (Singla and Reiter, 2006). Defects in cilia formation have been linked to several diseases, including retinal degeneration, cystic kidney disease, and Bardet-Biedl syndromes (Gerdes et al., 2009). Several BBS genes have been identified to be responsible for Bardet-Biedl syndromes; however, how these gene products lead to ciliogenesis and Bardet-Biedl syndromes are just beginning to be explored (Jin et al., 2010; Nachury et al., 2007). Given the analogy of cilia formation and prospore membrane formation, we seek to gain insights from how prospore membrane formation is regulated, and hopefully, apply our knowledge to cilia formation.

Appendix 1

The role of *mug79⁺* during FSM assembly in *S. pombe*

Different classes of GEFs and/or their associated G proteins are found to be associated with basal bodies or cilia. For example, Rabin8 is directly associated with the BBS protein, BBS1 and is localized to the basal body (Nachury et al., 2007). Rabin8 is required for the activation and the entry of Rab8a into the cilium (Nachury et al., 2007). Moreover, BBS3 encodes an ARF-like (Arl) GTPase, Arl6 that is localized to the cilium (Jin et al., 2010). Arf (ADP ribosylation factors) and Arl GTPase family proteins are implicated in membrane trafficking and actin cytoskeleton remodeling (Gillingham and Munro, 2007). It has been reported that a GTP-bound conformation of Arl6 is responsible for sorting membrane proteins to cilia (Jin et al., 2010). The Sec7 family of GEFs is responsible for activating the Arf and Arl GTPases and seem to be involved in cilia formation as well (Bell et al., 2009). However, it still remains elusive how Arl6 is activated at cilia and how the different small GTPases coordinate with each other to mediate membrane trafficking at cilia.

FSM assembly provides a model system with parallels to study cilia formation. In order to gain more insight into how small G proteins regulate membrane formation, the role of *mug79⁺* in FSM assembly was examined. *mug79⁺* encodes a protein containing a divergent *SEC7* GEF domain that is required for spore formation in *S. pombe* (Martin-Castellanos et al., 2005) (Figure 5). In this study, we show that *mug79⁺* is essential for FSM assembly and might have a regulatory role in localizing the Rabin8 homologue, Spo13.

Figure 5. Domain diagram of Mug79. *mug79⁺* encodes a protein of 1318 amino acids that includes a predicted N-terminal coiled-coil domain, a central divergent Sec7 GEF domain, and a C-terminal PH domain.

Materials and Methods

Yeast strain construction

The strains used in this study are listed in Table 5. To construct a chromosomally GFP-tagged *mug79*$^+$ strain, the cassette containing a C-terminally positioned GFP was first generated by polymerase chain reaction (PCR) (Longtine et al., 1998) using pFA6a-*mug79*$^+$*C-term*-GFP(S65T)-KanMX6-*mug79*$^+$*3'UTR* as a template and HJO239 and HJO238 as primers. JLP18 (a gift from Janet Leatherwood) and HJP1 were than transformed with the PCR products to generate HJP2 (*mug79*$^+$-*GFP-Kan*^{r}) and HJP4 (*spo13-B82 mug79*$^+$-*GFP-Kan*^{r}), respectively.

HJP3 (*mug79ΔKan*^{r}) and HJP6 (*spo13-B82 mug79ΔKan*^{r}) were constructed by deleting *mug79*$^+$ in JLP18 and HJP1, respectively, by PCR-based gene deletion using pFA6a-*mug79*$^+$*5'UTR*-GFP(S65T)-KanMX6-*mug79*$^+$*3'UTR* as a template and HJO241 and HJO242 as primers.

Plasmids

The strains used in this study are listed in Table 6.

To construct pFA6a-GFP(S65T)-KanMX6-*mug79*$^+$*3'UTR*, pFA6a-GFP(S65T)-KanMX6 (Longtine et al., 1998) was used as the vector backbone. The *mug79*$^+$*3'UTR* were amplified from *S. pombe* genomic DNA by oligos HJO237 and HJO238. The PCR products were purified, digested with PmeI and SacI, and cloned into similarly digested pFA6a-GFP(S65T)-KanMX6.

To make pFA6a-*mug79*$^+$*C-term*-GFP(S65T)-KanMX6-*mug79*$^+$*3'UTR*, the *mug79*$^+$*C-term* was amplified by HJO239 and HJO240, digested with BamHI and PacI, and cloned into similarly digested GFP(S65T)- KanMX6-*mug79*$^+$*3'UTR*. To make the plasmid of pFA6a-*mug79*$^+$*5'UTR*-GFP(S65T)- KanMX6-*mug79*$^+$*3'UTR*, the *mug79*$^+$*5'UTR* was amplified by HJO241 and HJO242, digested with BamHI and PacI, and cloned into similarly digested GFP(S65T)- KanMX6-*mug79*$^+$*3'UTR*.

For pJRU-MCS2-P$_{mug79}$-*mug79*$^+$-GFP and pJRU-MCS2-P$_{mug79}$-*ΔNmug79*–GFP, pJRU-MCS2 was used as vector backbone. The *mug79*$^+$ promoter (−800 upstream of

first ATG) was amplified from *S. pombe* genomic DNA by oligos HJO269 and HJO270. The PCR products was purified, digested with KpnI and SpeI, and cloned into similarly digested pJRU-MCS2 to create pJRU-MCS2-P$_{mug79}$. The *mug79$^+$*-GFP was PCR amplified using genomic DNA of HJP2 (*mug79$^+$-GFP-Kan^r*) as a template and HJO259 and HJO198 as oligos. A SpeI-BamHI–digested PCR fragment was cloned into similarly digested pJRU-MCS2-P$_{mug79}$. Likewise, the *ΔNmug79*–GFP was PCR amplified by HJO272 and HJO198, digested with BamHI and SpeI, and cloned into pJRU-MCS2-P$_{mug79}$ to make pJRU-MCS2-P$_{mug79}$-*ΔNmug79*–GFP.

Fluorescence microscopy

Freshly transformed *S. pombe* cells were cultured in 3 ml of EMM2 (3 g/l potassium hydrogen phthalate, 2.2 g/l sodium phosphate dibasic, 5 g/l ammonium chloride, 20 g/l dextrose, 2.1 g/l minimal salts, 0.2 g/l vitamins, and 3 mg/l trace elements), with selective supplements (75 µg/ml adenine and 225 µg/ml histidine) for 24 h. The cells were precipitated, washed twice with 1 ml EMM-N sporulation medium (3 g/l potassium hydrogen phthalate, 2.2 g/l sodium phosphate dibasic, 20 g/l dextrose, 2.1 g/l minimals, 0.2 g/l vitamins, and 3 mg/l trace elements). The cells were induced to enter meiosis by incubating in 3 ml of EMM-N at room temperature. After 12-15h incubation in the EMM-N, aliquots of cells were examined in an Axioplan2 microscope (Carl Zeiss, Thornwood, NY). Fluorescence images were obtained by using Axiovision release 4.7.

Table 5 Strains used in appendix 1

Strain	Genotype	Source
HJP1	*h90 ura4-294 leu1-32 spo13-B82*	(Yang and Neiman, 2010)
HJP2	*h90 ura4-D18 leu1-32 his3-127 mug79⁺-GFP-Kan^r*	This study
HJP3	*h90 ura4-D18 leu1-32 his3-127mug79ΔKan^r*	This study
HJP4	*h90 ura4-294 leu1-32 spo13-B82 mug79⁺-GFP-Kan^r*	This study
HJP6	*h90 ura4-294 leu1-32 spo13-B82 mug79ΔKan^r*	This study
JLP18	*h90 ura4-D18 leu1-32 his3-127*	This study

Table 6 Plasmids used in appendix 1

Plasmid	Selected Features	Source
pJRU-MCS2	Exp, $ars1$, $ura4^+$	(Moreno et al., 2000)
pJRU-MCS2-P$_{Spspo13}$-$Spspo13^+$-mRFP1	Exp, $ars1$, $ura4^+$	(Yang and Neiman, 2010)
pJRU-MCS2-P$_{mug79}$-$mug79^+$-GFP	Exp, $ars1$, $ura4^+$	This study
pJRU-MCS2-P$_{mug79}$-GFP	Exp, $ars1$, $ura4^+$	This study
pJRU-MCS2-P$_{mug79}$-$\Delta Nmug79$-GFP	Exp, $ars1$, $ura4^+$	This study
FY532 (pREP41-GFP-$psy1^+$)	Exp, $ars1$, $LEU2$	(Nakamura et al., 2001)
pFA6a-GFP(S65T)- KanMX6		(Longtine et al., 1998)
pFA6a-GFP(S65T)- KanMX6-$mug79^+3'UTR$		This study
pFA6a-$mug79^+C$-term-GFP(S65T)- KanMX6-$mug79^+3'UTR$		This study
pFA6a-$mug79^+5'UTR$ -GFP(S65T)- KanMX6-$mug79^+3'UTR$		This study

Results

Mug79 is localized to the SPBs at early Meiosis II

To examine the localization of Mug79, a chromosomal copy of *mug79*⁺ was C-terminally tagged with GFP. Consistent with report that *mug79*⁺ is a meiotically upregulated gene (Martin-Castellanos et al., 2005), the fluorescence signals of Mug79-GFP were most prominent at early Meiosis II and appeared as four foci. Mug79-GFP co-localized with Spo13-mRFP1, indicating that Mug79 is localized to the Meiosis II SPBs (Figure 6).
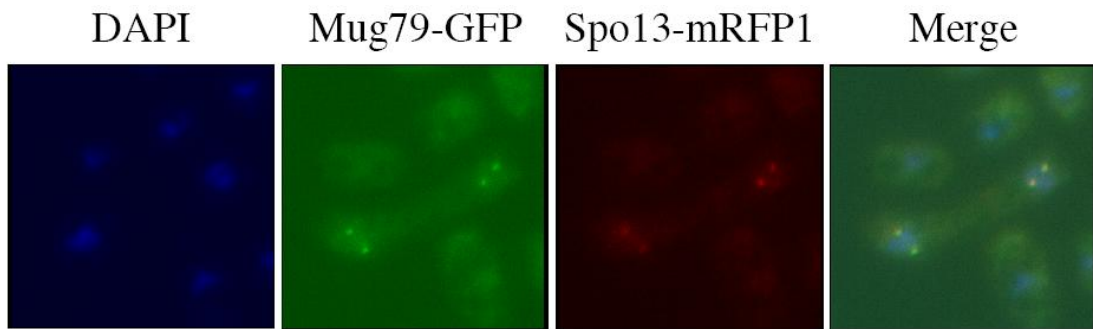

Figure 6. Mug79 is localized to the SPB at early Meiosis II. A plasmid carrying Spo13-mRFP1 was transformed into the strain, HJP2 (*mug79*⁺-GFP). Spo13-mRFP1 is a marker for the Meiosis II SPB. Cells were sporulated, fixed by ethanol, and stained with DAPI to monitor the cell stage.

A *mug79Δ* mutant is defective in FSM assembly

mug79⁺ is required for spore formation in *S. pombe* (Martin-Castellanos et al., 2005). In order to know how *mug79⁺* might regulate sporulation, I examined the phenotype of FSM assembly in the *mug79Δ* mutant. GFP-Psy1 was used to monitor the FSM assembly. In wild type, GFP-Psy1 is localized to the plasma membrane during vegetative growth and Meiosis I and shifts to the FSMs during Meiosis II. However, in the *mug79Δ* mutant, GFP-Psy1 is clustered in the cytoplasm rather than labeling FSM-like structures during Meiosis II (Figure 7). This result suggests that the sporulation defect of the *mug79Δ* mutant is due to a failure to assemble FSMs.

mug79⁺ is required for Spo13 localization

FSM assembly is initiated at the Meiosis II SPB and requires Spo13, one of the MOP components (Nakase et al., 2008). The above results show that Mug79 also localizes to the Meiosis II SPB and is essential for initiation of FSM assembly; therefore, I tested whether Spo13 is localized to the SPBs in the *mug79Δ* mutant.

In the *spo13-B82* mutant, Spo13-mRFP1 labels the Meiosis II SPBs, where FSM assembly is initiated (Figure 8A). Notably, the signal of Spo13-mRFP1 was much weaker in the *mug79Δspo13-B82* double mutant. In contrast, localization signal of Mug79-GFP at SPB is not affected in the *spo13-B82* mutant (Figure 8B). These observations suggest that Mug79 localization is independent of Spo13, but recruitment of Spo13 to the Meiosis II SPB is regulated by Mug79.
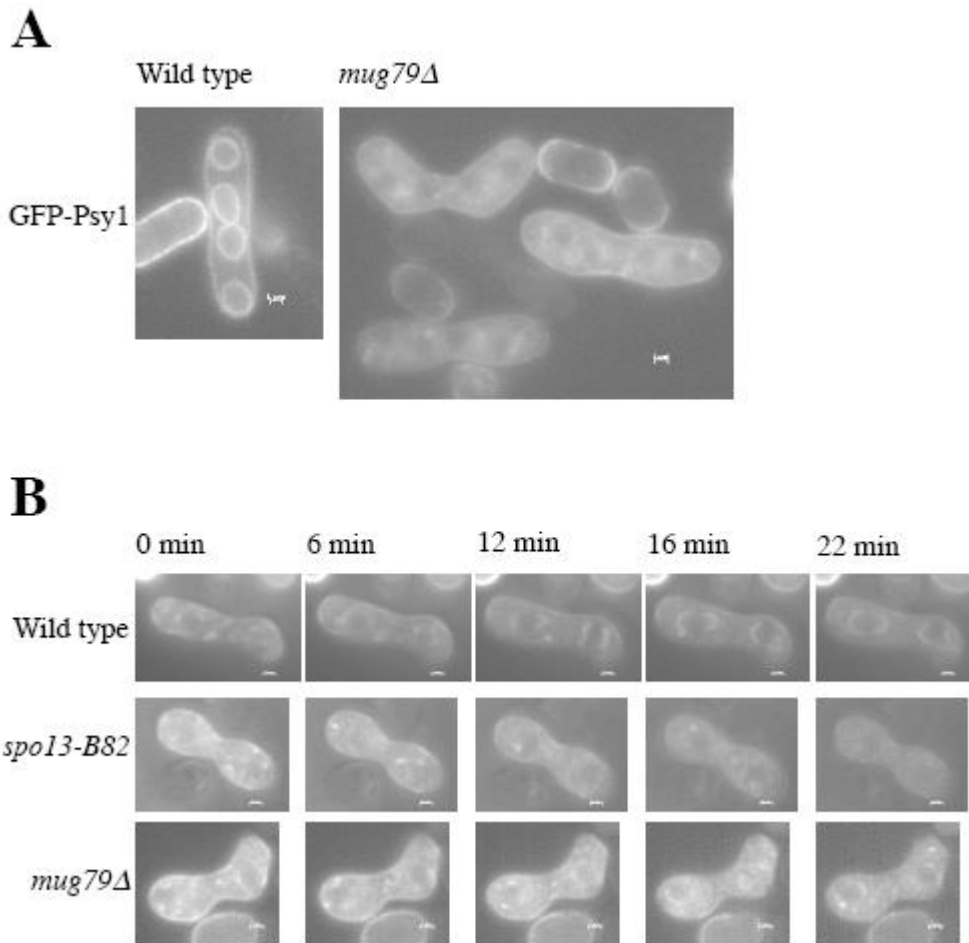
Figure 7. *mug79*⁺ **is required for FSM assembly.** A plasmid carrying GFP-Psy1 was transformed into wild-type cells, *spo13-B82* mutant cells, and *mug79Δ* mutants. (A) FSM assembly was examined by localization of GFP-Psy1. FSMs can be observed by the fluorescence signals of GFP-Psy1 during Meiosis II in the wild type, but not in the *mug79Δ* mutant. (B) Initiation of FSM assembly was monitored through live imaging of GFP-Psy1. At the onset of Meiosis II, GFP-Psy1 was dispersed in the cytoplasm (0 min). Expanded FSMs can be observed in the wild-type cells in 20 minutes. No apparent FSM-like structures were observed in the *spo13-B82* or *mug79Δ* mutants, although there were clusters of GFP-Psy1 in the cytoplasm.
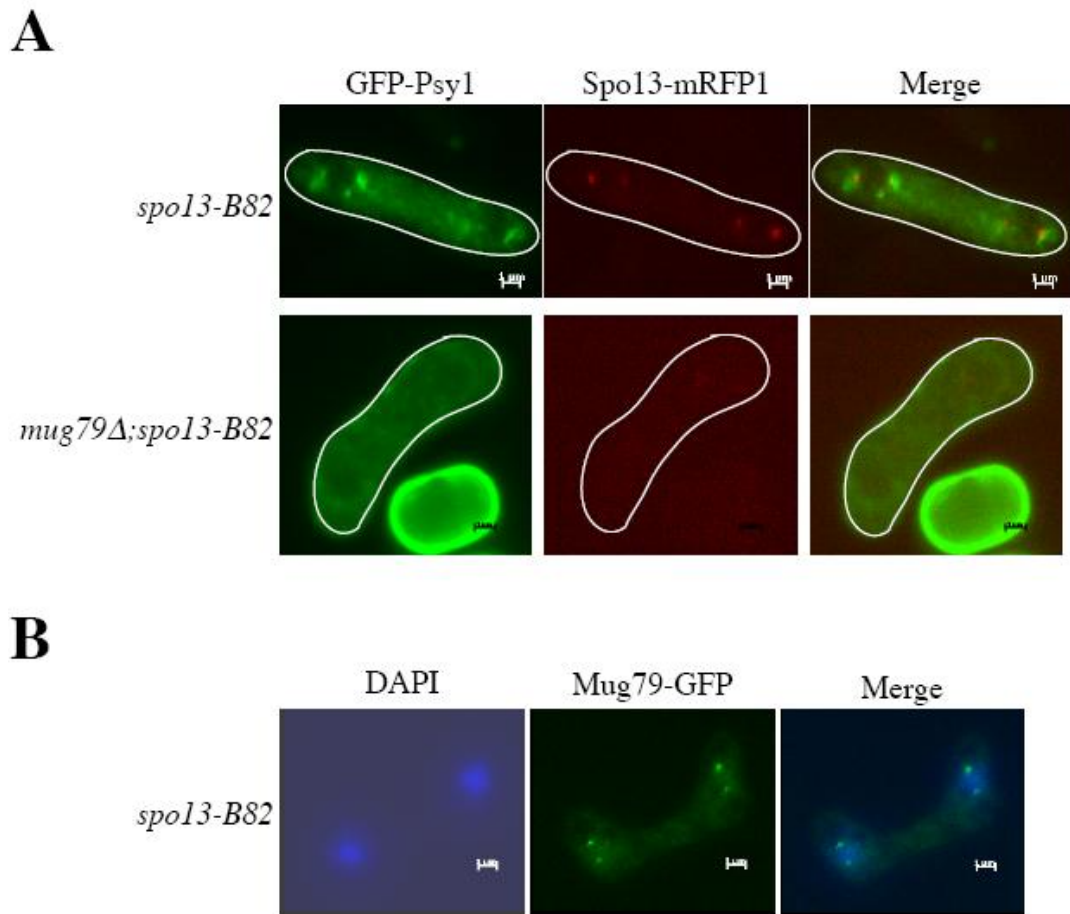
Figure 8. *mug79*⁺ is required for proper Spo13 localization, but not vice versa. (A) Fluorescence intensity of Spo13-mRFP1 is weak in the *mug79Δ* mutant. Plasmids carrying GFP-Psy1 or Spo13-mRFP1 were co-transformed into the *spo13-B82 or mug79Δ spo13-B82* mutants. (B) Mug79-GFP is localized properly in the *spo13-B82* mutant. PCR products containing the GFP tag and the selectable marker (*kanʳ*) were inserted at the C terminus of *mug79*⁺ through homologous recombination in the *spo13-B82* mutant.

ΔNMug79-GFP displays persistent signal at the nucleus throughout Meiosis II

mug79⁺ encodes a protein that includes a predicted N-terminal coiled-coil domain, a centrally divergent Sec7 GEF domain, and a C-terminal PH domain. I first examined whether the N-terminal domain (amino acids 1-690) is necessary for Mug79 function in FSM assembly. Plasmids carrying *mug79*⁺*-GFP* or an N-terminal truncation version, *ΔNmug79-GFP,* were transformed into the *mug79Δ* mutant. Although *mug79*⁺*-GFP* rescues the sporulation defect of the *mug79Δ* mutant up to 80% sporulation frequency, cells expressing *ΔNmug79-GFP* cannot sporulate.

The fluorescence signal of Mug79-GFP is most obvious at early Meiosis II SPB, and soon disappears during separation of sister chromatids (data not shown). Unlike the transient fluorescence signal of Mug79-GFP at the SPBs, the fluorescent signal of ΔNMug79-GFP is persistent throughout the Meiosis II and accumulated at the nucleus (Figure 9). These observations suggest that the N-terminal region (amino acids 1-690) of Mug79 is necessary for spore formation and may regulate the protein stability and localization of Mug79.
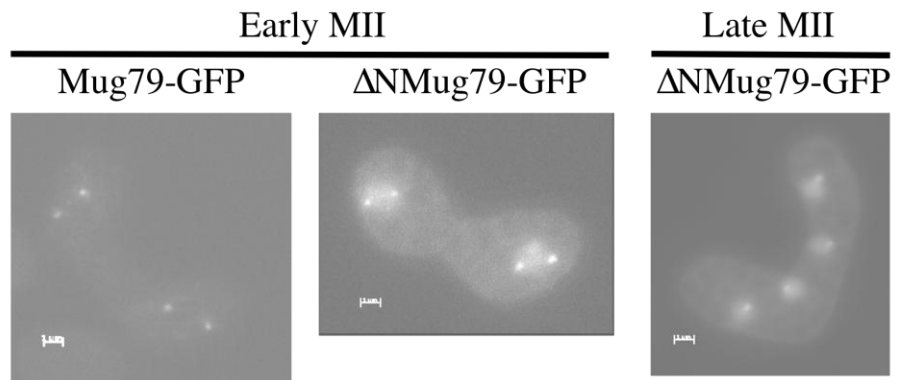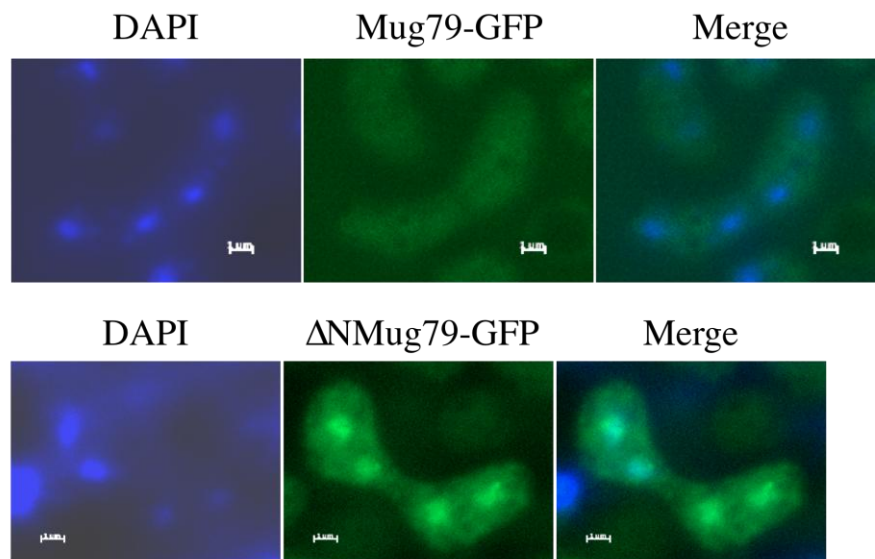
Figure 9. An N-terminal truncation of Mug79-GFP is mislocalized. (A) Mug79-GFP appears as four foci at early Meiosis II, while ΔNMug79-GFP accumulates in the nuclei during Meiosis II. (B) Mug79-GFP disappears at late Meiosis II, while ΔNMug79-GFP is still present. The cell stage is marked by DAPI staining.

Conclusions

In this study, I showed that Mug79 is transiently localized at the early Meiosis II SPBs is essential for FSM assembly. The localization of Mug79 is independent of one of the MOP components, Spo13. On the other hand, Spo13 localization requires *mug79*$^+$. Moreover, disruption of Mug79 N-terminal region affects the protein stability and localization. ΔNMug79-GFP is not functional and displays persistent nuclear localization through Meiosis II, suggesting that Mug79 needs to be tightly regulated during FSM assembly.

Future work will emphasize how Mug79 regulates FSM assembly and how Mug79 is regulated during sporulation. To further dissect the function of Mug79, it will be informative to see if the Sec7 GEF domain and the PH domain are required for FSM assembly and/or Spo13 localization. The mislocalization of Spo13 in the *mug79*Δ mutant raises the possibility that Mug79 is required for the Meiosis II SPB modification. This idea can be tested by examining the localization of the other MOP components, Spo2 and Spo15, in the *mug79*Δ mutant.

Appendix 2

The role of *YPT1* during prospore membrane formation in *S. cerevisiae*

When examining the fate of GFP-Snc1 expressed from the *CLB2* promoter, which is shut down during sporulation, it was found that GFP-Snc1 synthesized from vegetative cells moved from the plasma membrane to the prospore membrane (Morishita et al., 2007). Interestingly, however, the fate of GFP-Sso1 expressed from *CLB2* promoter was different as this protein accumulated in the vacuole instead of moving to the prospore membrane (Figure 10). Thus, the Sso1 functioning at the prospore membrane is newly synthesized protein. The different behavior of Snc1 and Sso1 during sporulation implys two different vesicular transport pathways to the prospore membrane: (1) vesicle trafficking from Golgi to prospore membrane, and (2) vesicle trafficking from plasma membrane or a cytosol compartment to prospore membrane. The two vesicular transport pathways could be mediated by different Rab GTPases. The goal of this study is to identify the Rab GTPases that mediate vesicle trafficking to prospore membrane.
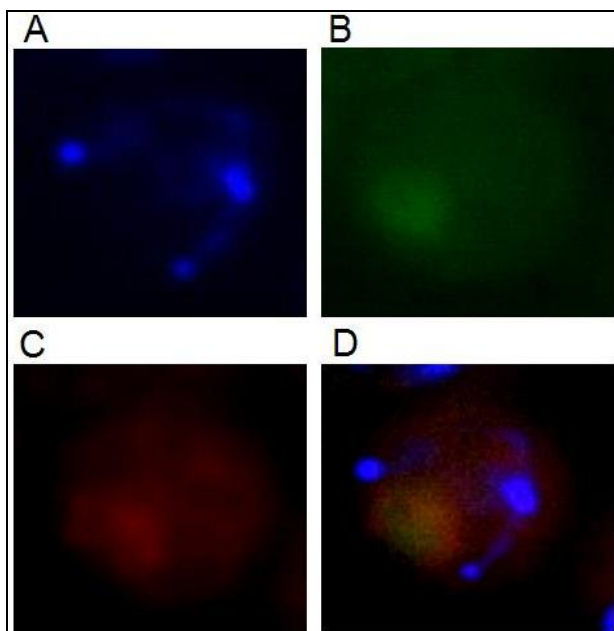

Figure 10. GFP-Sso1 synthesized from the vegetative growth is transported to the vacuole during sporulation.
(A) DAPI staining of Meiosis II chromatin.
(B) The signal of GFP-Sso1.
(C) The signal of FM4-64 marks vacuolar membrane.
(D) Merge. Note that GFP-Sso1 is surrounded by the signal of FM4-64, indicating that GFP-Sso1 is inside vacuole.

Materials and Methods

Yeast strain construction

The strains used in this study are listed in Table 7.

A *ypt1Δ* heterozygous diploid, HJ1, was constructed by deleting *YPT1* in AN120 by PCR-based gene deletion using pFA6a-His3MX6 as a template and HJO1 and HJO2 as primers. pRS416-*TEFpr-YPT1* was transformed into HJ1, and the resulting transformants were sporulated and dissected to get two opposite mating types of Ura$^+$ His$^+$ segregants. The two segregants were mated to get the *ypt1Δ* homozygous diploid, HJ7.

To get the *SEC4/YPT1* chimera mutants, HJ10, HJ11, HJ12, and HJ13, the plasmids of NRB420, NRB483, NRB500, and NRB471 were linearized by *BstX1* and integrated into the chromosomal *LEU2* locus of an *ypt1Δ* homozygous diploid carrying *pCEN-URA3-YPT1*, respectively. The transformed strains were then grown onto 5-FOA plate to select out the *URA3*-plasmid..

Plasmids

The plasmids used in this study are listed in Table 8. To construct pRS416*TEFpr-YPT1*, *YPT1* was first PCR amplified from pRS416*TEFpr*-GFP*YPT1* by HNO1041 and HNO1042. A XbaI–XhoI-digested PCR fragment was cloned into similarly digested pRS416TEF(Mumberg et al., 1995) .

pRS414*TEF*pr-*ypt1*^{I41M} was constructed by PCR site-directed mutagenesis against pRS416*TEFpr-YPT1* using HJO235 and HJO236 as primers.

pGADGH-*YPT1* and pGADGH-*YPT1ΔC* were constructed by cloning respective XbaI-XhoI-digested PCR products of *YPT1* and *YPT1ΔC* into SpeI-XhoI-digested pGADGH. *YPT1* was PCR amplified from pRS416*TEFpr*-GFP*YPT1* by HJO85 and HNO1042, and *YPT1ΔC* was PCR amplified from pRS416*TEFpr*-GFP*YPT1* by HJO85 and HJO86. PCR site-directed mutagenesis was targeted against pGADGH-*YPT1* or pGADGH-*YPT1ΔC* to generate pGADGH-*ypt1*^{S22N} and pGADGH-*ypt1*^{S22N}*ΔC* by HJO89 and HJO90. Likewise, pGADGH-*ypt1*^{N121I} and

pGADGH-*ypt1*^{N121I}*ΔC* were derived from pGADGH-*YPT1* and pGADGH-*YPT1ΔC* by site-directed mutagenesis using HJO93 and HJO94.

pRS424*SPO20pr-YPT1*, pRS424SPO20pr-*ypt1*^{S22N}, pRS424SPO20pr-*ypt1*^{N121I}, pRS424*SPO20pr-YPT1ΔC*, pRS424SPO20pr-*ypt1*^{S22N}*ΔC*, and pRS424SPO20pr-*ypt1*^{N121I}*ΔC* were constructed by cloning XbaI-XhoI-digested fragments containing *YPT1*, *ypt1*^{S22N}, *ypt1*^{N121I}, *YPT1ΔC*, *ypt1*^{S22N}*ΔC*, or *ypt1*^{N121I}*ΔC* into SpeI-XhoI-digested pRS424SPO20pr.

pRS306*SPS4pr* was constructed by cloning a SacI-SpeI-digested PCR fragment of *SPS4* promoter (-1000 upstream of first ATG) into similarly digested pRS306 (Sikorski and Hieter, 1989). The *SPS4* promoter was amplified from genomic DNA by oligos HJO166 and HJO177.

pRS426*CLB2pr-GFPSSO1* was constructed by cloning a SacI-BamHI-digested PCR fragment of *CLB2* promoter (-1000 upstream of first ATG) into similarly digested pRS426*TEFpr-GFPSSO1* (H. Nakanishi). The *CLB2* promoter was amplified from genomic DNA by oligos HJO50 and HJO56.

Sporulation assay

For measuring sporulation frequency, the strains to be tested were grown overnight on selective media, and then replica plated to sporulation medium. After 24 h, spore formation was quantified by direct observation in the light microscope.

For fluorescence microscopic observation, liquid sporulation was applied. Cells were grown in YPD (20g/l bactopeptone, 10g/l yeast extract, and 50ml/l 40% dextrose) or selective medium for overnight. The overnight culture was diluted into YPA (20g/l potassium acetate, 20g/l bactopeptone, and 10g/l yeast extract) as OD660 was about 0.2-0.3, and grown until the OD660 reached 1.2 (about 15-24 hours). The cells were shifted from YPA to 2% potassium acetate to sporulate. After sporulation in 2% potassium acetate for 6 hours, the cells were fixed, stained with DAPI and observed under fluorescence microscope.

Table 7 Strains used in appendix 2

Strain	Genotype	Source
HI58	MAT**a**/MATα ARG4/arg4-NspI his3△SK/his3△SK ho△::LYS2/ho△::LYS2 leu2/leu2 lys2/lys2 RME1/rme1::LEU2 ura3/ura3 trp1::hisG/trp1::hisG sso1△::his5+/sso1△::his5+ MPC54-RFP::URA3	(*Nakanishi et al., 2006*)
HJ1	MATa/MAT arg4/arg4-NspI his3SK/his3SK ho::LYS2/ho::LYS2 leu2/leu2 lys2/lys2 RME1/rme1::LEU2 trp1::hisG/trp1::hisG ura3/ura3 YPT1/ ypt1△his5+	This study
HJ7	MATa/MAT ARG4/arg4-NspI his3SK/his3SK ho::LYS2/ho::LYS2 leu2/leu2 lys2/lys2 RME1/rme1::LEU2 trp1::hisG/trp1::hisG ura3/ura3 ypt1△his5+/ ypt1△his5+	This study
HJ10	MATa/MAT ARG4/arg4-NspI his3△SK /his3△SK ho::LYS2/ho::LYS2 leu2/leu2 lys2/lys2 trp1::hisG/trp1::hisG ura3/ura3 ypt1△his5+/ ypt1△his5++pRS416TEF-YPT1	This study
HJ11	MATa/MAT ARG4/arg4-NspI his3△SK /his3△SK ho::LYS2/ho::LYS2 leu2/leu2 lys2/lys2 trp1::hisG/trp1::hisG ura3/ura3 ypt1△his5+/ ypt1△his5+ YPT1::LEU2	This study
HJ12	MATa/MAT ARG4/arg4-NspI his3△SK /his3△SK ho::LYS2/ho::LYS2 leu2/leu2 lys2/lys2 trp1::hisG/trp1::hisG ura3/ura3 Yp-EF^{S4}::LEU2	This study

Table 7 Strains used in appendix 2 (Continued)

Strain	Genotype	Source
	ypt1Δhis5+/ ypt1Δhis5+ Yp-L7ˢ⁴::LEU2	
HJ13	*MATa/MATα ARG4/arg4-NspI his3ΔSK /his3ΔSK ho::LYS2/ho::LYS2*	This study
	leu2/leu2 lys2/lys2 trp1::hisG/trp1::hisG ura3/ura3	
	ypt1Δhis5+/ ypt1Δhis5+ S4-(EF, L7, HV)ʸᵖ::LEU2	

Table 8 Plasmids used in appendix 2

Plasmids	Source
pRS416TEFpr-YPT1	This study
pRS416TEFpr-GFPYPT1	H. Nakanishi
pRS416TEFpr-GFPSEC4	H. Nakanishi
pRS416TEFpr-GFPYPT6	H. Nakanishi
pRS416TEFpr-GFPYPT31	H. Nakanishi
NRB420 (*LEU2, YPT1*)	(Brennwald and Novick, 1993)
NRB483 (*LEU2*, Yp-EF^{S4})	(Brennwald and Novick, 1993)
NRB500 (*LEU2*, Yp-L7^{S4})	(Brennwald and Novick, 1993)
NRB471 (*LEU2, S4-(EF, L7, HV)^{Yp}*)	(Brennwald and Novick, 1993)
pGADGH	Greg Hannon
pGADGH-*YPT1*	This study
pGADGH-*ypt1*^{S22N}	This study
pGADGH-*ypt1*^{N121I}	This study
pGADGH-*YPT1ΔC*	This study
pGADGH-*ypt1*^{S22N}*ΔC*	This study
pGADGH-*ypt1*^{N121I}*ΔC*	This study
pRS424SPO20pr	(Nakanishi et al., 2004)

Table 8 Plasmids used in appendix 2 (Continued)

Plasmids	Source
pRS424SPO20pr- $YPT1$	This study
pRS424SPO20pr-$ypt1^{S22N}$	This study
pRS424SPO20pr-$ypt1^{N121I}$	This study
pRS424SPO20pr- $YPT1\Delta C$	This study
pRS424SPO20pr- $ypt1^{S22N}\Delta C$	This study
pRS424SPO20pr- $ypt1^{N121I}\Delta C$	This study
pRS306SPS4pr	This study
pRS306SPS4pr- $ypt1^{N121I}\Delta C$	This study
pRS414TEFpr-$ypt1^{I41M}$	This study
pRS426CLB2pr-GFPSSO1	This study
pRS406GFP-SNC1	(Lewis et al., 2000)

Results

GFP-Ypt1 is localized to the SPB during Meiosis II

In order to determine which Rab GTPase(s) regulates prospore membrane vesicular transport, the localization of the Rab proteins, Sec4, Ypt1, Ypt6, and Ypt31, relative to the SPB during sporulation was examined (Figure 10). To visualize the Rab GTPase and SPB, the Rab proteins were N-terminally tagged with GFP and expressed under the *TEF2* promoter, and the SPB was labeled by RFP-tagged MPC54 (a MOP component). Because Rab GTPases cycle between membrane compartments, I used an *sso1Δ* mutant (HI58), which accumulates the vesicles around the MOP without prospore membrane formation, to facilitate the observation of Rab GTPase localization.

We found that GFP-Ypt1 and GFP-Sec4 are localized at the SPBs in sporulating *sso1Δ* cells. It is not unexpected to see GFP-Sec4 at the SPBs since it is known that *SEC4* is required for prospore membrane formation (Neiman, 1998). The finding of GFP-Ypt1 at SPBs raises the possibility that Ypt1 might also regulate membrane fusion at prospore membrane.

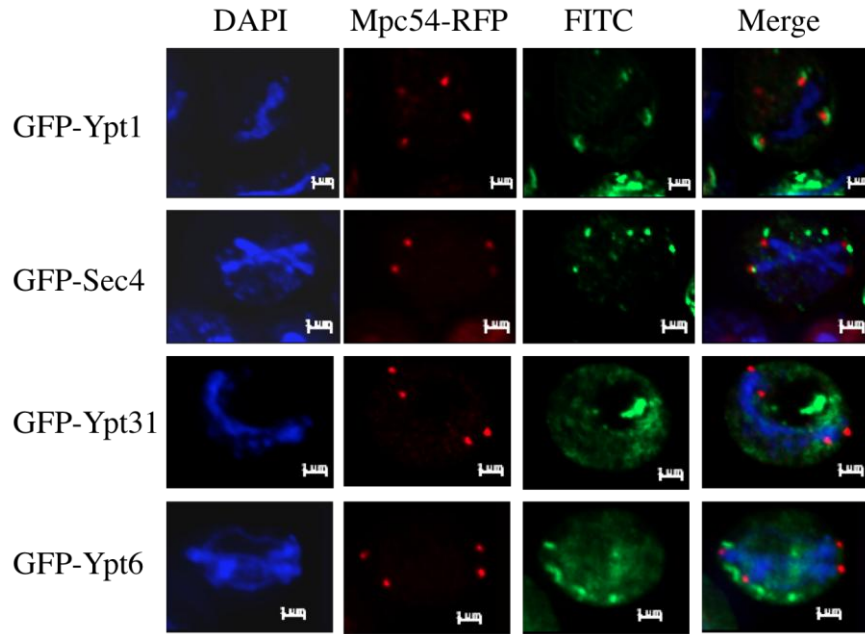|	DAPI	Mpc54-RFP	FITC	Merge
GFP-Ypt1				
GFP-Sec4				
GFP-Ypt31				
GFP-Ypt6				

Figure 11. GFP-Ypt1 localizes to SPBs at Meiosis II. The Meiosis II chromatin masses are labeled by DAPI staining, and the SPBs are indicated by Mpc54-RFP. Each Rab GTPase is visualized by N-terminal tagged GFP.

SEC4/YPT1 chimeras exhibit sporulation defect

YPT1 is an essential gene, which makes us unable to analyze the sporulation defect of *ypt1Δ* mutants. We therefore sought *ypt1* alleles that allow good vegetative growth, but show a sporulation defect. Several *SEC4/YPT1* chimeras have been constructed in order to identify the domain(s) required for specific function of Sec4 and Ypt1 (Brennwald and Novick, 1993). Among these *SEC4/YPT1* chimeras, the chimeras of *S4-(EF, L7, HV)^{Yp}, Yp-HV^{S4}, Yp-L7^{S4}*, and *Yp-EF^{S4}* fail to complement the growth defect of a *sec4Δ* mutant, but can complement the growth defect of an *ypt1Δ* mutant (Figure 11A).

I then examined if these *SEC4/YPT1* chimeras can support sporulation in a *ypt1Δ* mutant. Homozygous *ypt1Δ* diploids expressing the *SEC4/YPT1* chimera constructs integrated into the chromosome at the *LEU2* site were examined for sporulation defects. Compared to the 80% sporulation frequency of wild-type *YPT1*, the sporulation frequency of S4-(EF, L7, and HV)^{Yp} mutant was 10% and of Yp-EF^{S4} mutant was 30%. The Yp-L7^{S4} mutant displayed no spore formation at all (Figure 11B). Noticeably, the Yp-L7^{S4} mutant grew much slower than *YPT1* wild type cells (data not shown); therefore, I suspect that the sporulation defect of Yp-L7^{S4} mutant might be a secondary effect accumulated from the growth defect of vegetative cells. However, more careful examination for the Meiosis progression of Yp-L7^{S4} mutant is required. In sum, all the chimera mutants I have analyzed show sporulation defects, indicating an essential role of *YPT1* during sporulation. Nonetheless, the result that the *S4-(EF, L7, HV)^{Yp}, Yp-L7^{S4}*, and *Yp-EF^{S4}* chimeras all show sporulation defects does not allow a clear determination of which specific domains are required for *YPT1* function in spore formation.
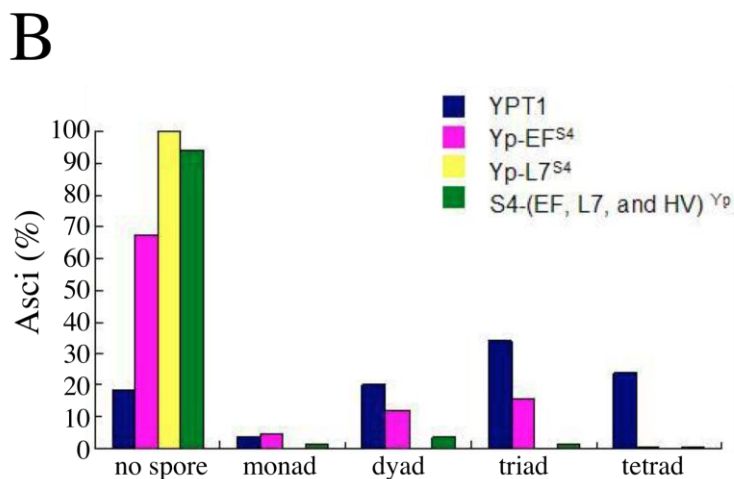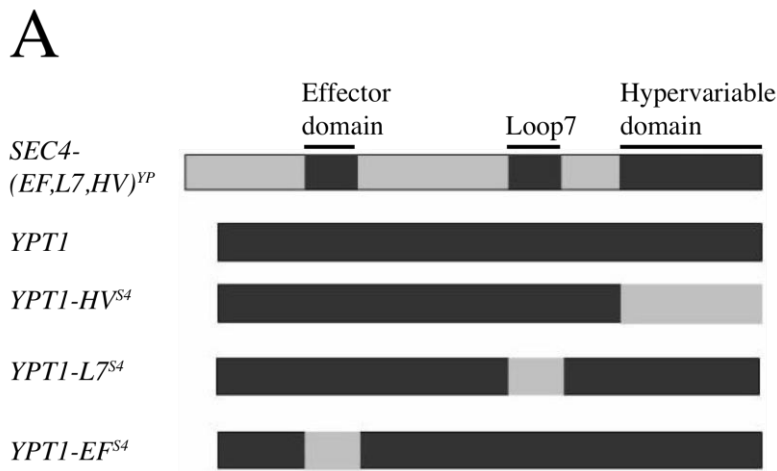
Figure 12. *SEC4/YPT1* **chimeras show sporulation defect.** (A) Diagram of the *SEC4/YPT1* chimeras of *SEC4-(EF, L7, HV)^{Yp}*, *YPT1-HV^{S4}*, *YPT1-L7^{S4}*, and *YPT1-EF^{S4}*. Gray bars represent sequences from Sec4, and black bars represent sequences from Ypt1. YP=*YPT1*; S4=*SEC4*; EF= effector domain; L7= Loop7; HV= Hypervariable domain. (B) Homozygote *ypt1Δ* diploids expressing the *SEC4/YPT1* chimera constructs integrated into the chromosome at the *LEU2* site were examined for sporulation frequency. As a control, an *ypt1Δ* homozygote expressing *YPT1* in the same plasmid was also examined. The X-axis represents the numbers of spores in an ascus. The Y-axis represents the percentages of cells were observed.

Ectopic expression of the *ypt1*^{N121I} dominant-negative allele in wild-type cells leads to sporulation defect

I next tried to block *YPT1* function by overexpression the dominant-negative form, *ypt1*^{N121I} in wild-type cells during sporulation. Interestingly, the prospore membrane fails to capture the nuclei in the *ypt1*^{N121I} dominant-negative mutant (Figure 12B). An observation from early electron microscopic studies showed that Meiosis II SPBs detached from prospore membranes after membrane closure. The phenotype of the *ypt1*^{N121I} mutant might reflect slow growing prospore membranes due to an incomplete early block of vesicle trafficking from ER to the Golgi. Alternatively, Ypt1 might regulate associations between the SPBs and the prospore membranes.
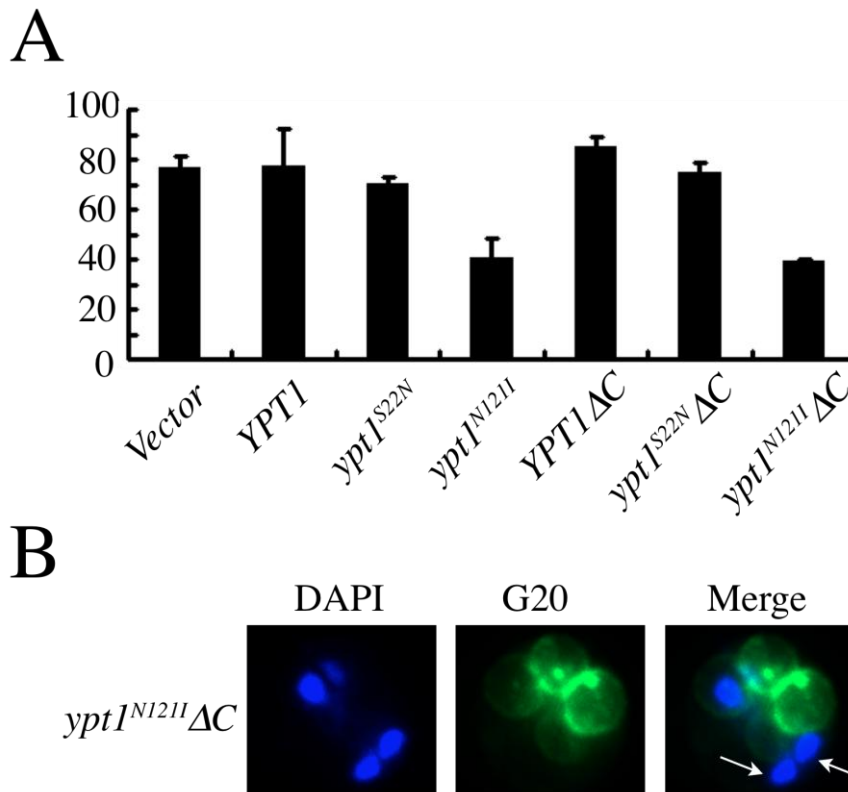
Figure 13. The *ypt1^{N121I}* allele shows sporulation defect.

(A) Various mutant forms of *ypt1* were expressed under *SPO20* promoter from 2μ plasmids in wild-type cells (AN120). Cells transformed with the vector alone or the plasmids carrying *YPT1* were included as controls. Ypt1^{N121I} is unable to bind guanine nucleotide and locked in nucleotide-free form. Ypt1^{S22N} may hold in the GDP-bound conformation. Ypt1ΔC deletes the C-terminal cysteines that are necessary for lipid modification and thus the membrane association of Ypt1.

(B) Prospore membranes fail to capture the nuclei in cells expressing *ypt1^{N121I}ΔC* from an integrating plasmid. The prospore membranes are labeled by G20. Arrowheads indicated un-captured nuclei by the prospore membranes. *ypt1^{N121I}ΔC* driven by *SPS4* promoter were integrated in the *URA3* locus in the wild-type cells. The cells expressing *ypt1^{N121I}ΔC* from the integrating plasmid are almost absent in sporulation (0.1% sporulation frequency, n=600).

An *ypt1^I41M* mutant that shows GFP-Snc1 recycling defect sporulates well

In vegetative cells, it is known that Snc1 at the cell surface undergoes endocytosis and resecretion via the Golgi back to the plasma membrane (Lewis et al., 2000). During sporulation, it was found that GFP-Snc1 synthesized from vegetative cells was moved from the plasma membrane to the prospore membrane (Morishita et al., 2007). I then asked if the GFP-Snc1 is en route from the Golgi to the prospore membrane during sporulation by examining the sporulation frequency of an *ypt1^I41M* allele. The *ypt1^I41M* allele is defective in GFP-Snc1 retrieval from endosome to Golgi (Sclafani et al., 2010). A *CEN-TRP1*-plasmid carrying *ypt1^I41M* was transformed into HJ7 (*ypt1Δ/ ypt1Δ*; *pCEN-URA3-YPT1*). The transformed strains were grown on a plate containing 5-fluoroorotic acid (5-FOA) to select for loss of the *URA3*-plasmid containing wild-type *YPT1*. Surprisingly, the *ypt1^I41M* allele sporulates well (Figure 13), suggesting that vesicular transport of GFP-Snc1 to the prospore membrane is independent of Ypt1-mediated endosome to Golgi retrieval.
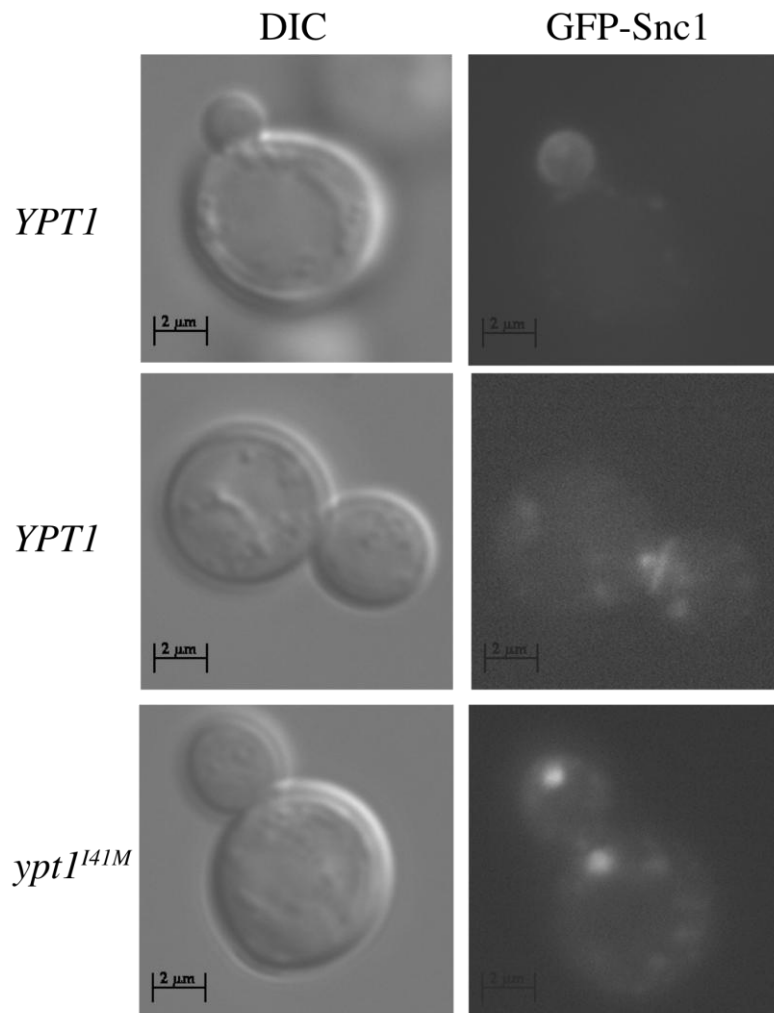
Figure 14. The *ypt1^I41M* allele *s*hows GFP-Snc1 recycling defect. GFP-Snc1 localization was examined in homozygous *ypt1Δ* diploids expressing *YPT1* or *ypt1^I41M* on a *CEN-TRP1*-plasmid. GFP-Snc1 is found on the plasma membrane or bud neck in the wild type, while GFP-Snc1 appeared as internal punctae in the *ypt1^I41M* mutant (also see Sclafani et al., (2010)). The *ypt1^I41M* mutant can sporulate as well as the wild type (70% sporulation frequency).

Conclusions

GFP-Ypt1 and GFP-Sec4 are both localized at the SPBs in sporulating cells, suggesting that Sec4 and Ypt1 might mediate two distinct vesicular transport pathways to prospore membrane. It is known that Sec4 mediates trafficking to prospore membrane of post-Golgi vesicles (Neiman, 1998). Intriguingly, GFP-Snc1 synthesized from vegetative cells was moved from the plasma membrane to the prospore membrane (Morishita et al., 2007). Moreover, the analysis of the $ypt1^{I41M}$ mutant shows that GFP-Snc1 retrieval from endosome to Golgi is not required for sporulation. Taken together, the behavior of GFP-Snc1 during sporulation suggests that there is a vesicular transport pathway from plasma membrane or endosome to prospore membrane. The future work will need to identify more proteins that undertake this route to the prospore membrane and examine how this vesicular transport pathway is mediated, in which Ypt1 might play a role.

Several sporulation-specific *ypt1* alleles have been identified, including the *SEC4/YPT1* chimera mutants and the $ypt1^{N121I}$ mutant. How these mutant alleles affect sporulation remains an open question.

References

Aalto, M.K., J. Jantti, J. Ostling, S. Keranen, and H. Ronne. 1997. Mso1p: a yeast protein that functions in secretion and interacts physically and genetically with Sec1p. *Proc Natl Acad Sci U S A*. 94:7331-7336.

Aalto, M.K., H. Ronne, and S. Keranen. 1993. Yeast syntaxins Sso1p and Sso2p belong to a family of related membrane proteins that function in vesicular transport. *Embo J*. 12:4095-104.

Adams, I.R., and J.V. Kilmartin. 1999. Localization of core spindle pole body (SPB) components during SPB duplication in Saccharomyces cerevisiae. *J Cell Biol*. 145:809-23.

Bajgier, B.K., M. Malzone, M. Nickas, and A.M. Neiman. 2001. *SPO21* is required for meiosis-specific modification of the spindle pole body in yeast. *Mol Biol Cell*. 12:1611-1621.

Becker, T., A. Volchuk, and J.E. Rothman. 2005. Differential use of endoplasmic reticulum membrane for phagocytosis in J774 macrophages. *Proc Natl Acad Sci U S A*. 102:4022-6.

Bell, A.J., C. Guerra, V. Phung, S. Nair, R. Seetharam, and P. Satir. 2009. GEF1 is a ciliary Sec7 GEF of Tetrahymena thermophila. *Cell Motil Cytoskeleton*. 66:483-99.

Bock, J.B., H.T. Matern, A.A. Peden, and R.H. Scheller. 2001. A genomic perspective on membrane compartment organization. *Nature*. 409:839-41.

Bos, J.L., H. Rehmann, and A. Wittinghofer. 2007. GEFs and GAPs: critical elements in the control of small G proteins. *Cell*. 129:865-877.

Brennwald, P., B. Kearns, K. Champion, S. Keranen, V. Bankaitis, and P. Novick. 1994. Sec9 is a SNAP-25-like component of a yeast SNARE complex that may be the effector of Sec4 function in exocytosis. *Cell*. 79:245-58.

Brennwald, P., and P. Novick. 1993. Interactions of three domains distinguishing the Ras-related GTP-binding proteins Ypt1 and Sec4. *Nature*. 362:560-3.

Bresch, C., G. Muller, and R. Egel. 1968. Genes involved in meiosis and sporulation of a yeast. *Mol Gen Genet*. 102:301-306.

Bucking-Throm, E., W. Duntze, L.H. Hartwell, and T.R. Manney. 1973. Reversible arrest of haploid yeast cells in the initiation of DNA synthesis by a diffusible sex factor. *Exp Cell Res*. 76:99-110.

Byers, B. 1981. Cytology of the yeast life cycle, p.59-96. In J. N. Strathern, E. W. Jones, and J. R. Broach (ed.), The molecular biology of the yeast Saccharomyces: life cycle and inheritance. Cold Spring Harbor Laboratory Press, Cold Spring Harbor, N.Y.

Cai, Y., H.F. Chin, D. Lazarova, S. Menon, C. Fu, H. Cai, A. Sclafani, D.W. Rodgers, E.M. De La Cruz, S. Ferro-Novick, and K.M. Reinisch. 2008. The structural basis for activation of the Rab Ypt1p by the TRAPP membrane-tethering complexes. *Cell*. 133:1202-1213.

Carr, C.M., E. Grote, M. Munson, F.M. Hughson, and P.J. Novick. 1999. Sec1p binds to SNARE complexes and concentrates at sites of secretion. *J Cell Biol*. 146:333-44.

Celio, G.J., M. Padamsee, B.T. Dentinger, R. Bauer, and D.J. McLaughlin. 2006. Assembling the Fungal Tree of Life: constructing the structural and biochemical database. *Mycologia*. 98:850-9.

Chang, L., and K.L. Gould. 2000. Sid4p is required to localize components of the septation initiation pathway to the spindle pole body in fission yeast. *Proc Natl Acad Sci U S A*. 97:5249-54.

Christianson, T.W., R.S. Sikorski, M. Dante, J.H. Shero, and P. Hieter. 1992. Multifunctional yeast high-copy-number shuttle vectors. *Gene*. 110:119-22.

Chu, S., J. DeRisi, M. Eisen, J. Mulholland, D. Botstein, P.O. Brown, and I. Herskowitz. 1998. The transcriptional program of sporulation in budding yeast. *Science*. 282:699-705.

Coluccio, A., E. Bogengruber, M.N. Conrad, M.E. Dresser, P. Briza, and A.M. Neiman. 2004a. Morphogenetic pathway of spore wall assembly in Saccharomyces cerevisiae. *Eukaryot Cell*. 3:1464-75.

Coluccio, A., M. Malzone, and A.M. Neiman. 2004b. Genetic evidence of a role for membrane lipid composition in the regulation of soluble NEM-sensitive factor receptor function in Saccharomyces cerevisiae. *Genetics*. 166:89-97.

Coluccio, A.E., R.K. Rodriguez, M.J. Kernan, and A.M. Neiman. 2008. The yeast spore wall enables spores to survive passage through the digestive tract of Drosophila. *PLoS One*. 3:e2873.

Craighead, M.W., S. Bowden, R. Watson, and J. Armstrong. 1993. Function of the *ypt2* gene in the exocytic pathway of *Schizosaccharomyces pombe*. *Mol Biol Cell*. 4:1069-1076.

Diamond, A.E., J.S. Park, I. Inoue, H. Tachikawa, and A.M. Neiman. 2009. The anaphase promoting complex targeting subunit Ama1 links meiotic exit to cytokinesis during sporulation in *Saccharomyces cerevisiae*. *Mol Biol Cell*. 20:134-145.

Dong, G., M. Medkova, P. Novick, and K.M. Reinisch. 2007. A catalytic coiled coil: structural insights into the activation of the Rab GTPase Sec4p by Sec2p. *Mol Cell*. 25:455-462.

Elkind, N.B., C. Walch-Solimena, and P.J. Novick. 2000. The role of the COOH terminus of Sec2p in the transport of post-Golgi vesicles. *J Cell Biol*. 149:95-110.

Fasshauer, D., W. Antonin, M. Margittai, S. Pabst, and R. Jahn. 1999. Mixed and non-cognate SNARE complexes. Characterization of assembly and biophysical properties. *J Biol*

Chem. 274:15440-6.

Fasshauer, D., R.B. Sutton, A.T. Brunger, and R. Jahn. 1998. Conserved structural features of the synaptic fusion complex: SNARE proteins reclassified as Q- and R-SNAREs. *Proc Natl Acad Sci U S A*. 95:15781-6.

Gao, X.D., H. Tachikawa, T. Sato, Y. Jigami, and N. Dean. 2005. Alg14 recruits Alg13 to the cytoplasmic face of the endoplasmic reticulum to form a novel bipartite UDP-N-acetylglucosamine transferase required for the second step of N-linked glycosylation. *J Biol Chem*. 280:36254-36262.

Gerdes, J.M., E.E. Davis, and N. Katsanis. 2009. The vertebrate primary cilium in development, homeostasis, and disease. *Cell*. 137:32-45.

Gillingham, A.K., and S. Munro. 2007. The small G proteins of the Arf family and their regulators. *Annu Rev Cell Dev Biol*. 23:579-611.

Graf, C.T., D. Riedel, H.D. Schmitt, and R. Jahn. 2005. Identification of functionally interacting SNAREs by using complementary substitutions in the conserved '0' layer. *Mol Biol Cell*. 16:2263-74.

Gromley, A., A. Jurczyk, J. Sillibourne, E. Halilovic, M. Mogensen, I. Groisman, M. Blomberg, and S. Doxsey. 2003. A novel human protein of the maternal centriole is required for the final stages of cytokinesis and entry into S phase. *J Cell Biol*. 161:535-45.

Gromley, A., C. Yeaman, J. Rosa, S. Redick, C.T. Chen, S. Mirabelle, M. Guha, J. Sillibourne, and S.J. Doxsey. 2005. Centriolin anchoring of exocyst and SNARE complexes at the midbody is required for secretory-vesicle-mediated abscission. *Cell*. 123:75-87.

Grosshans, B.L., A. Andreeva, A. Gangar, S. Niessen, J.R. Yates, 3rd, P. Brennwald, and P. Novick. 2006a. The yeast lgl family member Sro7p is an effector of the secretory Rab GTPase Sec4p. *J Cell Biol*. 172:55-66.

Grosshans, B.L., D. Ortiz, and P. Novick. 2006b. Rabs and their effectors: achieving specificity in membrane traffic. *Proc Natl Acad Sci U S A*. 103:11821-7.

Gruneberg, U., K. Campbell, C. Simpson, J. Grindlay, and E. Schiebel. 2000. Nud1p links astral microtubule organization and the control of exit from mitosis. *Embo J*. 19:6475-88.

Guo, W., D. Roth, C. Walch-Solimena, and P. Novick. 1999. The exocyst is an effector for Sec4p, targeting secretory vesicles to sites of exocytosis. *Embo J*. 18:1071-1080.

Guth, E., T. Hashimoto, and S.F. Conti. 1972. Morphogenesis of ascospores in Saccharomyces cerevisiae. *J Bacteriol*. 109:869-80.

Hattendorf, D.A., A. Andreeva, A. Gangar, P.J. Brennwald, and W.I. Weis. 2007. Structure of the yeast polarity protein Sro7 reveals a SNARE regulatory mechanism. *Nature*.

446:567-71.

Hayles, J., and P. Nurse. 1989. A review of mitosis in the fission yeast Schizosaccharomyces pombe. *Exp Cell Res*. 184:273-86.

Herskowitz, I. 1988. Life cycle of the budding yeast Saccharomyces cerevisiae. *Microbiol Rev*. 52:536-53.

Hirata, A., and C. Shimoda. 1994. Structural modification of spindle pole bodies during meiosis II is essential for the normal formation of ascospores in *Schizosaccharomyces pombe*: ultrastructural analysis of *spo* mutants. *Yeast*. 10:173-183.

Hoyer-Fender, S. 2010. Centriole maturation and transformation to basal body. *Semin Cell Dev Biol*. 21:142-7.

Ishikawa, H., A. Kubo, S. Tsukita, and S. Tsukita. 2005. Odf2-deficient mother centrioles lack distal/subdistal appendages and the ability to generate primary cilia. *Nat Cell Biol*. 7:517-24.

Jahn, R., and R.H. Scheller. 2006. SNAREs--engines for membrane fusion. *Nat Rev Mol Cell Biol*. 7:631-43.

Jantti, J., M.K. Aalto, M. Oyen, L. Sundqvist, S. Keranen, and H. Ronne. 2002. Characterization of temperature-sensitive mutations in the yeast syntaxin 1 homologues Sso1p and Sso2p, and evidence of a distinct function for Sso1p in sporulation. *J Cell Sci*. 115:409-20.

Jaspersen, S.L., and M. Winey. 2004. The budding yeast spindle pole body: structure, duplication, and function. *Annu Rev Cell Dev Biol*. 20:1-28.

Jin, H., S.R. White, T. Shida, S. Schulz, M. Aguiar, S.P. Gygi, J.F. Bazan, and M.V. Nachury. 2010. The conserved Bardet-Biedl syndrome proteins assemble a coat that traffics membrane proteins to cilia. *Cell*. 141:1208-19.

Jones, S., C. Newman, F. Liu, and N. Segev. 2000. The TRAPP complex is a nucleotide exchanger for Ypt1 and Ypt31/32. *Mol Biol Cell*. 11:4403-4411.

Kassir, Y., D. Granot, and G. Simchen. 1988. IME1, a positive regulator gene of meiosis in S. cerevisiae. *Cell*. 52:853-62.

Katz, L., and P. Brennwald. 2000. Testing the 3Q:1R "rule": mutational analysis of the ionic "zero" layer in the yeast exocytic SNARE complex reveals no requirement for arginine. *Mol Biol Cell*. 11:3849-58.

Knop, M., K.J. Miller, M. Mazza, D. Feng, M. Weber, S. Keranen, and J. Jantti. 2005. Molecular interactions position Mso1p, a novel PTB domain homologue, in the interface of the exocyst complex and the exocytic SNARE machinery in yeast. *Mol Biol Cell*. 16:4543-56.

Knop, M., and E. Schiebel. 1998. Receptors determine the cellular localization of a

gamma-tubulin complex and thereby the site of microtubule formation. *Embo J*. 17:3952-67.

Knop, M., and K. Strasser. 2000. Role of the spindle pole body of yeast in mediating assembly of the prospore membrane during meiosis. *Embo J*. 19:3657-67.

Kooijman, E.E., V. Chupin, B. de Kruijff, and K.N. Burger. 2003. Modulation of membrane curvature by phosphatidic acid and lysophosphatidic acid. *Traffic*. 4:162-74.

Kooijman, E.E., V. Chupin, N.L. Fuller, M.M. Kozlov, B. de Kruijff, K.N. Burger, and P.R. Rand. 2005. Spontaneous curvature of phosphatidic acid and lysophosphatidic acid. *Biochemistry*. 44:2097-102.

Krapp, A., P. Collin, A. Cokoja, S. Dischinger, E. Cano, and V. Simanis. 2006. The Schizosaccharomyces pombe septation initiation network (SIN) is required for spore formation in meiosis. *J Cell Sci*. 119:2882-91.

Lagow, R.D., H. Bao, E.N. Cohen, R.W. Daniels, A. Zuzek, W.H. Williams, G.T. Macleod, R.B. Sutton, and B. Zhang. 2007. Modification of a hydrophobic layer by a point mutation in syntaxin 1A regulates the rate of synaptic vesicle fusion. *PLoS Biol*. 5:e72.

Lewis, M.J., B.J. Nichols, C. Prescianotto-Baschong, H. Riezman, and H.R. Pelham. 2000. Specific retrieval of the exocytic SNARE Snc1p from early yeast endosomes. *Mol Biol Cell*. 11:23-38.

Lin, Y., and G.R. Smith. 1995. Molecular cloning of the meiosis-induced *rec10* gene of *Schizosaccharomyces pombe*. *Curr Genet*. 27:440-446.

Liu, S., K.A. Wilson, T. Rice-Stitt, A.M. Neiman, and J.A. McNew. 2007. In vitro fusion catalyzed by the sporulation-specific t-SNARE light-chain Spo20p is stimulated by phosphatidic acid. *Traffic*. 8:1630-43.

Lo, H.C., L. Wan, A. Rosebrock, B. Futcher, and N.M. Hollingsworth. 2008. Cdc7-Dbf4 regulates NDT80 transcription as well as reductional segregation during budding yeast meiosis. *Mol Biol Cell*. 19:4956-67.

Longtine, M.S., A. McKenzie, 3rd, D.J. Demarini, N.G. Shah, A. Wach, A. Brachat, P. Philippsen, and J.R. Pringle. 1998. Additional modules for versatile and economical PCR-based gene deletion and modification in *Saccharomyces cerevisiae*. *Yeast*. 14:953-61.

Lynn, R.R., and P.T. Magee. 1970. Development of the spore wall during ascospore formation in Saccharomyces cerevisiae. *J Cell Biol*. 44:688-92.

Maeda, Y., J. Kashiwazaki, C. Shimoda, and T. Nakamura. 2009. The *Schizosaccharomyces pombe* syntaxin 1 homolog, Psy1, is essential in the development of the forespore membrane. *Biosci Biotechnol Biochem*. 73:339-345.

Marshall, W.F. 2009. Centriole evolution. *Curr Opin Cell Biol*. 21:14-9.

Martin-Castellanos, C., M. Blanco, A.E. Rozalen, L. Perez-Hidalgo, A.I. Garcia, F. Conde, J. Mata, C. Ellermeier, L. Davis, P. San-Segundo, G.R. Smith, and S. Moreno. 2005. A large-scale screen in S. pombe identifies seven novel genes required for critical meiotic events. *Curr Biol*. 15:2056-62.

Mathieson, E.M., Y. Suda, M. Nickas, B. Snydsman, T.N. Davis, E.G. Muller, and A.M. Neiman. 2010. Vesicle Docking to the Spindle Pole Body Is Necessary to Recruit the Exocyst During Membrane Formation in Saccharomyces cerevisiae. *Mol Biol Cell*.

McNew, J.A. 2008. Regulation of SNARE-mediated membrane fusion during exocytosis. *Chem Rev*. 108:1669-86.

McNew, J.A., F. Parlati, R. Fukuda, R.J. Johnston, K. Paz, F. Paumet, T.H. Sollner, and J.E. Rothman. 2000. Compartmental specificity of cellular membrane fusion encoded in SNARE proteins. *Nature*. 407:153-9.

Mellman, I., and G. Warren. 2000. The road taken: past and future foundations of membrane traffic. *Cell*. 100:99-112.

Mendonsa, R., and J. Engebrecht. 2009. Phosphatidylinositol-4,5-bisphosphate and phospholipase D-generated phosphatidic acid specify SNARE-mediated vesicle fusion for prospore membrane formation. *Eukaryot Cell*. 8:1094-105.

Moens, P.B. 1971. Fine structure of ascospore development in the yeast Saccharomyces cerevisiae. *Can J Microbiol*. 17:507-10.

Moens, P.B., and E. Rapport. 1971. Spindles, spindle plaques, and meiosis in the yeast Saccharomyces cerevisiae (Hansen). *J Cell Biol*. 50:344-61.

Moreno, M.B., A. Duran, and J.C. Ribas. 2000. A family of multifunctional thiamine-repressible expression vectors for fission yeast. *Yeast*. 16:861-872.

Morishita, M., R. Mendonsa, J. Wright, and J. Engebrecht. 2007. Snc1p v-SNARE transport to the prospore membrane during yeast sporulation is dependent on endosomal retrieval pathways. *Traffic*. 8:1231-45.

Morozova, N., Y. Liang, A.A. Tokarev, S.H. Chen, R. Cox, J. Andrejic, Z. Lipatova, V.A. Sciorra, S.D. Emr, and N. Segev. 2006. TRAPPII subunits are required for the specificity switch of a Ypt-Rab GEF. *Nat Cell Biol*. 8:1263-9.

Mumberg, D., R. Muller, and M. Funk. 1995. Yeast vectors for the controlled expression of heterologous proteins in different genetic backgrounds. *Gene*. 156:119-122.

Munson, M., and F.M. Hughson. 2002. Conformational regulation of SNARE assembly and disassembly in vivo. *J Biol Chem*. 277:9375-81.

Nachury, M.V., A.V. Loktev, Q. Zhang, C.J. Westlake, J. Peranen, A. Merdes, D.C. Slusarski, R.H. Scheller, J.F. Bazan, V.C. Sheffield, and P.K. Jackson. 2007. A core complex of

BBS proteins cooperates with the GTPase Rab8 to promote ciliary membrane biogenesis. *Cell*. 129:1201-13.

Nair, J., H. Muller, M. Peterson, and P. Novick. 1990. Sec2 protein contains a coiled-coil domain essential for vesicular transport and a dispensable carboxy terminal domain. *J Cell Biol*. 110:1897-1909.

Nakagawa, Y., Y. Yamane, T. Okanoue, S. Tsukita, and S. Tsukita. 2001. Outer dense fiber 2 is a widespread centrosome scaffold component preferentially associated with mother centrioles: its identification from isolated centrosomes. *Mol Biol Cell*. 12:1687-97.

Nakamura-Kubo, M., T. Nakamura, A. Hirata, and C. Shimoda. 2003. The fission yeast *spo14$^+$* gene encoding a functional homologue of budding yeast Sec12 is required for the development of forespore membranes. *Mol Biol Cell*. 14:1109-1124.

Nakamura, T., H. Asakawa, Y. Nakase, J. Kashiwazaki, Y. Hiraoka, and C. Shimoda. 2008. Live observation of forespore membrane formation in fission yeast. *Mol Biol Cell*. 19:3544-3553.

Nakamura, T., J. Kashiwazaki, and C. Shimoda. 2005. A fission yeast SNAP-25 homologue, SpSec9, is essential for cytokinesis and sporulation. *Cell Struct Funct*. 30:15-24.

Nakamura, T., M. Nakamura-Kubo, A. Hirata, and C. Shimoda. 2001. The *Schizosaccharomyces pombe spo3$^+$* gene is required for assembly of the forespore membrane and genetically interacts with *psy1$^+$*-encoding syntaxin-like protein. *Mol Biol Cell*. 12:3955-3972.

Nakanishi, H., P. de los Santos, and A.M. Neiman. 2004. Positive and negative regulation of a SNARE protein by control of intracellular localization. *Mol Biol Cell*. 15:1802-15.

Nakanishi, H., M. Morishita, C.L. Schwartz, A. Coluccio, J. Engebrecht, and A.M. Neiman. 2006. Phospholipase D and the SNARE Sso1p are necessary for vesicle fusion during sporulation in yeast. *J Cell Sci*. 119:1406-15.

Nakanishi, H., Y. Suda, and A.M. Neiman. 2007. Erv14 family cargo receptors are necessary for ER exit during sporulation in Saccharomyces cerevisiae. *J Cell Sci*. 120:908-16.

Nakase, Y., M. Nakamura-Kubo, Y. Ye, A. Hirata, C. Shimoda, and T. Nakamura. 2008. Meiotic spindle pole bodies acquire the ability to assemble the spore plasma membrane by sequential recruitment of sporulation-specific components in fission yeast. *Mol Biol Cell*. 19:2476-2487.

Nakase, Y., T. Nakamura, A. Hirata, S.M. Routt, H.B. Skinner, V.A. Bankaitis, and C. Shimoda. 2001. The *Schizosaccharomyces pombe spo20$^+$* gene encoding a homologue of *Saccharomyces cerevisiae* Sec14 plays an important role in forespore membrane formation. *Mol Biol Cell*. 12:901-917.

Neiman, A.M. 1998. Prospore membrane formation defines a developmentally regulated

branch of the secretory pathway in yeast. *J Cell Biol*. 140:29-37.

Neiman, A.M. 2005. Ascospore formation in the yeast Saccharomyces cerevisiae. *Microbiol Mol Biol Rev*. 69:565-84.

Neiman, A.M., L. Katz, and P.J. Brennwald. 2000. Identification of domains required for developmentally regulated SNARE function in Saccharomyces cerevisiae. *Genetics*. 155:1643-55.

Nickas, M.E., C. Schwartz, and A.M. Neiman. 2003. Ady4p and Spo74p are components of the meiotic spindle pole body that promote growth of the prospore membrane in *Saccharomyces cerevisiae*. *Eukaryot Cell*. 2:431-445.

Nottingham, R.M., and S.R. Pfeffer. 2009. Defining the boundaries: Rab GEFs and GAPs. *Proc Natl Acad Sci U S A*. 106:14185-6.

Ortiz, D., M. Medkova, C. Walch-Solimena, and P. Novick. 2002. Ypt32 recruits the Sec4p guanine nucleotide exchange factor, Sec2p, to secretory vesicles; evidence for a Rab cascade in yeast. *J Cell Biol*. 157:1005-1015.

Oyler, G.A., G.A. Higgins, R.A. Hart, E. Battenberg, M. Billingsley, F.E. Bloom, and M.C. Wilson. 1989. The identification of a novel synaptosomal-associated protein, SNAP-25, differentially expressed by neuronal subpopulations. *J Cell Biol*. 109:3039-52.

Parlati, F., J.A. McNew, R. Fukuda, R. Miller, T.H. Sollner, and J.E. Rothman. 2000. Topological restriction of SNARE-dependent membrane fusion. *Nature*. 407:194-8.

Parlati, F., O. Varlamov, K. Paz, J.A. McNew, D. Hurtado, T.H. Sollner, and J.E. Rothman. 2002. Distinct SNARE complexes mediating membrane fusion in Golgi transport based on combinatorial specificity. *Proc Natl Acad Sci U S A*. 99:5424-9.

Paumet, F., B. Brugger, F. Parlati, J.A. McNew, T.H. Sollner, and J.E. Rothman. 2001. A t-SNARE of the endocytic pathway must be activated for fusion. *J Cell Biol*. 155:961-8.

Paumet, F., V. Rahimian, and J.E. Rothman. 2004. The specificity of SNARE-dependent fusion is encoded in the SNARE motif. *Proc Natl Acad Sci U S A*. 101:3376-80.

Pelham, H.R. 1999. SNAREs and the secretory pathway-lessons from yeast. *Exp Cell Res*. 247:1-8.

Pfeffer, S.R. 1999. Transport-vesicle targeting: tethers before SNAREs. *Nat Cell Biol*. 1:E17-22.

Poirier, M.A., W. Xiao, J.C. Macosko, C. Chan, Y.K. Shin, and M.K. Bennett. 1998. The synaptic SNARE complex is a parallel four-stranded helical bundle. *Nat Struct Biol*. 5:765-9.

Protopopov, V., B. Govindan, P. Novick, and J.E. Gerst. 1993. Homologs of the

synaptobrevin/VAMP family of synaptic vesicle proteins function on the late secretory pathway in S. cerevisiae. *Cell*. 74:855-61.

Rivera-Molina, F.E., and P.J. Novick. 2009. A Rab GAP cascade defines the boundary between two Rab GTPases on the secretory pathway. *Proc Natl Acad Sci U S A*. 106:14408-14413.

Rogers, K.K., P.D. Wilson, R.W. Snyder, X. Zhang, W. Guo, C.R. Burrow, and J.H. Lipschutz. 2004. The exocyst localizes to the primary cilium in MDCK cells. *Biochem Biophys Res Commun*. 319:138-43.

Rojas, R.J., R.J. Kimple, K.L. Rossman, D.P. Siderovski, and J. Sondek. 2003. Established and emerging fluorescence-based assays for G-protein function: Ras-superfamily GTPases. *Comb Chem High Throughput Screen*. 6:409-418.

Rudge, S.A., A.J. Morris, and J. Engebrecht. 1998. Relocalization of phospholipase D activity mediates membrane formation during meiosis. *J Cell Biol*. 140:81-90.

Rudge, S.A., V.A. Sciorra, M. Iwamoto, C. Zhou, T. Strahl, A.J. Morris, J. Thorner, and J. Engebrecht. 2004. Roles of phosphoinositides and of Spo14p (phospholipase D)-generated phosphatidic acid during yeast sporulation. *Mol Biol Cell*. 15:207-18.

Rudge, S.A., C. Zhou, and J. Engebrecht. 2002. Differential regulation of Saccharomyces cerevisiae phospholipase D in sporulation and Sec14-independent secretion. *Genetics*. 160:1353-61.

Sanderfoot, A.A., F.F. Assaad, and N.V. Raikhel. 2000. The Arabidopsis genome. An abundance of soluble N-ethylmaleimide-sensitive factor adaptor protein receptors. *Plant Physiol*. 124:1558-69.

Sato, Y., R. Shirakawa, H. Horiuchi, N. Dohmae, S. Fukai, and O. Nureki. 2007. Asymmetric coiled-coil structure with Guanine nucleotide exchange activity. *Structure*. 15:245-252.

Scales, S.J., B.Y. Yoo, and R.H. Scheller. 2001. The ionic layer is required for efficient dissociation of the SNARE complex by alpha-SNAP and NSF. *Proc Natl Acad Sci U S A*. 98:14262-7.

Sciorra, V.A., S.A. Rudge, J. Wang, S. McLaughlin, J. Engebrecht, and A.J. Morris. 2002. Dual role for phosphoinositides in regulation of yeast and mammalian phospholipase D enzymes. *J Cell Biol*. 159:1039-49.

Sclafani, A., S. Chen, F. Rivera-Molina, K. Reinisch, P. Novick, and S. Ferro-Novick. 2010. Establishing a role for the GTPase Ypt1p at the late Golgi. *Traffic*. 11:520-32.

Segev, N. 2001. Ypt and Rab GTPases: insight into functions through novel interactions. *Curr Opin Cell Biol*. 13:500-11.

Shen, J., D.C. Tareste, F. Paumet, J.E. Rothman, and T.J. Melia. 2007. Selective activation of

cognate SNAREpins by Sec1/Munc18 proteins. *Cell*. 128:183-95.

Shimoda, C. 2004. Forespore membrane assembly in yeast: coordinating SPBs and membrane trafficking. *J Cell Sci*. 117:389-396.

Sikorski, R.S., and P. Hieter. 1989. A system of shuttle vectors and yeast host strains designed for efficient manipulation of DNA in Saccharomyces cerevisiae. *Genetics*. 122:19-27.

Singla, V., and J.F. Reiter. 2006. The primary cilium as the cell's antenna: signaling at a sensory organelle. *Science*. 313:629-33.

Smits, G.J., H. van den Ende, and F.M. Klis. 2001. Differential regulation of cell wall biogenesis during growth and development in yeast. *Microbiology*. 147:781-94.

Snyder, M. 1994. The spindle pole body of yeast. *Chromosoma*. 103:369-80.

Sogaard, M., K. Tani, R.R. Ye, S. Geromanos, P. Tempst, T. Kirchhausen, J.E. Rothman, and T. Sollner. 1994. A rab protein is required for the assembly of SNARE complexes in the docking of transport vesicles. *Cell*. 78:937-48.

Sollner, T., S.W. Whiteheart, M. Brunner, H. Erdjument-Bromage, S. Geromanos, P. Tempst, and J.E. Rothman. 1993. SNAP receptors implicated in vesicle targeting and fusion. *Nature*. 362:318-24.

Sorensen, J.B., K. Wiederhold, E.M. Muller, I. Milosevic, G. Nagy, B.L. de Groot, H. Grubmuller, and D. Fasshauer. 2006. Sequential N- to C-terminal SNARE complex assembly drives priming and fusion of secretory vesicles. *Embo J*. 25:955-66.

Sorokin, S. 1962. Centrioles and the formation of rudimentary cilia by fibroblasts and smooth muscle cells. *J Cell Biol*. 15:363-77.

Stajich, J.E., M.L. Berbee, M. Blackwell, D.S. Hibbett, T.Y. James, J.W. Spatafora, and J.W. Taylor. 2009. The fungi. *Curr Biol*. 19:R840-5.

Stenmark, H. 2009. Rab GTPases as coordinators of vesicle traffic. *Nat Rev Mol Cell Biol*. 10:513-525.

Strop, P., S.E. Kaiser, M. Vrljic, and A.T. Brunger. 2008. The Structure of the Yeast Plasma Membrane SNARE Complex Reveals Destabilizing Water-filled Cavities. *J Biol Chem*. 283:1113-9.

Sutton, R.B., D. Fasshauer, R. Jahn, and A.T. Brunger. 1998. Crystal structure of a SNARE complex involved in synaptic exocytosis at 2.4 A resolution. *Nature*. 395:347-53.

Szebenyi, G., B. Hall, R. Yu, A.I. Hashim, and H. Kramer. 2007. Hook2 localizes to the centrosome, binds directly to centriolin/CEP110 and contributes to centrosomal function. *Traffic*. 8:32-46.

TerBush, D.R., T. Maurice, D. Roth, and P. Novick. 1996. The Exocyst is a multiprotein complex required for exocytosis in *Saccharomyces cerevisiae*. *Embo J*. 15:6483-6494.

Togneri, J., Y.S. Cheng, M. Munson, F.M. Hughson, and C.M. Carr. 2006. Specific SNARE complex binding mode of the Sec1/Munc-18 protein, Sec1p. *Proc Natl Acad Sci U S A*. 103:17730-5.

Virgin, J.B., J. Metzger, and G.R. Smith. 1995. Active and inactive transplacement of the *M26* recombination hotspot in *Schizosaccharomyces pombe*. *Genetics*. 141:33-48.

Walch-Solimena, C., R.N. Collins, and P.J. Novick. 1997. Sec2p mediates nucleotide exchange on Sec4p and is involved in polarized delivery of post-Golgi vesicles. *J Cell Biol*. 137:1495-1509.

Wang, W., and S. Ferro-Novick. 2002. A Ypt32p exchange factor is a putative effector of Ypt1p. *Mol Biol Cell*. 13:3336-43.

Weber, M., K. Chernov, H. Turakainen, G. Wohlfahrt, M. Pajunen, H. Savilahti, and J. Jantti. 2010. Mso1p regulates membrane fusion through interactions with the putative N-peptide-binding area in Sec1p domain 1. *Mol Biol Cell*. 21:1362-74.

Weber, T., B.V. Zemelman, J.A. McNew, B. Westermann, M. Gmachl, F. Parlati, T.H. Sollner, and J.E. Rothman. 1998. SNAREpins: minimal machinery for membrane fusion. *Cell*. 92:759-72.

Weimbs, T., K. Mostov, S.H. Low, and K. Hofmann. 1998. A model for structural similarity between different SNARE complexes based on sequence relationships. *Trends Cell Biol*. 8:260-2.

Whyte, J.R., and S. Munro. 2002. Vesicle tethering complexes in membrane traffic. *J Cell Sci*. 115:2627-37.

Wiederkehr, A., J.O. De Craene, S. Ferro-Novick, and P. Novick. 2004. Functional specialization within a vesicle tethering complex: bypass of a subset of exocyst deletion mutants by Sec1p or Sec4p. *J Cell Biol*. 167:875-887.

Winzeler, E.A., D.D. Shoemaker, A. Astromoff, H. Liang, K. Anderson, B. Andre, R. Bangham, R. Benito, J.D. Boeke, H. Bussey, A.M. Chu, C. Connelly, K. Davis, F. Dietrich, S.W. Dow, M. El Bakkoury, F. Foury, S.H. Friend, E. Gentalen, G. Giaever, J.H. Hegemann, T. Jones, M. Laub, H. Liao, N. Liebundguth, D.J. Lockhart, A. Lucau-Danila, M. Lussier, N. M'Rabet, P. Menard, M. Mittmann, C. Pai, C. Rebischung, J.L. Revuelta, L. Riles, C.J. Roberts, P. Ross-MacDonald, B. Scherens, M. Snyder, S. Sookhai-Mahadeo, R.K. Storms, S. Veronneau, M. Voet, G. Volckaert, T.R. Ward, R. Wysocki, G.S. Yen, K. Yu, K. Zimmermann, P. Philippsen, M. Johnston, and R.W. Davis. 1999. Functional characterization of the S. cerevisiae genome by gene deletion and parallel analysis. *Science*. 285:901-6.

Wolfe, K.H., and D.C. Shields. 1997. Molecular evidence for an ancient duplication of the entire yeast genome. *Nature*. 387:708-13.

Wurmser, A.E., T.K. Sato, and S.D. Emr. 2000. New component of the vacuolar class C-Vps complex couples nucleotide exchange on the Ypt7 GTPase to SNARE-dependent docking and fusion. *J Cell Biol*. 151:551-562.

Yang, B., L. Gonzalez, Jr., R. Prekeris, M. Steegmaier, R.J. Advani, and R.H. Scheller. 1999. SNARE interactions are not selective. Implications for membrane fusion specificity. *J Biol Chem*. 274:5649-53.

Yang, H.J., H. Nakanishi, S. Liu, J.A. McNew, and A.M. Neiman. 2008. Binding interactions control SNARE specificity in vivo. *J Cell Biol*. 183:1089-100.

Yang, H.J., and A.M. Neiman. 2010. A guaninine nucleotide exchange factor is a component of the meiotic spindle pole body in Schizosaccharomyces pombe. *Mol Biol Cell*. 21:1272-81.

Yoshimura, S., J. Egerer, E. Fuchs, A.K. Haas, and F.A. Barr. 2007. Functional dissection of Rab GTPases involved in primary cilium formation. *J Cell Biol*. 178:363-9.

Zhang, H. 2003. Binding platforms for Rab prenylation and recycling: Rab escort protein, RabGGT, and RabGDI. *Structure*. 11:237-9.

Zuo, X., W. Guo, and J.H. Lipschutz. 2009. The exocyst protein Sec10 is necessary for primary ciliogenesis and cystogenesis in vitro. *Mol Biol Cell*. 20:2522-9.